Cell-Surface Interactions Controlled by Surface Modifications with Polyelectrolyte Multilayers

Zur Erlangung des akademischen Grades eines

DOKTORS DER INGENIEURWISSENSCHAFTEN (DR.-ING.)

von der KIT-Fakultät für Chemieingenieurwesen und Verfahrenstechnik des Karlsruher Instituts für Technologie (KIT)
genehmigte

DISSERTATION

von

M.Sc. Alexander Rudt
aus Tübingen

Tag der mündlichen Prüfung: 15.05.2025

Erstgutachter: Prof. Dr.-Ing. Matthias Franzreb

Zweitgutachter: Prof. Dr. Rumen Krastev

Abstract (English)

The interaction between cells and medical implants occurs at their interface, where material surface properties play a crucial role. Cells do not directly interact with surfaces of the material but recognize biologically active proteins that adsorb to the material. This dissertation investigated cell-surface interactions by adjusting substrate surface properties and characterizing the biological cell responses in contact with these surfaces. Polyelectrolyte (PE) multilayer (PEM) coatings were used to precisely modify surfaces. Variations in surface properties were achieved through the use of synthetic and natural polyelectrolyte pairs, different terminations (negative or positive), and altered coating conditions. Surface properties such as zeta potential, water contact angle, roughness, surface viscosity, and surface elasticity were measured, revealing differences in the characteristics of modified surfaces. Protein adsorption on these modified surfaces was studied, showing that adsorption behavior varied with surface charge and intrinsic excess charge, influencing the amount of adsorbed proteins. Neutron reflectometry provided insights into the thickness, density, and water content of PEM films altered by protein adsorption. Experiments with endothelial cells (HUVEC) were conducted on modified surfaces to prove effects of surface properties on cellular behavior. The PEM modification system allowed surfaces to be switched from cell-adhesive to non-adhesive (and vice versa) and enabled precise control over the number of adhering cells, revealing several correlations with surface properties. Surface roughness and elasticity strongly correlated with cell adhesion. Higher amounts of adsorbed proteins correlated with greater numbers of adhered cells. Cells showed more affinity towards negatively charged surfaces with increasing shear viscosity and towards positively charged surfaces with decreasing shear viscosity. An increase in water content in PEM films directly correlated with an increase in the number of adhering cells. The dissertation also explored the immune response to surfaces. Human endothelial cells were brought into contact with these surfaces to simulate the precursor reaction of the immune response. The activation of the nuclear factor kappa B (Nf-κB) pathway and subsequent secretion of pro-inflammatory interleukins were measured. Higher surface roughness and elasticity were found to reduce pro-inflammatory signaling in cells stressed by foreign body surfaces. Certain PEM-modified surfaces significantly decreased the expression of pro-inflammatory signaling molecules, highlighting the potential for these modifications to improve the biocompatibility of medical implants. This finding is significant for biomedical applications, such as cardiovascular stents, where surface modifications can promote cell adhesion and reduce inflammation.

Zusammenfassung (Deutsch)

Die Interaktion zwischen Zellen und medizinischen Implantaten erfolgt an ihrer Grenzfläche, wobei Materialoberflächeneigenschaften eine entscheidende Rolle spielen. Zellen interagieren nicht direkt mit Oberflächen der Materialen, sondern erkennen biologisch aktive Proteine, die sich an das Material adsorbieren. Diese Dissertation untersuchte Zell-Oberflächen-Interaktionen, indem Oberflächeneigenschaften des Substrats verändert und die biologischen Zellreaktionen in Kontakt mit diesen Oberflächen charakterisiert wurden. Polyelektrolyt (PE)-Multischichtbeschichtungen (PEM) wurden verwendet um Oberflächen präzise zu modifizieren. Variationen von Oberflächeneigenschaften wurden durch Verwendung von synthetischen und natürlichen Polyelektrolytpaaren, unterschiedlichen Terminierungen (negativ oder positiv) und veränderten Beschichtungsbedingungen erreicht. Oberflächeneigenschaften wie Zeta-Potential, Wasserkontaktwinkel, Rauigkeit, Oberflächenviskosität und Elastizität wurden gemessen, wodurch Unterschiede in den Eigenschaften der modifizierten Oberflächen bestimmt wurden. Die Proteinadsorption auf diesen modifizierten Oberflächen wurde untersucht und zeigte, dass das Adsorptionsverhalten mit der Oberflächenladung und der intrinsischen Überschussladung variierte, was die Menge der adsorbierten Proteine beeinflusste. Neutronenreflektometrie lieferte Einblicke in die Dicke, Dichte und den Wassergehalt von PEM-Filmen, die durch Proteinadsorption verändert wurden. Experimente mit Endothelzellen (HUVEC) wurden auf diesen modifizierten Oberflächen durchgeführt, um Effekte auf Zellverhalten zu prüfen. Die PEM-Modifikation ermöglichte es, Oberflächen von zell-adhäsiv zu nicht-adhäsiv (und umgekehrt) zu wechseln und die Anzahl der haftenden Zellen präzise zu kontrollieren, wodurch mehrere Korrelationen mit den Oberflächeneigenschaften aufgedeckt wurden. Oberflächenrauigkeit und Elastizität korrelierten stark mit der Zelladhäsion. Höhere Mengen adsorbierender Proteine korrelierten mit einer höheren Anzahl anhaftender Zellen. Zellen zeigten mehr Affinität zu negativ geladenen Oberflächen mit zunehmender Scherviskosität und zu positiv geladenen Oberflächen mit abnehmender Scherviskosität. Eine Zunahme des Wassergehalts in PEM-Filmen korrelierte direkt mit einer Zunahme der Anzahl haftender Zellen. Die Dissertation untersuchte auch die Immunantwort auf diese Oberflächen. Menschliche Endothelzellen wurden mit diesen Oberflächen in Kontakt gebracht, um die Vorläuferreaktion der Immunantwort zu simulieren. Die Aktivierung des Nuklearfaktors Kappa B (Nf-κB)-Signalwegs und die anschließende Sekretion proinflammatorischer Interleukine wurden gemessen. Höhere Oberflächenrauigkeit und Elastizität zeigten eine Reduktion der proinflammatorischen Signalgebung in Zellen, die durch

Fremdkörperoberflächen gestresst wurden. Bestimmte PEM-modifizierte Oberflächen verringerten signifikant die Expression proinflammatorischer Signalmoleküle, was das Potenzial dieser Modifikationen zur Verbesserung der Biokompatibilität medizinischer Implantate hervorhebt. Diese Erkenntnis ist bedeutend für biomedizinische Anwendungen, wie z.B. kardiovaskuläre Stents, bei denen Oberflächenmodifikationen die Zelladhäsion fördern und Entzündungen reduzieren können.

Index

Chapter 1 – Introduction

In cell-surface interactions, the most important events occur at the interface between material and cells. Key surface properties relevant to these interactions include surface energy, surface charge, surface roughness, surface elasticity, and chemical composition. Cells possess mechanisms to recognize their own tissues and differentiate them from foreign materials. However, cells do not directly interact with biomaterial surfaces. Instead, membrane-located cellular receptor proteins recognize the body's own biologically active proteins that adsorb to material surfaces prior to cell interaction. Thus, cells communicate with biomaterial surfaces through the extracellular matrix and blood serum proteins that adsorb beforehand.

In today's medicine, the use of biomaterials is indispensable in a wide range of applications, including implants, protheses, tissue engineering and drug delivery systems. A biomaterial is any natural or synthetic material, that is engineered to interact with biological systems for a medical purpose. Particularly in the field of implantations, the interaction between biomaterial and host tissue can promote proper wound healing and integration or trigger inflammatory responses and potentially lead to implant failure. One of the main challenges after implantation is the potential rejection of a biomaterials by the host tissue. The interactions at the interface between tissue and material surface are crucial in determining whether a rejection reaction will occur.

The affinity of proteins for specific surfaces and the impact of surface properties on the conformation of adsorbing proteins are crucial for activating both the complement system and the coagulation cascade. The type, surface density, and conformation of adsorbed serum proteins provide information about the physical, chemical, and biological properties of the surface. The extracellular matrix acts as an extension of cellular sensing and a mediator between cells and surface-adsorbed serum proteins. After initial coverage of material surfaces with blood serum proteins, specific extracellular matrix proteins bind to the serum protein-covered surfaces. Surface properties affect the types and surface densities of adsorbing serum proteins, which in turn enable further adsorption of extracellular matrix proteins and the recognition by cells.

Fine-tuning these properties can alter subsequent cellular behavior, such as adhesion or activation of intracellular pathways. In-stent restenosis is a prominent example of cell-surface interactions. It occurs due to the synergistic effects of tissue injury and immunological processes caused by the presence of the stent implant. This can lead to excessive growth of scar tissue (neointimal hyperplasia) and the narrowing of the artery within the stent, potentially resulting in implant failure and the need for a second intervention.

This dissertation aims to study cell-surface interactions. Our hypothesis is that by fine-tuning implant material surface properties – such as hydrophobicity, surface energy, nano-roughness, and nano-elasticity – it is possible to stimulate cellular recognition mechanisms to reduce the expression of pro-inflammatory interleukins and subsequently diminish inflammatory processes, potentially reducing the incidence of inflammatory diseases such as in-stent restenosis.

Surfaces with defined surface properties were precisely constructed by coating of substrates with polyelectrolyte multilayers (PEM). Variations in surface properties were reached by alteration of the used polyelectrolytes, negative or positive termination of the coating, and by alteration of electrolyte concentration in the polyelectrolyte deposition solution. This allowed for the construction of modified surfaces with differences in zeta potential, hydrophobicity, surface roughness, surface elasticity (Young's modulus and shear modulus), and surface viscosity.

Protein adsorption on PEM-modified surfaces was studied using both a simple albumin solution and a complex cell culture medium. The amount of adsorbed proteins varied across the tested surfaces, which could be attributed to the surface charge and the intrinsic excess charge of the PEM films.

Human endothelial cells were cultivated on PEM-modified surfaces and showed different adhesion and activity on the tested surfaces. A strong correlation of cell adhesion with surface elasticity and surface roughness, as well as the amount of adsorbed proteins from cell culture medium was observed.

To simulate a stenting and initial host cell signaling like in in-stent restenosis, an experimental setup was established, in which confluent cells were approached and pressed from above with a medical steel surface. The immune response towards the surface was measured at three points of progress: the activation of nuclear factor kappa B pathway, the expression of mRNA coding for pro-inflammatory interleukins and the expression and secretion of interleukins.

Certain PEM modifications were identified that enable a significant reduction of pro-inflammatory interleukin expression on transcriptional and translational level by contact with the endothelial cells. A strong correlation between interleukin expression and surface properties was found in surface elasticity (Young's modulus) and roughness of the surface.

These findings underscore the importance of altering surface properties to enhance the biocompatibility of implant materials, potentially reducing adverse reactions and improving clinical outcomes in medical implantations.

Chapter 2 – Theory

Biomaterials are engineered materials designed to treat, augment, repair, or replace tissue or body functions lost due to illness or other causes. To achieve this, biomaterials must at least be in contact with biological tissue (e.g., wound dressings) or be inserted into the body near vital organs (e.g., pacemakers). The rejection of biomaterials by host tissue is one of the major challenges in the medical fields, particularly concerning implantations. Therefore, improving the design of biomaterials for better biocompatibility is an important area of study [Jandt & Cai 2007].

The interactions of biomaterial and tissue occurs at the interface between material surface and biological cells. A suitable material surface promotes complete wound healing and the proper integration of implants into host tissue. Conversely, an unsuitable surface can trigger an inflammatory response and potentially lead to implant failure. The emerging field of materiomics seeks to connect the physicochemical properties of materials with their overall biological effects [Cranford & Buehler 2012].
Mechanical properties are the primary consideration when selecting a material for implantation. For instance, steel is often chosen for its stiffness and robustness in joint prostheses, or for its spring effect in stents. However, the base material may encounter challenges during the integration process with host tissue. The interactions at the interface between tissue and material surface determine whether a rejection reaction will occur. To enhance biocompatibility, the surface of the base material can be modified, altering its surface properties to suit the specific application [Wintermantel & Ha 2009].

In nature, foreign materials do not belong into living bodies. If a foreign material invades the body, it is usually a harmful entity such as bacteria, viruses or inert materials during injury. To preserve vital functions, multicellular organisms evolved immensely complicated and powerful systems to deactivate and remove foreign materials from the body.

Cells possess mechanisms to recognize own tissues and differentiate own surfaces from surfaces of foreign materials. This process is very complex and involves various immunological systems, which are induced by local recognition and signaling of host cells in contact with the foreign body.

Biomaterials, although intended for beneficial purpose, remain foreign bodies that the human body will attempt to fight. The main challenge is to design materials with properties that are not recognized by the human body as hostile and will be accepted as its own tissue, which is a straightforward definition of biocompatibility for long-term implants.

2.1 Surfaces

Materials in biomedical applications are mainly chosen by their physical properties such as stiffness, robustness or elasticity. However, in cell-surface interactions, the most important events occur at the interface between material and cells, so to speak, at the surface of the biomaterial.

Surfaces are defined as boundary separating two different phases, such as solid-solid, liquid-gas or solid-gas interfaces [Butt & Kappl 2018].

The most important properties of surfaces with relevance to cell-surface interactions include: (1) Surface Energy. This is the excess energy at the surface of a material compared to its bulk. It influences adhesion, wetting, and surface reactions. (2) Surface Charge. The distribution of electrical charges on a surface, which affects electrostatic interactions and colloidal stability. (3) Surface Roughness. The texture of a surface, which can impact friction, adhesion, and wettability. (4) Surface Elasticity. The response of surfaces and interfaces to mechanical stresses and deformations. (5) Chemical Composition. The elements and compounds present on a surface, determining its reactivity and interaction with other substances [Butt & Kappl 2018].

2.1.1 Surface energy

Surface energy is the excess energy at the surface of a material compared to its bulk. It influences phenomena such as adhesion, wetting, and surface reactions. The surface energy can be related to work of adhesion (W_{12}) between two phases using the Young-Dupré equation (eq. 1), where γ_1 and γ_2 are the surface energies of the two phases and γ_{12} is the interfacial energy between them.

$$W_{12} = \gamma_1 + \gamma_2 - \gamma_{12} \qquad \text{(eq. 1)}$$

In practical terms, the Young's equation (eq. 2) can be used to analyze contact angle measurements of a liquid drop on a solid surface:

$$\gamma_{SV} = \gamma_{SL} + \gamma_{LV}\cos(\Theta) \qquad \text{(eq. 2)}$$

, where γ_{SV} is the surface energy of the solid-vapor interface; γ_{SL} is the surface energy of the solid-liquid interface; γ_{LV} is the surface tension of the liquid (liquid-vapor interface); and Θ is the contact angle, which is the angle formed at the junction of the liquid, solid and vapor phases.

The surface energy is a general material constant that is independent on liquids in contact with the surface. For analysis of a substrates surface energy, contact angle measurements with different polar and disperse liquids, and modelling are required.

The contact angle measurement of a single liquid (e.g., water) is specific to the interface between the liquid and the surface. Therefore, it is always labeled with the corresponding liquid (e.g., contact angle of water) and can be used to compare liquid-surface interactions of different surfaces. For example, measuring the contact angles of water allows for the comparison of the hydrophobicity of various surfaces.

2.1.2 Surface charge, surface potential and zeta potential

Surface charge refers to the distribution of electrical charges on a surface due to ions, protonation or deprotonation. Surface charge density is commonly measured in coulombs per square meter and describes the charge distribution on the surface.

Surface potential is the electric potential at the surface of a material, which is influenced by the surface charge and the surrounding medium. Surface potential is a more application-oriented definition in physics and electrochemistry. It directly relates how materials behave in practical scenarios, such as in chemical reactions at surfaces.

The relation of surface charge and surface potential is derived from the Gouy-Chapman theory and described by the Grahame equation (eq. 3):

$$\sigma = \sqrt{8c_0\varepsilon\varepsilon_0 k_B T} \cdot sinh\left(\frac{e\psi_0}{2k_B T}\right) \quad \text{(eq. 3)}$$

, where σ is the surface charge density in C/m^2; ε is the dielectric constant of the medium; ε_0 is the constant of permittivity of free space, approx. $8.854 \cdot 10^{-12}$ F/m; c_0 is the bulk ion concentration in mol/m^3; k_B is the Boltzmann constant, approx. $1.381 \cdot 10^{-23}$ J/K; T is the temperature in K; e is the elementary charge constant, approx. $1.602 \cdot 10^{-19}$ C; and ψ_0 is the surface potential in V.

At low potentials, the Grahame equation is shortened to eq. 4, where abbreviations are as above, with addition of the Debye length (λ_D):

$$\sigma = \sqrt{8c_0\varepsilon\varepsilon_0 k_B T} \cdot \frac{e\psi_0}{2k_B T} = \frac{\varepsilon\varepsilon_0\psi_0}{\lambda_D} \quad \text{(eq. 4)}$$

In the concept of electric double layer, the stern layer is in direct proximity with the surface and the slipping plane is a certain distance away from the surface. Whereas surface potential is the electric potential at the surface, zeta potential (ζ potential) is the electric potential at the slipping plane. The direct measurements of surface potentials are challenging and require precise control and measurements of the surfaces. Zeta potential is easier to measure experimentally using techniques such as electrophoretic light scattering and serves as a practical proxy for the surface potential.

The relationship between zeta potential and surface potential is complex and depends on the ionic strength of the solution and the distance from the surface to the slipping plane. A commonly used approximation in the context of the Debye-Hückel theory for low ionic strengths can be summarized as (eq. 5):

$$\zeta \approx \psi_0 \exp(-\kappa d) \qquad \text{(eq. 5)}$$

, where ζ is the zeta potential; ψ_0 is the surface potential; κ is the inverse Debye length, which depends on the ionic strength of the solution; and d is the distance from the surface to the slipping plane.

Therefore, zeta potential is directly related to surface potential and surface charge, making it relevant for colloidal chemistry and electrokinetics. One advantage is that it can be relatively easily measured on complicated surfaces, such as those that are not perfectly planar, rough or undefined.

2.1.3 Surface roughness

Surface roughness is the texture of a surface, characterized by the presence of peaks and valleys. It impacts friction, adhesion and wettability. Nano-scaled Surface roughness can be calculated from measured topographic imaging by atomic force microscopy (AFM). There are different mathematical definitions of roughness, with variation in emphasis on certain features. The most common definitions of surface roughness are:

$$R_a = \frac{1}{MN} \sum_{k=0}^{M-1} \sum_{j=0}^{N-1} |z(x_k, y_i)| \qquad \text{(eq. 6)}$$

Average Roughness R_a is calculated by eq. 6 on topographic images (e.g., obtained by AFM). Here R_a is average roughness; M, N are length and width of the image; x, y are lateral coordinates and z is the vertical coordinate [DIN 4768, ASME B46.1].

$$R_q = \sqrt{\frac{1}{MN}\sum_{k=0}^{M-1}\sum_{j=0}^{N-1}[(z(x_k, y_i)]^2} \quad \text{(eq. 7)}$$

Root mean squared Roughness R_q is calculated by eq. 7 on topographic images. Here R_q is root mean squared roughness; M, N are length and width of image; x, y are lateral coordinates and z is the vertical coordinate [ISO 4287/1 ASME B46.1].

$$R_t = z_{max} - z_{min} \quad \text{(eq. 8)}$$

Peak-to-valley Roughness R_t is calculated by eq. 8. Here R_t is the Peak-to-Valley roughness, z_{max} is the highest pixel and z_{min} is the lowest pixel [ASME B46.1].

2.1.4 Surface elasticity

Surface elasticity refers to the ability of a surface or interface to resist deformation when subjected to mechanical stresses. It is a measure of how surface tension changes with deformation, reflecting the elastic properties of the surface layer. The surface elasticity can affect the surface energy of a material. When a surface is elastic, it can deform in response to the adsorption of molecules, particles, proteins or biological cells, which can increase or decrease the surface energy depending on the nature of the interaction. A deformation of the surface due to elasticity can alter the number and nature of adsorption sites, which changes the adsorption capacity of the surface. The kinetics of surface reactions, including adsorption and desorption, are influenced by elasticity because it affects the activation energy needed for these processes [Butt & Kappl 2018, Vogl *et al.* 2021].

For bulk materials with ordered fiber networks or surfaces, the direction of applied stress significantly influences the resulting strain, which is described by different models. The two primary directions stress can be applied to a surface are along the surface (horizontal) and orthogonal to the surface (vertical). Young's modulus describes the elasticity under vertical stress, while the shear modulus pertains to horizontal stress. Figure 2.1 illustrates Young's modulus and shear modulus along with their corresponding definitions.

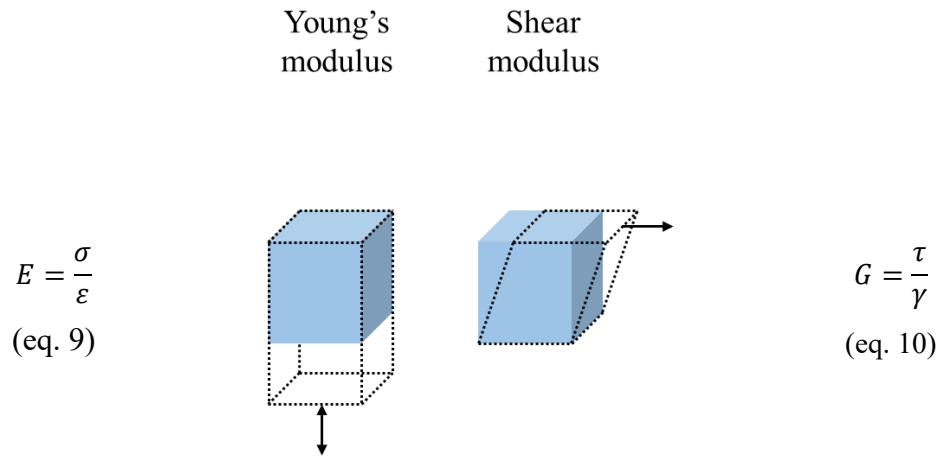

Fig. 2.1. Elasticity under vertical elongation or compression and elasticity under shear strain. The Young's modulus (E) is the relationship between compressive stress (σ) and axial strain (ε). The shear stress (G) is defined as the ratio of shear stress (τ) to the shear strain (γ).

The relationship between Young's modulus (eq. 9) and shear modulus (eq. 10) can be determined using the Poisson's ratio (υ), a material constant that describes volumetric changes under mechanical stress (eq. 11).

$$G = \frac{E}{[2(1+\upsilon)]} \qquad \text{(eq. 11)}$$

Unifying the horizontally and vertically acting elasticities is not advantageous due to their potentially differing effects on adsorption kinetics. In addition, the Poisson's ratio can be affected by the depth of an indentation, especially in nanoindentation tests. The depth of indentation influences the measurement of mechanical properties, including the Poisson's ratio, due to factors like material heterogeneity and surface effects [Hu & Hassan 2019].

2.1.5 Chemical composition

The chemical composition of a surface determines its reactivity and interaction with other substances. It includes the elements and compounds present on the surface [Butt & Kappl 2018]. Some important examples are:

- Hydroxyl Groups (-OH) – the hydroxyl group is polar and can form hydrogen bonds and makes the molecule more reactive towards nucleophiles and electrophiles.
- Carbonyl Group (C=O) – e.g., aldehydes and ketones are highly polar making the carbon atom electrophilic. This makes aldehydes and ketones reactive towards nucleophiles, leading to addition reactions.
- Carboxyl Group (-COOH) – e.g., carboxylic acids. The carboxyl group is acidic and can donate a proton (H+), making carboxylic acids reactive in acid-base reactions. It also participates in esterification and amidation reactions.
- Amino Group (-NH2) – e.g., amines. The amino group is basic and can accept a proton, making amines reactive in acid-base reactions. It also makes the molecule nucleophilic, allowing it to participate in substitution and addition reactions.
- Halogen Group (-X, where X = F, Cl, Br, I) – e.g., alkyl halides. Halogens are electronegative and make the carbon atom they are attached to electrophilic. This makes alkyl halides reactive towards nucleophiles, leading to substitution and elimination reactions.

2.2 Cellular recognition of biomaterial surfaces

Cells can not directly interact with biomaterial surfaces. Membrane-located cellular receptor proteins are only able to recognize the body's own biologically active proteins that adsorb to material surfaces prior to cell interaction.

Cellular recognition of material surfaces is a complex, multi-faceted process. The initial event is the adsorption of proteins from the blood serum, which attach to specific properties on surface to self-activate and change their conformation. Adsorbed active blood serum proteins can be bound by proteins from the extra cellular matrix (ECM) of cells, which transfer signals to cellular receptors. Thus, cells do not directly interact with biomaterial surfaces, but cross-talk by extracellular matrix with blood serum proteins that adsorbed beforehand. The type, surface density and conformation of adsorbed serum proteins present information about physical, chemical and biological properties of the surface.

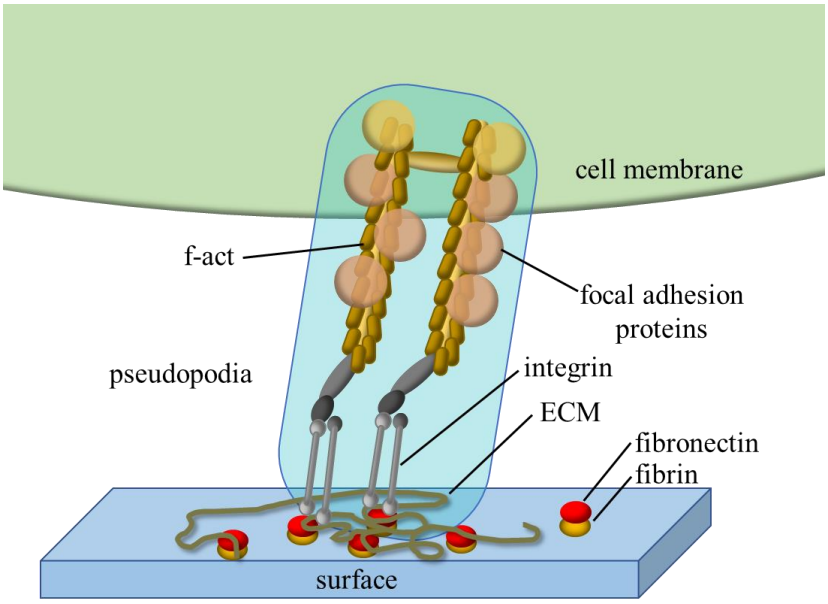

Fig. 2.2. Scheme of cellular recognition of surfaces. Blood serum protein fibronectin adsorbs on specific spots on the surface and is transformed to fibrin. Fibronectin (an ECM protein) interconnects fibrin binding spots with collagen fibers of the ECM. These complexes are recognized and bound by integrins (cellular receptors) and transduce surface information (e.g., integrin density, ECM stiffness) inside the cell. Redrawn according to [Vrana *et al.* 2016].

Figure 2.2 illustrates cellular interactions with a biomaterial surface. Initially, the blood serum protein fibrinogen adsorbs to the surface and is enzymatically converted into fibrin during the blood coagulation cascade. Fibrin binds to fibronectin, an ECM protein expressed by adhering cells. This interaction allows ECM collagen to bind and interact with cellular receptors

(integrins), facilitating cellular responses such as focal adhesion protein assembly, force transduction to the cytoskeleton via actin filaments, and subsequent cell behaviors such as adhesion, migration, and wound healing [Vaca *et al.* 2020, Weisel & Litvinov 2017].

2.2.1 Extracellular matrix

The extracellular matrix (ECM) plays a crucial role in cell-surface recognition. It consists of a network of extracellular macromolecules like collagen, enzymes, glycoproteins and hydroxyapatite. The ECM components show high biochemical, structural and functional diversity. The ECM components show affinity towards specific physical, biochemical and biomechanical cues on surfaces. Types, surface density and conformations of specific blood serum proteins in synergy with specific ECM proteins, that adsorbed on surface, act like a complementary key to specific cellular integrin receptors [Vrana *et al.* 2016].

Mechanical microenvironment surface properties such as stiffness, porosity and topography rearrange native ECM components to supramolecular structures like fibers and meshes, which either directly interact with cellular integrins or indirectly by presentation of nanocanonical growth factors to cells [Vrana *et al.* 2016].

2.2.2 Integrins and toll-like receptors

Cells interact with ECM proteins including collagen, fibronectin, laminin, vitronectin and others mainly through integrins and proteoglycan receptors. Integrins are transmembrane cell surface receptors that bind to different types of ECM components and play a key role in regulation of many cellular processes such as adhesion, proliferation and apoptosis [Petreaca & Martins-Green *et al.* 2007].

Integrins and toll-like receptors (TLR) are transmembrane proteins, which translate extracellular signals such as presence of biological signaling molecules or exposed serum/ECM proteins to biochemical intracellular signals. Both, integrins and TLR, directly contribute to Nf-κB pathway activation or deactivation with the subsequent expression of pro-inflammatory interleukins [Vrana *et al.* 2016].

Integrins can mediate inflammatory responses upon contact with biomaterials [Zaveri *et al.* 2014]. In [Nakashima *et al.* 1999] it was observed that integrin receptors CD11b/CD18 on human macrophages recognized titanium alloy particles and induced the expression of pro-

inflammatory cytokines TNFα and IL6. The interleukin expression only happened if LPS was previously adsorbed on the titanium alloy particles, indicating that these receptors only activate when in coordination with CD14 and TLR4 [Zaveri *et al.* 2014]. This observation highlights the co-regulation of certain integrins to induce intracellular pathways [Vrana *et al.* 2016].

Toll-like receptors (TLR) bind to a wide range of exogenous and endogenous structurally conserved molecules name pathogen-associated molecular patterns (PAMPs). Upon binding to ligands TLR initiate intracellular signaling through adaptor molecules MyD88 and TRIF, which can activate the transcription factor Nf-κB and other regulatory factors leading to the expression of pro-inflammatory cytokines.

2.3 Protein adsorption on biomaterial surfaces

There are over 200 different proteins in blood serum that may interact with a biomaterials surface [Wintermantel & Ha 2009]. The adsorbing serum proteins play a crucial part in initializing the innate immunity, including the blood coagulation cascade and the complement system.

Protein adsorption on material surfaces happens before any cell interaction takes place. Protein adsorption on solid surfaces is a complex event depending on biological, chemical environmental factors and physico-chemical properties of the surface. Surface properties such as chemical composition, contact angle, hydrophobicity, surface charge, and topography not only influence the types and density of adsorbing blood proteins but also facilitate the conversion of certain proteins from their deactivated form to their enzymatically active form [William *et al.* 2009]. The affinity of proteins for specific surfaces and the impact of surface properties on the conformation of adsorbing proteins are crucial for activating both the complement system and the coagulation cascade [Mitra 2020].

Proteins are mainly driven to surfaces by diffusion, thermal convection and flow. At the surface proteins tend to attach and lose their degree of freedom, which is often accompanied by conformation changes [Barbucci & Magnani 1994, Billsten *et al.* 1995, Fang & Szleifer 2001, Horbett & Brash 1995]. A prime example of proteins that auto-activate when adsorbing to surfaces are the blood clotting factors XII and VII, which experience several conformational transformations and eventually lead to the production of thrombin (an enzyme), which cleaves fibrinogen to produce fibrin. Auto-activation upon adsorption by conformation changes is also found in several types of collagens, platelets, nucleic acids and large poly-phosphate molecules [Renné *et al.* 2012].

Several factors at molecular level determine the protein adsorption behavior on surfaces. Protein properties like size, surface charge and rate of unfolding affect the speed of adsorption. The adsorption speed of smaller proteins with increased mobility is increased. Proteins near their isoelectric point feature more charged groups, which may interact stronger with the surface. Structurally instable proteins with an increased rate of folding/unfolding have higher contact rate with the surface and adsorb faster [Mitra 2020].

Several properties of solid surfaces particularly increase the protein adsorption. A higher surface area (e.g., by increased surface roughness) provides more contact possibilities with proteins. The surface composition, in particular amount, density and spacing of polar, hydrophobic regions as wells as negatively or positively charged regions affect the adsorption speed, adsorption strength and potentially conformational changes of proteins. Heterogeneity of functional groups on surfaces enables certain proteins with mixed regions to adsorb that usually would not be able to adsorb on homogenous surfaces. Figure 2.3 illustrates a protein with several functional regions adsorbing on a heterogenous surface. The protein interacts with the surface by ionic, hydrophobic or charge transfer processes depending on the character of the surface and the structure and surface nature of the protein molecule.

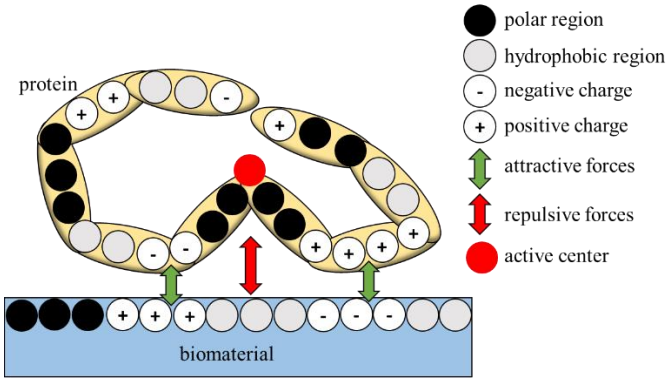

Fig. 2.3. Scheme of an adsorbing protein that interacts physico-chemically with a complementary heterogeneous surface through polar, hydrophobic, or charged regions. Redrawn according to [Mitra 2020].

The majority of soluble proteins do not possess a rigid structure and can flex, coil, bent and fold. The conformation in solution is held in the lowest state of free energy, which is regarded as the native state conformation. Adsorbed proteins continue undergoing conformational changes to reach an energetically favorable state with formation of new hydrogen bonds, van der Waals or electrostatic interactions with the surface. Exposed binding sites may enable biological characteristics that could be enzymatic, growth factors, signaling molecules or hormones. These conformational changes can be influenced by chemical factors (such as pH-value), biological

factors (proteins and enzymes in proximity) and surface properties of the substrate [Han *et al.* 2023]. One such example is serum albumin in cell culture medium, which can expose new epitopes upon adsorption, potentially affecting biocompatibility and triggering the immune response [Han *et al.* 2023, Matsarskaia *et al.* 2020]. Figure 2.4 illustrates the conformational change of an adsorbing protein by interaction with physico-chemical surface properties. In figure 2.5 a protein conformation in solution is stabilized by a chaperone protein. Upon adsorption the synergistic binding site on the serum protein binds to the material surfaces and displaces the chaperone, which leads to conformational change and exposure of an active center [Schmidt *et al.* 2009].

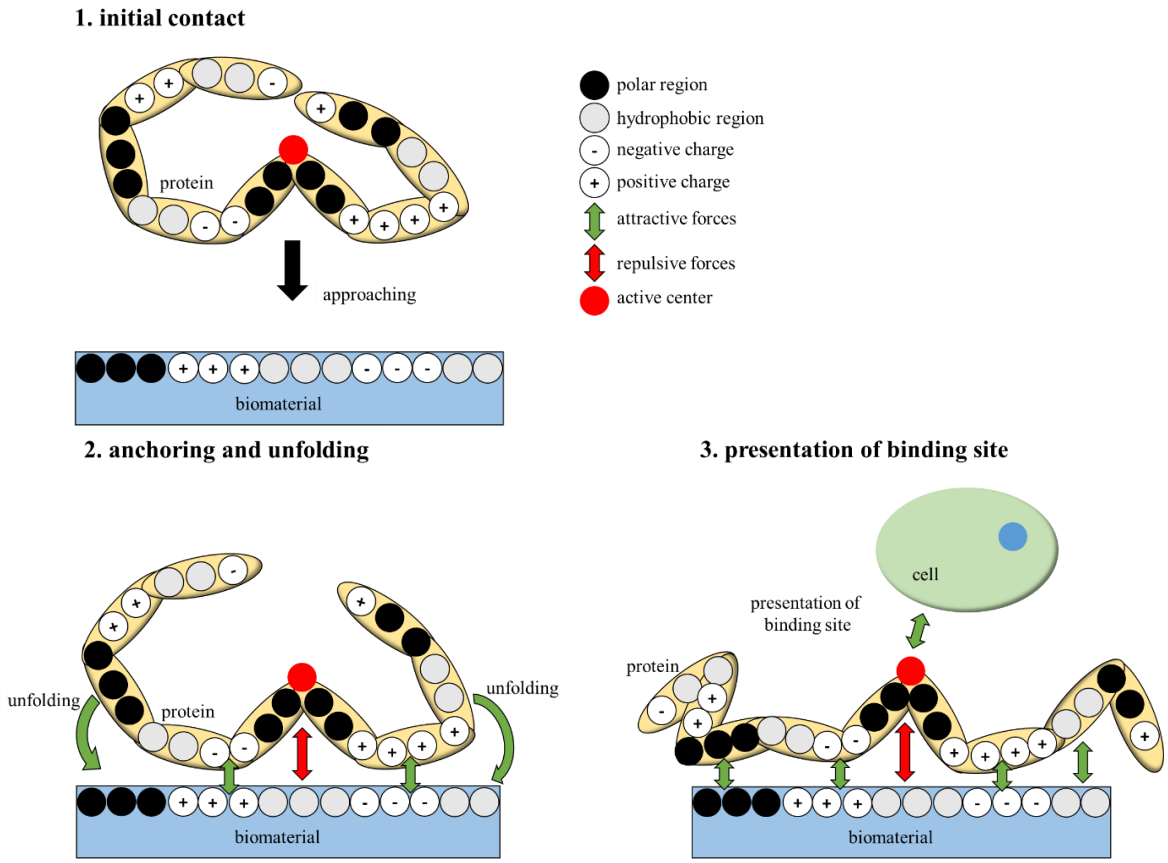

Fig. 2.4. Scheme of auto-activation of conformational change of a serum protein upon adsorbing on biomaterial surfaces. (1) The initial contact is directed by physical diffusion and leads to physico-chemical adsorption of complementary regions (polar, unpolar, negatively or positively charged) between protein and surface (2). An adequate surface leads to unfolding of the anchored protein, which may lead to exposure of binding sites (active center), which can be recognized by other proteins, enzymes or cells (3).

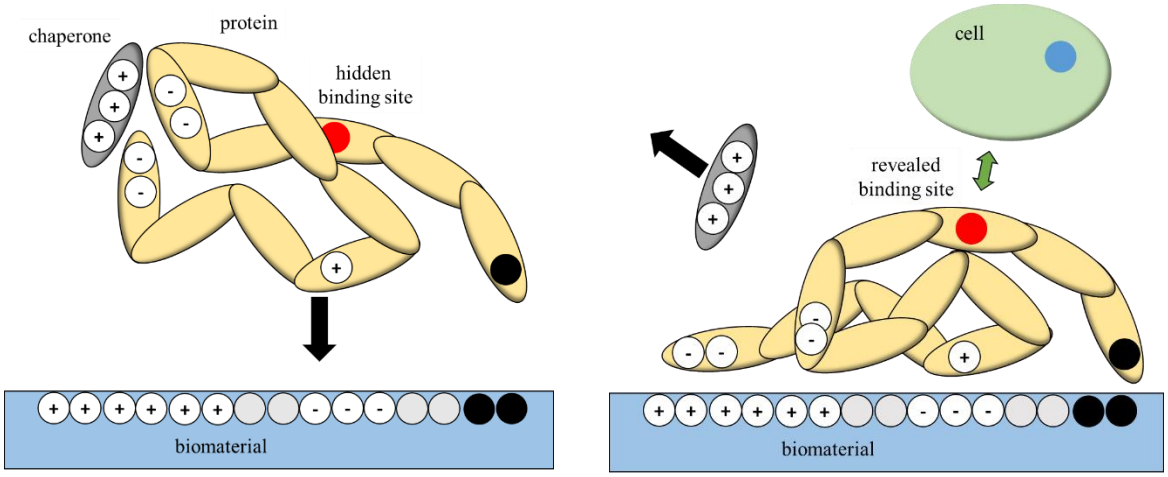

Fig. 2.5. Scheme of auto-activation of conformational change of a chaperon-bound serum protein upon adsorbing on biomaterial surfaces. The chaperone protein stabilizes protein conformation in solution to inhibit function and false activation. Upon adsorption the synergistic binding site on the serum protein bind to the surface, releasing the chaperone by competitive adsorption. The release of the chaperone leads to unfolding of the serum protein and presentation of an active binding site/ active center. Redrawn according to [Schmidt *et al.* 2009].

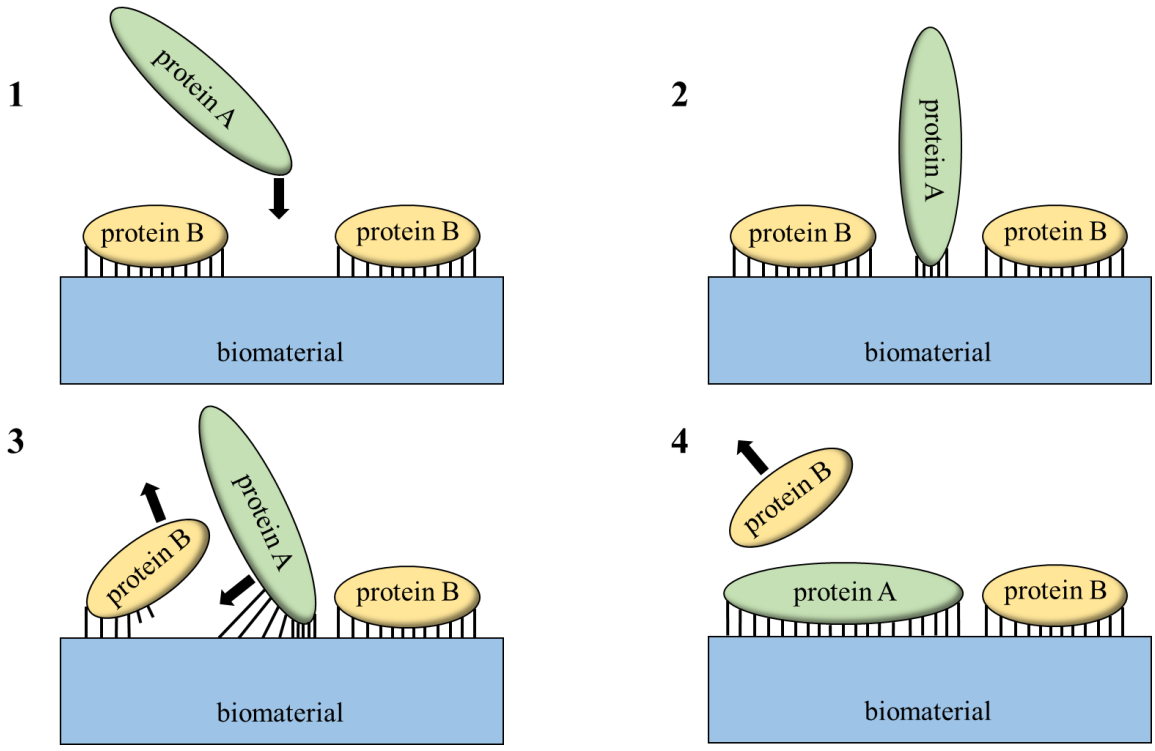

Fig. 2.6. Schematic representation of the Vroman effect: Lower molecular weight proteins (B) in higher concentrations are the first to adsorb onto surfaces. Larger, slower proteins (A) arrive later and, due to their higher affinity for the surface, displace the smaller proteins (B). Redrawn according to [Mitra 2020].

Upon adsorption to material surfaces some proteins denature to expose binding sites that can be recognized by several types of integrins (e.g., Mac-1, CD11b/CD18) and RGD binding integrins. Surface-adsorbed proteins of blood coagulation cascade include kininogen, fibrinogen, factor X, and complement component C3b. Simultaneously, non-specific adsorption of Ig and C3 components of the complement launch classical and alternative complement pathways [Vrana *et al.* 2016].

The presence of multiple interacting proteins adds to the complexity of protein adsorption. At all times a competitive adsorption is present between different species of proteins with varying concentrations, sizes, mobilities and compositions. A well accepted principle of adsorption of multiple proteins is described by the Vroman effect [Vroman *et al.* 1980]. Smaller protein species in higher concentrations adsorb first and are displaced by larger proteins with higher binding forces over time. The Vroman effect is illustrated in figure 2.6.

2.3.1 Thermodynamics of protein adsorption

Protein adsorption behavior can be described by Gibbs' and Langmuir models.

The fundamental principle of Gibbs free energy is applicable to determine the spontaneous process of general protein adsorption on surfaces.

$$\Delta G_{ads}^{0} = \Delta H_{ads} - T\Delta S_{ads} < 0 \qquad \text{(eq. 12)}$$

Gibbs free energy change (ΔG_{ads}^{0}) must be negative in order to achieve spontaneous adsorption. Although a small increase of enthalpy (ΔH_{ads}) is generated during adsorption, the high increase of entropy (ΔS_{ads}) shifts change of the free energy in the negative, due to release of a vast number of water molecules in compensation for one adsorbing protein. Thus, if protein adsorption happens, the event is always spontaneous and, without active intervention, it is viewed as almost irreversible [Dee *et al.* 2002, Kubiak *et al.* 2015, Mitra 2020].

A more complex Gibbs energy depiction by [Vogler 2012] takes into consideration the free energy gains due to hydrophobic effects working on the protein molecules, the free energy cost of displacing the vicinal water or surface dehydration and the free energy gains of protein-protein and protein-surface interactions [Vogler 2012, Mitra 2020].

The steady state can be described by three component free energy expression [Vogler 2012]:

$$\Delta G^0_{ads} = \Delta G^0_{hydrophobic} + \Delta G^0_{dehydration} + \Delta G^0_{interaction} \quad \text{(eq. 13)}$$

The hydrophobic effect ($\Delta G^0_{hydrophobic}$) contributes to energy gain by expelling protein molecules from solution and recovering hydrogen bonds between water molecules and proteins. The dehydration effect ($\Delta G^0_{dehydration}$) releases water molecules from interfaces at the material surface and the protein surface, increasing the entropy and costing the free energy. Finally, the interaction effect ($\Delta G^0_{interaction}$) contributes to energy gains by the ability of protein to connect to the surface or connect to previously adsorbed proteins forming a multilayer. This effect depends on protein properties like concentration, size, functional groups and the ability to form multilayers as well as adsorbent surface properties like surface area, surface energy and complementary functional groups.

The interaction of multiple proteins with varying mobility and surface affinity was described by the Vroman effect. Multiple protein mixtures include proteins with higher and lower affinity towards surfaces and different adsorption behavior and kinetics.

The hydrophobic and dehydration effects are approximately constant for all blood proteins and their mixtures, including serum and plasma protein, per mass of protein. The interaction effect is protein specific and surface specific and as such governs the adsorption of specific proteins on certain surfaces. For protein adsorption to occur, the free energy gains by hydrophobic effect and interaction effect must exceed the energetic cost of moving water out of the interphase (hydrophobic effect) by adsorbing protein. In multi protein solutions the interaction effect governs the type of adsorbing proteins and the occurrence of protein displacement by other adsorbing proteins (Vroman effect).

In general, the protein adsorption can be described by the Langmuir isotherm. Initially the surface is empty and the proteins adsorb in quick succession. The steady loading of proteins on the surface occupies the space and adsorption speed is decreased and eventually haltered. However, deviations from the Langmuir model occur by conformational changes of proteins upon adsorption (spreading, reorientation), the occurrence of multilayers and protein interactions like competitive adsorption, especially in multi protein solutions.

2.3.2 Surface energy and role of water

Surface energy directly affects biological responses at interfacial events like complement activation, blood coagulation and cell adhesion. In theory, surface energy controls water structure at close proximity to the interface, which is associated with reactivity of biological responses with hydrogen bridges [Bair *et al.* 1969]. At molecular level, the terms hydrophobicity and hydrophilicity describe the nature of long-range forces (van der Waals forces, electrostatic interactions) experienced by the water molecules close to the interface. Hydrophilic surfaces attract water molecules and increase water interfacial tension and the density of the water structure close to the interface. The water in the water structure near hydrophilic surfaces have more occupied hydrogen bridges and a changed chemical reactivity (chemical potential) compared to bulk water. Whereas, hydrophobic surfaces result in less-dense network of water with more open hydrogen bridges [Lee *et al.* 1984, Mitra 2020, Vogler 1998]. The reactivity of interfacial structure of water plays and important role in protein adsorption and protein conformation changes [Andrade & Hlady 1987, Lee *et al.* 1984, Vogler 1998].

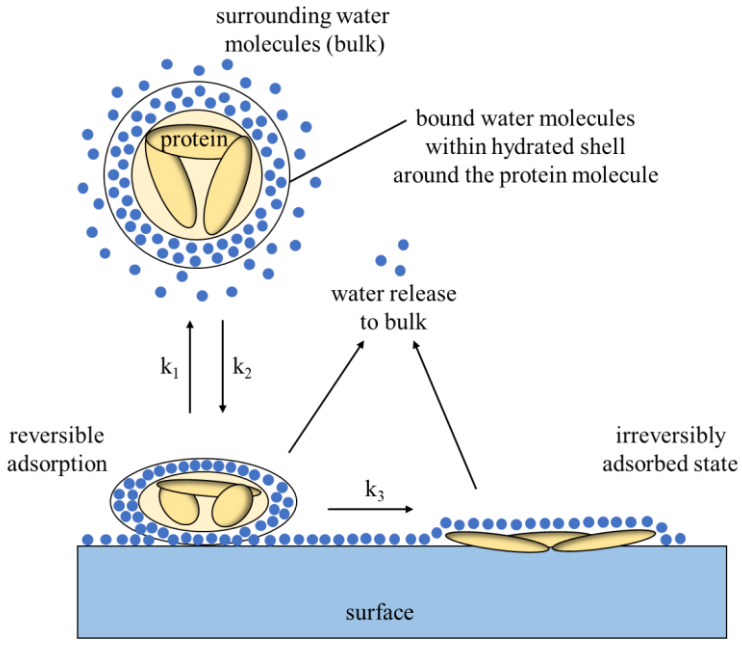

Fig. 2.7. Scheme of a protein adsorption on a solid surface. Water molecules in water structures around the protein and on the surface of the substrate are relatively denser compared to bulk water. Upon adsorption the water shells are released and the protein irreversibly adsorbs to the surface. Redrawn according to [Mitra 2020].

Water molecules are bound around proteins in aqueous media, contributing to the tertiary, native state of conformation. Charged and hydrophilic functional groups on proteins lead to formation of multilayered hydrated shells [Chattoraj & Mitra 1977]. As proteins approach surfaces, water molecules on surface and hydrated shells of the proteins are displaced by protein-surface bonds,

which contributes to increase of entropy. Figure 2.7 illustrates a protein with a stabilized structure by a hydrated shell adsorbing to a surface.

2.4 Cell adhesion on implant surfaces

The only way to stop ongoing inflammatory responses on implant materials without the use of medication is real integration of the foreign material into the host tissue. Host cell adhesion an optimal surface would enable the host to 'accept' the alien material and enable full wound healing. The adhesion of cells governs the health state of the host tissue and is mandatory for real integration of subcutaneous implants. One possibility to bypass this condition is the use of a bioresorbable material that after serving its purpose resorbs and is replaced by endogenous (body's own) tissue. However, many types of implants are designed to stay fully functional for decades of the patient's lifetime. For example, pacemakers must not be covered by fibrotic tissue to ensure their functionality.

After the initial adsorption of blood serum proteins on the biomaterial surface, surrounding cells start approaching (migrating towards) and sensing the biomaterial surface via ECM to determine the substrate compatibility for adhesion. In order to do this, cells utilize transmembrane receptors that have biochemical affinity for specific proteins (e.g., RGD sequence). Important parameters for determining substrate compatibility are type of proteins (integrin binding), density of proteins (integrin ligand spacing) and mechanical properties of the underlying substrate. For sensing of mechanical properties, the receptors connect with the cytoskeleton and are able to 'pull' on the material surface. Other surface parameters such as roughness, surface charge and surface energy may change the type or conformation of adsorbing proteins, also the presentation and the accessibility of the proteins for cellular sensing. The cell receptors not only are involved in cell adhesion, migration and proliferation but also regulate cellular behavior such as gene expression, differentiation, angiogenesis, tissue healing and consequently the integration of the biomaterial [Degasne *et al.* 1999, Karimi *et al.* 2018].

Adhesion formation, maturation and disassembly are continuously driven by a balance of actin polymerization and actomyosin contraction. These processes are dependent on contractile nature of cell type, the composition and the mechanical properties of ECM substrate such as compliance, dimensionality and fiber orientation [Geiger *et al.* 2009, Pelham & Wang 1997, Ridley *et al.* 2003, Vicente-Manzanares *et al.* 2009].

Cells of the myeloid linage such as neutrophils and macrophages show small dynamic adhesion (nascent adhesion) to enable rapid movement on ECM substrates, whereas contractile cells such as fibroblasts, endothelial cells and smooth muscle cells form stable adhesions (focal adhesion).

Cell adhesion to biomaterials is influenced by proteins that adsorb onto their surfaces. Surfaces with varying properties facilitate differential binding of cellular integrins to the adsorbed protein layer [Keselowsky *et al.* 2003 & 2005, Lan *et al.* 2005, Lee *et al.* 2006]. These material-dependent variations in cell adhesion and cytoskeletal rearrangement are associated with differences in the phosphorylation of FAK and ERK [Allen *et al.* 2006, Garcia & Boettiger 1999], as well as the recruitment of talin, α-actinin, and paxillin [Keselowsky *et al.* 2004]. This suggests that variations in downstream integrin signaling contribute to morphological differences observed in adherent cells on material surfaces with different surface properties.

2.4.1 Protein adsorption and cell adhesion

In contrast to unspecific hydrogen bonding, electrostatic, polar and hydrophobic binding of proteins on surfaces, the prevalent interaction between cells and surface-adsorbed proteins is based on receptor-mediated communication. The extracellular matrix (ECM) acts as an extension of cellular sensing and a mediator between cells and serum proteins. After initial coverage of material surfaces with blood serum proteins, the next instance is the binding of specific extracellular matrix proteins to the serum protein covered surfaces.
Blood serum proteins, such as albumins, globulins, and fibrinogen, are primarily produced and released by the liver into the bloodstream, or in *in-vitro* experiments are added via cell culture media. In contrast, ECM molecules like fibronectin, vitronectin, laminin, and collagen are locally expressed by adhering cells and are specifically tailored to the needs of the tissue or organs.

The adhesion process is driven by recognition and interaction of cellular receptors like integrins and toll-like receptors with adsorbed ECM proteins. These receptors are transmembrane proteins with the function to relate extracellular signals to intracellular biochemical signaling affecting a number of biochemical pathways and transduction of forces to the exoskeleton.
The receptors are distributed on the cell membrane with a specific density and spacing between them. For optimal recognition of surfaces the corresponding ligand density (e.g. fibronectin) on the surfaces materials must exceed the density of receptors on the cell membrane. The dependence of cell adhesion on ligand density on surfaces was measured and described in

[Selhuber-Unkel *et al.* 2010]. Figure 2.8 illustrates an adhering cell on surfaces with varying ligand density on surfaces. Surfaces which enable high ligand density (spacing ≤ 50 nm) leads to strong adhesion and spreading of cells, whereas surfaces with few possible contact points lead to weak adhesion and hindered cellular spread.

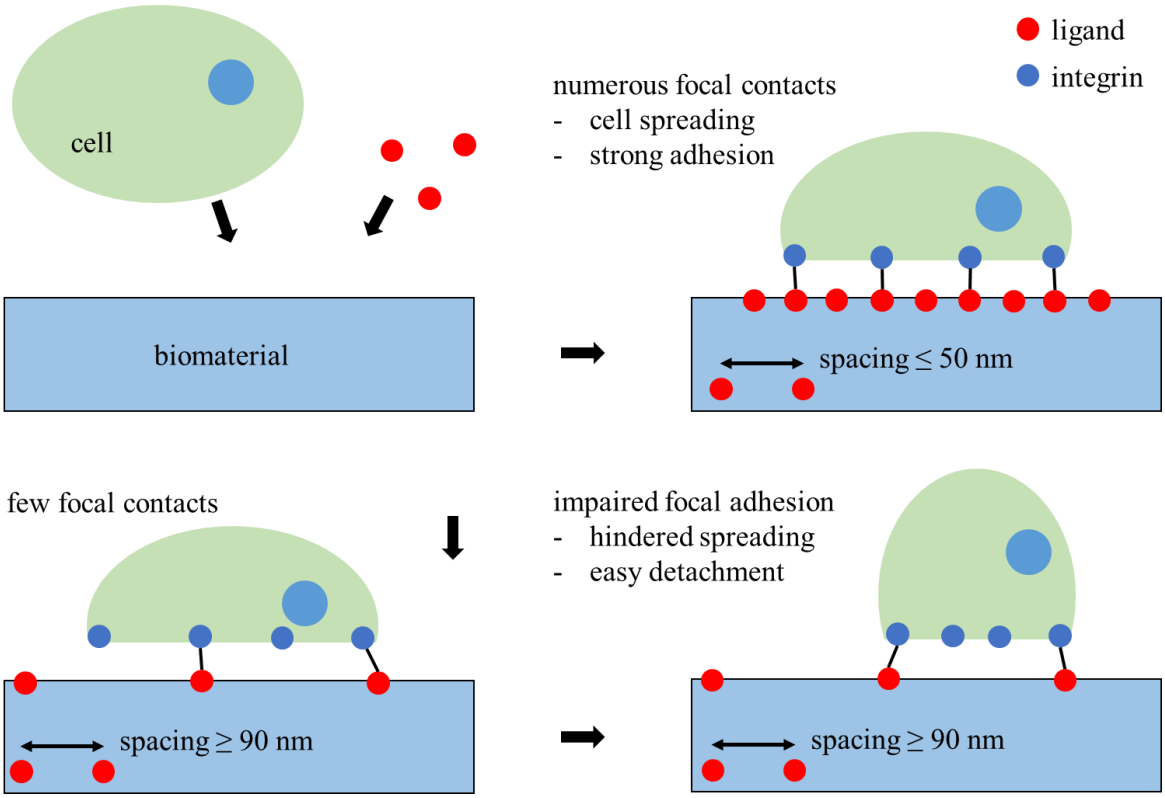

Fig. 2.8. Effect of spacing of fibronectin on material surfaces on the adhesion behavior of cells. According to [Selhuber-Unkel *et al.* 2010], a certain density (spacing ≤ 50 nm) of surface adsorbed ligands (e.g., fibronectin) is necessary to reach strong cell adhesion and cell spreading. Fewer contact spots (spacing ≥ 90 nm) lead to easy detachment, impaired focal adhesion and spreading.

Surface properties such as electrostatic, polar and hydrophobic regions directly affect the types and surface densities of adsorbing serum proteins, which in turn enable further adsorption of ECM proteins such as fibronectin. Thus, finetuning these properties is a possible way to alter subsequent cellular behavior such as adhesion or activation of intracellular pathways.

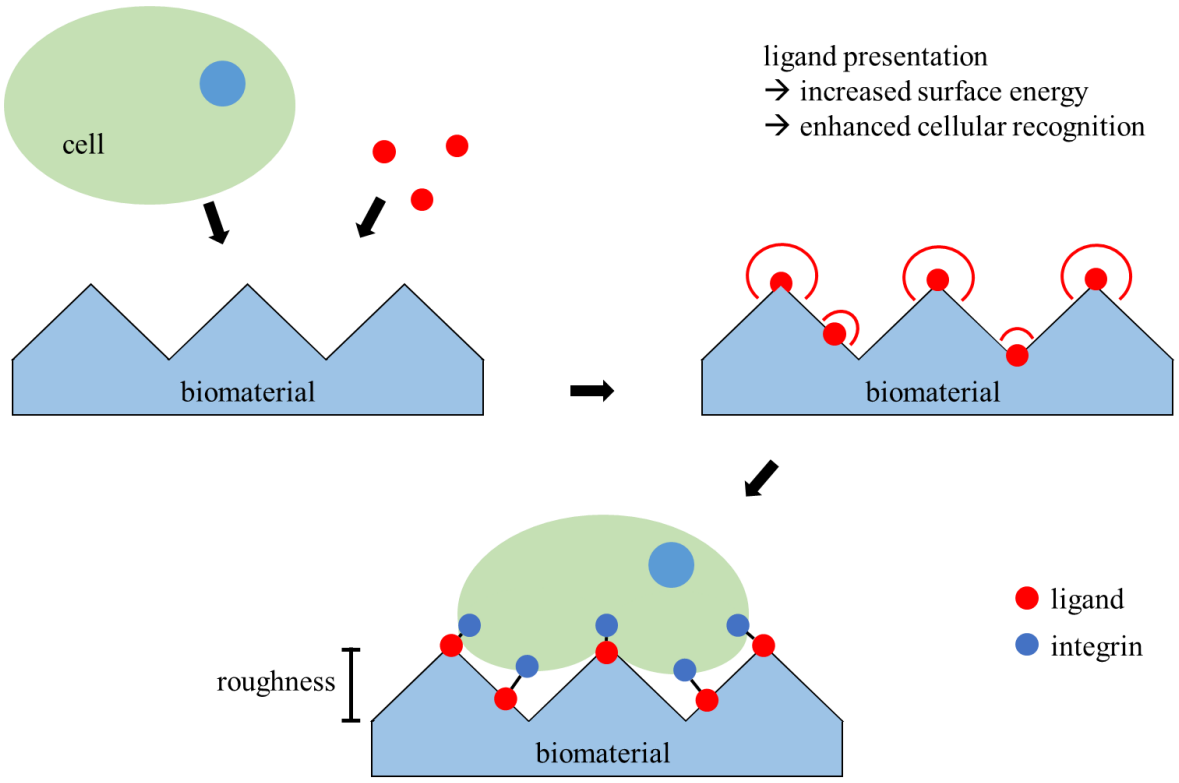

Fig. 2.9. Effect of surface roughness on ligand surface energy and presentation. Compared to plain surfaces, increased roughness enhances the surface energy of ligands adsorbed on elevated topographic peaks, potentially leading to improved cellular recognition.

Surface roughness (or topography and porosity) is a crucial property for cellular recognition. Increased roughness enhances the surface area, enabling more proteins to adsorb onto it. Additionally, presenting ligands on topographically elevated areas increases the surface energy of these molecules at the molecular level, enhancing cellular recognition (illustrated in figure 2.9). The impact of surface roughness on cellular adhesion has been documented in numerous studies [Majhy *et al.* 2021, Olarte-Plata *et al.* 2020, and sources therein]. In the engineering of medical implants, surface roughness is widely recognized as a powerful tool to improve implant integration into tissue.

2.5 In-stent restenosis as prime example for cell-surface interactions

In-stent restenosis is one of the most prominent clinically relevant examples of cell-surface interactions. It occurs due to synergistic effects of tissue injury and inflammation caused by the stent (a foreign body) and the excessive growth of scar tissue (neointimal hyperplasia). This process can lead to the narrowing of the artery within the stent, potentially resulting in implant failure and the need for a second intervention [Istanbullu *et al.* 2021, Maleknia *et al.* 2020].

In this dissertation in-stent restenosis is focused as a prime example of cell-surface interactions.

Our hypothesis is that by fine-tuning implant material surface properties - such as hydrophobicity, surface energy, nano-roughness and nano-stiffness - it is possible to stimulate cellular mechanosensing and integrin/toll-like receptor recognition mechanisms to reduce the expression of pro-inflammatory interleukins and subsequently diminish inflammatory processes, potentially reducing the incidence of in-stent restenosis.

2.5.1 Stenosis and in-stent restenosis

Arterial stenosis is the narrowing or constriction of an artery due to buildup of atherosclerotic plaque. This condition can reduce or block blood flow leading to serious health issues. The reduced blood flow or blockage caused by stenosis can deprive tissues of oxygen and nutrients, leading to cell death and organ damage. Stenosis is one of the main causes of life-threatening conditions such as apoplectic strokes (ischemic strokes) and heart attacks (myocardial infarctions) [Indolfi *et al.* 2003].

The first introduced treatment of stenosis was balloon angioplasty. This procedure involves inflating a small balloon inside the narrowed artery to widen it and improve blood flow.

Restenosis is the re-narrowing of a blood vessel at the same site after it has been treated with balloon angioplasty. This process is based on the body's healing response, involving smooth muscle cell proliferation and negative remodeling. After balloon angioplasty the injury to the arterial wall triggers a healing response. Smooth muscle cells proliferate and migrate to the site of injury, contributing to neointimal hyperplasia (thickening of the arterial wall) [Cao *et al.* 2022, Curcio *et al.* 2011, Huynh & Heo 2021, Jaminon *et al.* 2019, Newby & Zaltsman 1999].

Over time, stenting (placing a small mesh tube inside the artery) has become a common adjunct to balloon angioplasty to help keep the artery open longer. The coronary stent implantation is

widely accepted to severely reduce the restenosis rate in comparison to balloon angioplasty [Indolfi *et al.* 2003].

The introduction of coronary stents has significantly reduced the restenosis rate compared to balloon angioplasty alone, however bare metal stents also showed a certain inherent risk of restenosis.

The in-stent restenosis (ISR) is the narrowing of the blood vessel within the confines of the stent [Mitra *et al.* 2006]. Histologically, in-stent restenosis is distinct from restenosis after balloon angioplasty and follows a different mechanism. Remodeling of the vessel wall does not occur, instead, the narrowing is primarily due to smooth muscle cell proliferation [Indolfi *et al.* 2003]. A specific trait of in-stent restenosis is the mandatory role of inflammation caused by the body's reaction to the presence of the foreign body inside the blood vessel [Maleknia *et al.* 2020, Mitra *et al.* 2006, Welt & Rogers 2002].

A major advancement in addressing in-stent restenosis was the introduction of drug-eluting stents (DES). DES release medication that inhibits smooth muscle proliferation, significantly reducing the incidence of in-stent restenosis compared to bare-metal stents (BMS).

However, DES have introduced new potential long-term complications such as in-stent thrombosis. Due to the release of cytostatic medication, the DES might not be covered by endothelial cells during the healing process. This incomplete endothelialization can lead to the formation of blood clots inside the stent. Although the risk of in-stent thrombosis (IST) is relatively low, this complication is serious and potentially life-threatening. Blood clots can abruptly occlude blood vessels and lead to strokes and heart attacks. The seriousness of in-stent thrombosis requires careful management and prevention strategies such as prolonged dual antiplatelet therapy [Koźlik *et al.* 2023, Kuramitsu *et al.* 2021, Navarese *et al.* 2014].

The enhancement of stent surface-cell interactions is a crucial area of research. By optimizing these interactions, the aim is to improve integration of both bare-metal stents (BMS) and drug-eluting stents (DES). This can help in reducing restenosis and minimizing long-term complications like in-stent thrombosis [Istanbullu & Akdogan 2022].

2.5.2 Mechanisms of in-stent restenosis

In the course of balloon angioplasty or stenting, the mature atherosclerotic plaque is crushed, and the entire artery is stretched by the inflation of the balloon under high pressure. The process begins with injury to the endothelial cells during the operation. This injury, along with the

presence of the stent, triggers the release of von Willebrand factors (VWF) from the stressed endothelial cells to recruit and activate platelets.

Platelets recognize immobilized VWF and start adhering to the vessel walls [Welt & Rogers 2002]. Platelets and fibrin actively deposit at the point of injury where the platelets activate and express adhesion molecules such as P-selectin on their cell walls [Costa & Simon 2005, Welt & Rogers 2002]. Circulating leukocytes, such as neutrophils and monocytes, recognize the signals from activated platelets via receptors like P-selectin glycoprotein ligand. The leukocytes then adhere to the vessel wall and begin to roll along it. This process is known as leukocyte rolling [Costa & Simon 2005, Welt & Rogers 2002].

Simultaneously, pro-inflammatory cytokines such as TNF-α, IL-1β, IL-6, and chemokines such as IL-8 are expressed and released by stressed and injured host cells at the site of injury. These chemoattractants are produced constantly and diffuse in all directions, causing a buildup of a concentration gradient with the highest concentration at the point of injury [Costa & Simon 2005, Welt & Rogers 2002].

The leukocytes, rolling along the vessel wall, transduce signals from both - adhesion receptors and chemokine receptors [McEver 2010]. Under the influence of chemokines, the leukocytes bind tightly to leukocyte integrin (Mac-1) class adhesion molecules via direct attachment to platelet receptors such as GPIbα and through crosslinking with fibrinogen to the GP IIb/IIIa receptors [Welt & Rogers 2002]. The increasing binding near the point of injury causes leukocytes to roll slower and eventually arrest, which is essential for migration through the vasculature into underlying tissues.

The interactions of leukocyte ligands with platelet selectins mediate tethering and rolling, and interactions of leukocyte integrins with chemokines mediate arrest and migration [McEver 2010]. As the leukocytes approach the site of injury, the increasing concentration of chemokines amplifies the activation of integrins, which leads to stronger adhesion and results in a firm attachment. A leukocyte stops rolling when the adhesive bond can withstand the force required to balance the maximal force and torque applied to the cell by the blood flow [McEver 2010].

Migration of leukocytes across the platelet-fibrin layer and diapedesis into the tissue is driven by chemical gradients of chemokines such as IL-8 released from host endothelial cells, smooth muscle cells, and resident macrophages [Costa & Simon 2005].

Typically, neutrophils are the first type of leukocyte responding and arriving at the point of injury, where they initiate the inflammation by releasing chemokines and attracting additional

immune cells such as monocytes. Transmigrated monocytes differentiate to macrophages and orchestrate further inflammatory responses.

The release of growth factors by mostly macrophages stimulates the smooth muscle cells to migrate from the media into the neointima. The resulting neointima consists of smooth muscle cells, extracellular matrix, and macrophages recruited over several weeks [Costa & Simon 2005].

Over a long period, the artery is remodeled by extra cellular matrix (ECM) protein degradation and resynthesis. This causes a shift to fewer cells and more ECM in the plaque. In mature restenotic plaque, the ECM is the major component and is composed of collagen subtypes and proteoglycans. In the final phase, the narrowed vessel is reendothelialized [Costa & Simon 2005].

2.5.3 Inflammation in in-stent restenosis

The recruitment and activation of leukocytes, including neutrophils, plays a crucial role in the inflammatory response leading to in-stent restenosis. The role of neutrophil-mediated oxidative burst in post-stent inflammatory process has been documented in [Inoue *et al.* 2008]. Several studies have shown early recruitment of neutrophils after vascular injury and the persistence of neutrophil products in the vessel wall [Jorgenson *et al.* 1988, Richardson *et al.* 1990]. The association between neutrophils and restenosis has been demonstrated in several clinical studies [Inoue *et al.* 2008, Neumann *et al.* 1996, and references therein].

2.5.4 Role of inflammatory signaling molecules IL-1ß, IL-6 and IL-8 in in-stent restenosis

The focus of this dissertation is set on the expression of IL-1ß, IL-6 and IL-8 by endothelial cells when activated with injury (by stimulation with tumor necrosis factor alpha) and stimulated by pressure with medial steel surface with specifically modified surface properties.

Cytokines and chemokines play a crucial role in the inflammatory responses associated with in-stent restenosis. In in-stent restenosis, messenger molecules such as cytokines Interleukin 1-ß and IL-6 and chemokines such as IL-8 are initially expressed by host cells of the blood vessel including endothelial cells, which are the first point of contact during stenting. The initial signaling of host cells leads to recruitment of immune cells such as neutrophils that heavily amplify the signaling by expressing similar messenger molecules in higher numbers.

The nuclear factor kappa-light-chain-enhancer of activated B cells (NF-κB) represents a family of transcription factors regulating aspects of innate and adaptive immune functions serving as

mediator of inflammatory responses [Sun 2017]. The NF-κB pathway regulates all aspects of inflammatory responses by mediating induction of various pro-inflammatory genes in innate immunity. It is the central pathway of activating the inflammasome by inducing expression of pro-inflammatory membrane proteins (e.g., selectins), cytokines (e.g., IL-1ß, IL-6) and chemokines (e.g., IL-8) in cells [Lawrence 2009, Sutterwala *et al.* 2014, Tak & Firestein 2001].

A plethora of messenger molecules are involved in the process. In this thesis the focus is set on two important pro-inflammatory interleukins, IL-1ß and IL-6, and a chemokine, IL-8. These interleukins have following roles and functions when expressed by endothelial cells during initial phases of in-stent restenosis:

Interleukin-1 beta (IL-1ß) is a highly potent pro-inflammatory cytokine that plays a pivotal role in early stages of the inflammatory response. Similar to tumor necrosis factor alpha (TNFα) it is expressed by endothelial cells during injury to alert and induce events in neighboring endothelial cells, which were not directly affected by injury. IL-1ß receptors on the endothelium induce the production of other pro-inflammatory cytokines like IL-6 to further amplify the inflammatory response [Dinarello 2005, Dinarello *et al.* 2012, Chan & Schroder 2020] and induce expression of tissue factors drastically increasing the adhesiveness of the endothelial cell surface for immune cells, which facilitates the recruitment of leukocytes to the site of injury [Bevilacqua *et al.* 1985, Turner *et al.* 2007].

Interleukin-6 (IL-6) is key mediator in the inflammatory response following stent implantation. IL-6 enhances the recruitment of leukocytes at the site of injury [Pyrillou *et al.* 2020], and in conjunction with growth factors promotes the proliferation and migration of vascular smooth muscle cells contributing to neointimal formation, which is the primary cause of in-stent restenosis [Maleknia *et al.* 2020].

Interleukins IL-1ß and IL-6 play a pivotal role in mediating systemic fever and the acute phase response. Both cytokines are responsible for stimulating acute phase protein synthesis and give rise to inflammatory cytokine production, as well as the production and activation of leukocytes like neutrophils and monocytes.

Interleukin-8 (IL-8) is a chemotactic factor with two primary functions. This chemokine induces chemotaxis (movement in response to a chemical stimulus) in leukocytes, causing them to migrate towards the site of injury. The second function is the stimulation of diapedesis (passage of cells through intact vessel walls) of leukocytes inside the tissue at the site of injury. In fact, IL-8 is one of the two most important chemotaxins for neutrophil diapedesis [Delves & Roitt *et al.* 1998].

The essential role of IL-8 in acute inflammation was demonstrated by [Harada *et al.* 1994]. Their study showed that the application of an anti-IL-8 antibody treatment prevented neutrophil-dependent tissue damage and neutrophil infiltration. This finding highlighted the causative role of IL-8 in acute inflammation by recruiting and activating neutrophils [Harada *et al.* 1994]. According to Harada, inhibiting IL-8 presents a promising target for therapeutic investigations in inflammatory diseases, particularly acute ones. Other experimental studies have demonstrated the specific importance of IL-8 and its receptors for restenosis. Antibody blockage of IL-8 [Rogers 1998] or its receptor (Mac-1) [Simon *et al.* 2000] significantly reduced the occurrence of neointimal thickening in animal studies [Inoue *et al.* 2003, Rogers *et al.* 1998, Simon *et al.* 2000].

2.6 Surface modifications of biomaterials

One effective approach to prevent adverse biological reactions while preserving the native physical properties of biomaterials is the modification of their surfaces to mimic tissue properties, thereby disguising the foreign material from the host tissues. Among various surface modifications, such as chemical (e.g., acidic polishing) or physical (e.g., electro polishing) methods [O'Brien & Carroll 2009], coating the substrate with a second material possessing specific surface properties is particularly suitable. This method can modify various surfaces without altering the fundamental mechanical properties, such as tensile strength or compressive strength, of the base materials.

Mechanical properties are the primary consideration when selecting a material for implantation. For instance, steel is often chosen for its stiffness and robustness in joint prostheses or for its spring effect in stents. However, the base material may encounter challenges during the integration process with host tissue. The interactions at the interface between tissue and material determine whether a rejection reaction will occur. To enhance biocompatibility, the surface of the base material can be modified using various methods, thereby altering its surface properties to suit the specific application [Wintermantel & Ha 2009].

The two main directions of surface modification are either the physical or chemical surface modification of the base material or the covering and masking of the base material by a second material with specific surface properties. The surface modifications change physical surface properties such as micro-, nano-roughness and surface stiffness, when compared to bulk

properties of the base material. Chemical surface modifications such as oxidation may change roughness and surface chemistry.

The type of surface modification employed is highly dependent on the application and intended purpose of the biomaterial. Common procedures for micro structuring of surfaces are silicon micro mechanics (etching processes, chemical vapor deposition, photolithography), LIGA procedure (lithography, electroplating, molding), laser micro material processing, micro machining and micro spark erosion (limited to conductive materials). Examples of applications for physical/chemical surface modifications are miniaturized instruments for endoscopic surgery, vascular prostheses (stents) and micro containers for cell cultures [Wintermantel & Ha 2009].

The deposition of a second material, or surface coating, can alter various surface properties, including roughness, surface stiffness, chemical functionality, and even biological functionality through the deposition of bioactive molecules. The functionality of the second-material coating can be maintained in thin layers at the micro- and nanoscale. Commercial coating techniques for biomaterials primarily utilize vacuum, plasma, and ionization principles for material deposition. Examples include hydroxyapatite coatings on dental implants using plasma spraying techniques and atmospheric plasma spraying of bioactive films based on calcium carbonate. Thin layer techniques include salinization and plasma-induced grafting [Wintermantel & Ha 2009].

2.7 Polyelectrolyte multilayers

Polyelectrolyte multilayers (PEMs) are a polymer-based surface modification, which enables the controlled alteration of several surface properties like surface charge, hydrophobicity, roughness and stiffness in nano range.

The basic principle of Polyelectrolyte Multilayers (PEM) thin-film production process is the alternating exposure of a charged substrate to solutions of positively and negatively charged polyelectrolytes (PE) as demonstrated by [Decher *et al.* 1992]. Each step of substrate exposure to PEs in solution leads to deposition of a self-assembled charged layer of PEs on the surface. The substrate surface charge is inverted by adsorption of PEs and enables the subsequent adsorption of the oppositely charge PEs. Bilayer (one positively and one negatively charged PE layer) deposition can be repeated till a layered complex with desired thickness and unique properties is formed [Schönhoff 2003].

Many PE combinations can be used for production of multilayers. The utilized PEs can be synthetic such as e.g., poly(ethylenimine), poly(styrene sulfonate) and poly(allyamine hydrochloride) or from natural origin such as e.g., hyaluronic acid and chitosan (figure 2.10).

Synthetic strong polyanion:

Poly(styrene sulfonate)

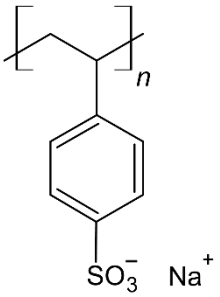

Synthetic weak polycation:

Poly(allylamine hydrochloride)

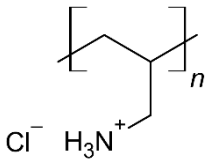

Natural weak polyanion:

Hyaluronic acid

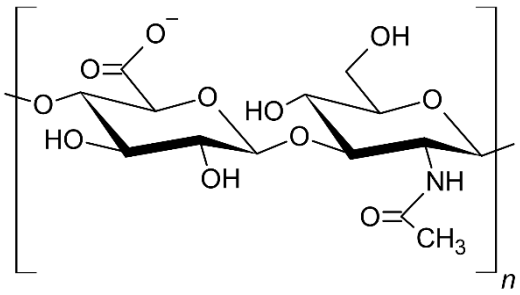

Natural weak polycation:

Chitosan

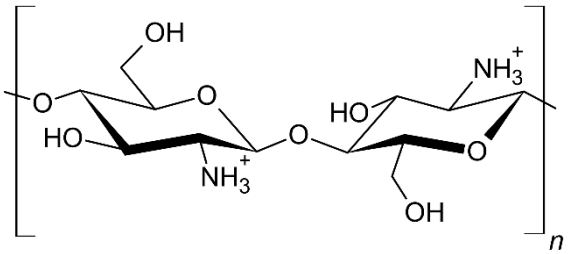

Fig. 2.10. Examples of polyelectrolytes suitable for polyelectrolyte multilayer formation. The synthetic polyelectrolytes poly(styrene sulfonate) and poly(allylamine hydrochloride) have sulfonic and amine based functional groups. The natural polysaccharides hyaluronic acid and chitosan feature carboxy acids and amino groups as functional groups. Drawn with ACD/ChemSketch.

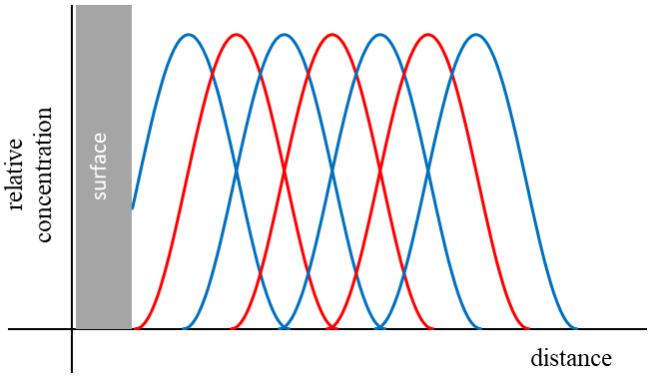

Fig. 2.11. Scheme of segment distribution in multilayers along the surface normal. Blue and red lines correspond to polyanions and polycations, respectively. Redrawn according to [Decher 1997].

The polyelectrolyte deposition solutions normally contain dissolved polyelectrolytes, counterions (electrolytes such as NaCl) and have a set pH-value. Main driving forces of the PE adsorption from solution on surfaces are electrostatic interactions, hydrophobic interactions between polymer segments, and entropic effects by release of counterions (electrolytes) from the surface.

The polyelectrolyte (PE) layers do not adsorb as isolated static blocks. Instead, PEs penetrate into the previously adsorbed multilayers, interconnecting with the earlier deposited PE layers, as illustrated in figure 2.11. This creates the possibility for deeper PE layers to interact with subsequently adsorbing molecules, such as proteins.

2.7.1 Electrostatic interactions in polyelectrolyte multilayers

In PEM multilayer formation the Coulomb's law helps explain the interactions between charged groups on different layers. The strength and nature of these interactions are fundamental to the formation and stability of multilayers. The Debye length determines the range over which electrostatic interactions between charged groups are significant. A shorter Debye length indicates stronger screening, meaning that the electrostatic interactions are more localized. The Bjerrum length helps determine the strength of interactions between charged groups on the same or different layers. If the distance between charges is less than the Bjerrum length, electrostatic interactions dominate over thermal motion.

The **Coulomb's law** describes the electrostatic force between two point charges. It states that the magnitude of the force (F) between two charges is directly proportional to the product of the charges (Q_1Q_2), multiplied by the Coulomb's constant (k), and inversely proportional to the square of the distance between them (r) (shown in eq. 14):

$$F = k\frac{Q_1Q_2}{r^2} \qquad \text{(eq. 14)}$$

In PEM formation, the Coulomb's law explains the attraction and repulsion forces between charged groups, driving the adsorption of layers.

The **Debye length** is a measure of a charge carrier's net electrostatic effect in solution and how far its electrostatic effect persists. The Debye length is a crucial parameter for electrolytes in solution. It represents the distance over which the electric potential decreases by a factor of (1/e)

due to the increasing electrical screening of charges within a spherical volume, known as the Debye sphere, whose radius is the Debye length. It was defined by [Debye *et al.* 1923] as:

$$l_D = \sqrt{\frac{\epsilon k_B T}{n e^2}} \quad \text{(eq. 15)}$$

, where l_D is the Debye length, ϵ is the permittivity of the medium, k_B is the Boltzmann constant, T is the absolute temperature, n is the number density of charge carriers and e is the elementary charge.

The distance over which mobile charge carriers (like ions in a solution) screen out electric fields. The Debye length describes how far the electrostatic effects of a charge can extend in a medium before being neutralized by other charges. In multilayer formation, the Debye length influences the thickness of the electrical double layer and extent of charge screening, affecting how layers interact.

The **Bjerrum length** is the distance at which the electrostatic interaction between two elementary charges is comparable in magnitude to the thermal energy scale. It essentially sets a scale for the strength of electrostatic interactions in a given medium. The electrostatic interaction strength between monovalent ions is described in [Bjerrum *et al.* 1959] by the equation

$$l_B = \frac{e^2}{4\pi\epsilon k_B T} \quad \text{(eq. 16)}$$

, where l_B is the Bjerrum length, e is the elementary charge, ϵ is the permittivity of the medium, k_B is the Boltzmann constant and T is the absolute temperature.

If the distance between two elementary charges is greater than the Bjerrum length (l_B), the electrostatics are weak and thermal energy predominates. Conversely, if the distance is less than the Bjerrum length (l_B) than electrostatics are stronger.

2.7.2 Polyelectrolytes in solutions at different electrolyte concentration

In PE solutions, like-charged functional groups on a molecule backbone repel each other, resulting in a more linear conformation of PE molecules. The addition of electrolytes (counter ions) to the deposition solution shields the charged groups and decreases the repulsion of like-charged groups. The concentration and type of electrolytes affect the strength of the shielding [Andreeva *et al.* 2016], leading to a decrease in Debye length (which is the length of interaction between two charged groups on one PE backbone). The reduced repulsion of the charged groups

allows PE molecules in solution to move more freely and adopt a more coiled conformation (as illustrated in figure 2.12).

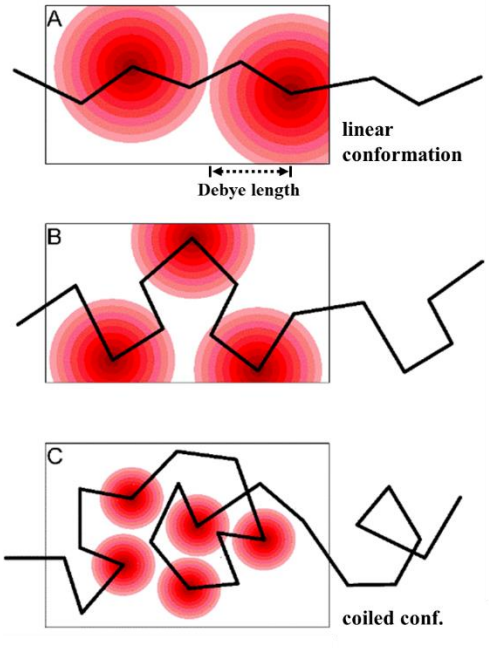

A: In the absence of added electrolytes, the Debye-Hückel interaction reduces the PE size (R) is given by

$$R \sim Na\sqrt[3]{\frac{f_B^2}{a}} \text{ (eq. 17)}$$

, where N the number of monomers; a the size of a monomer; f the fraction of charged monomers.

B & C: At very high ionic strength, the electrostatic interaction is short range and equivalent to an excluded volume interaction.
The corresponding excluded volume parameter (υ_{el}) is

$$\upsilon_{el} = 4\pi l_B \frac{f^2}{l_D} \text{ (eq. 18)}$$

, where f is the fraction of charged monomers; l_B the Bjerrum length and l_D the Debye length
[Decher & Schlenoff 2002].

Fig. 2.12. Scheme of polyelectrolyte conformation in deposition solutions with different electrolyte (counter ion) concentrations: (A) electrolyte-free, (B) low, and (C) high electrolyte concentration. By the decrease of effective repulsion between like-charged groups, the conformation of polyelectrolyte chains is changed from stretched and linear (A) to more coiled (B) and highly coiled (C) conformations. (A) In the absence of added electrolytes, the Debye-Hückel interaction reduces the standard Coulomb interaction. (B) As electrolytes are added, the chain is not fully elongated and bends. The persistence length is predicted to decrease with the electrolyte concentration by l_D^{-1} or l_D^{-2}, where l_D is the Debye screening length. (C) At even higher electrolyte concentrations, the PE chains eventually overlap and form blobs.

2.7.3 Polyelectrolytes at surfaces from deposition solution with different electrolyte concentration

Polyelectrolytes (PEs) in deposition solutions adsorb onto solid surfaces that carry an electrical charge opposite to that of the polymer. For uncharged surfaces, plasma treatment or the deposition of an adhesion agent, such as poly(ethylene imine), can be used to impart charges to the surface. When PEs adsorb onto the surface, they release electrolytes (counter ions) that were stabilizing their conformation in the solution.

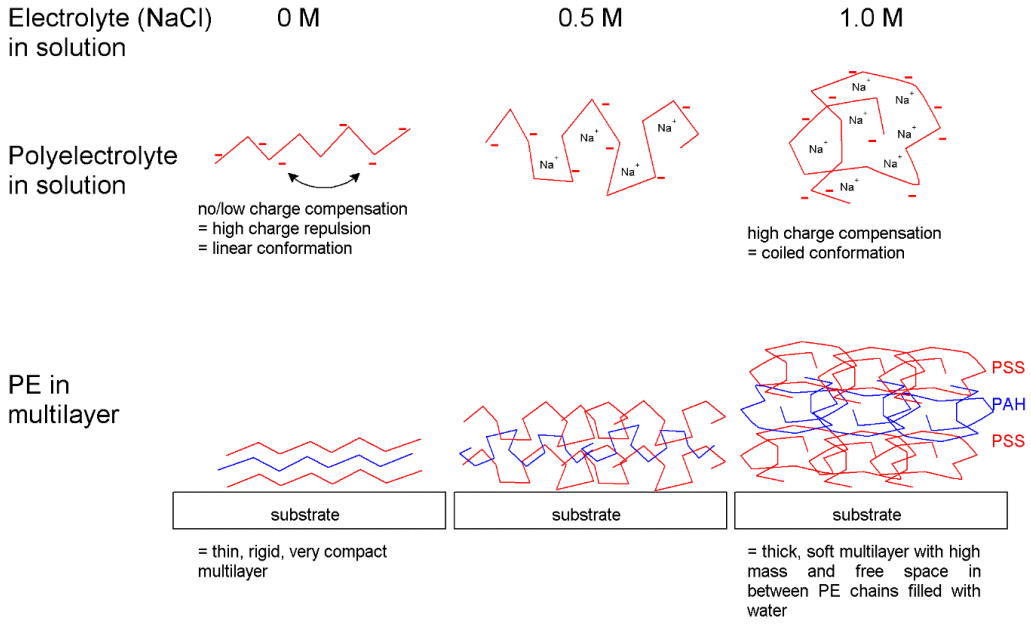

Fig. 2.13. Effect of electrolyte concentration in polyelectrolyte deposition solution on the conformation of adsorbed polyelectrolyte chains in multilayers. An increased concentration of electrolytes in the deposition solution leads to increased shielding of functional groups on polyelectrolytes and decreases the radius of gyration of the molecules in solution. Adsorbing polyelectrolytes partly retain the conformation changes and produce a multilayer with changed properties such as thickness and elasticity.

The electrolyte concentration in the PE deposition solution influences the conformation of the PEs that adsorb onto the surface. At very low electrolyte concentrations, PEs do not form large loops, and the thickness of the adsorbed layer is approximately the thickness of a single adsorbed chain [Decher & Schlenoff 2002]. At higher electrolyte concentrations, PEs adopt a more coiled conformation. Upon adsorption onto surfaces, PEs partially retain their conformation, resulting in polyelectrolyte multilayer coatings with varying properties such as thickness and elasticity (as shown in figure 2.13). The type and concentration of electrolytes used in the deposition solution are powerful tools for controlling the thickness and other properties of the layers over a wide range [Decher *et al.* 1992].

2.7.4 Excess charge in polyelectrolyte multilayers

Polyelectrolyte multilayers (PEMs) exhibit several important properties that make them highly versatile and useful in modifying surfaces. The thickness of PEMs can be precisely controlled by adjustment of layers during the layer-by-layer (LbL) deposition process and other factors such as electrolyte concentration and pH-value of deposition solutions. The surface charge of PEMs can be set to positive or negative by selection of the last deposited PE layer (so-called termination and tuned by selecting different PE. However, not only the terminating layer affects

the charge and reactivity of a PEM multilayer. One fascinating property is that intrinsic PE chains retain excess charges and might be contribute to reactivity at the surface of a PEM.

Polyelectrolytes (PEs) in solution are stabilized by their corresponding counterions. Upon adsorption on surfaces, the PE charges interact with the charges of previously deposited PE layers in the multilayer, leading to the release of counterions. PE layer adsorption is consistently driven by charge overcompensation, where each new layer introduces more charges than are neutralized by the preceding layer [Zan *et al.* 2012]. This overcompensation varies based on environmental factors and the type of PE. If the charge overcompensation varies between polyanions and polycations, the overall charge of the multilayer can be either positively or negatively in excess. This excess charge is stabilized by counterions associated with the excess charges. Introducing other adsorbing molecules, such as proteins, into the system may result in interactions between these excess charges and the adsorbing molecules.

Chapter 3 - Modification of surfaces with polyelectrolyte multilayers and their characterization

The study of the relation between the properties of material surfaces such as surface energy, surface charge, nano-scaled roughness and elasticity and the reaction of biological cells to these physical properties is a main goal of this work. The dependence of cell adhesion, cell proliferation and viability on the changed surfaces were studied as this is an important problem for the interaction between the implants and the body of the human patients. The contact between the biological tissue and the implants takes place at the surface of the implant material. Thus, surface modulations are important to be studied to gain understanding of interactions between biological tissue and implants.

The polyelectrolyte (PE) multilayer (PEM) systems for surface coatings have shown great potential to be used as coatings for medical devices and extensively applied in different studies. The PEM coatings have a thickness of only few hundred nanometers and thus do not change the microscopic structure of the surface, but still allow to tune it very precisely at molecular level. It has already been shown in the literature how small changes in the deposition conditions of the PEM influence their structure [Büscher *et al.* 2002, Decher *et al.* 1992].

This chapter summarizes the used PEM surface modifications, their preparation and their physicochemical characterization. These coatings were applied and studied throughout the whole thesis.

Polyelectrolyte multilayers (PEM) are prepared from alternating deposition of cationic and anionic polyelectrolytes (PE) from aqueous solution. Different polyelectrolytes (different molecular weight, charge density, chain rigidity), number of layers and deposition conditions such as temperature, pH-value, concentration of polyelectrolytes or electrolytes (counter ions) in the deposition solution significantly alter the physico-chemical surface properties.

In this work two PE pairs were used to build PEM, these are:

- **PSS/PAH**: Synthetic
  strong polyanion Poly(Styrene Sulfonate) (PSS) and
  weak polycation Poly(Allylamine Hydrochloride) (PAH)
- **HA/CHI**: Natural
  weak polyanion Hyaluronic Acid (HA) and
  weak polycation deacetylated Chitosan (CHI).

Each of the PEM coating systems were finished with either the polycation or with the respective polyanion resulting in positive and negative surface charges.

3.1 Surface modification procedure by polyelectrolyte multilayers (PEM)

The surfaces were modified by Polyelectrolyte Multilayer (PEM) coatings using Layer-by-Layer deposition technique [Decher *et al.* 1992]. All coatings were prepared using polyethyleneimine (PEI) as adhesion promoting layer. Glass slides, silicon wafers/blocks, Au-quartz-crystal-microbalance sensor crystals were used as substrates for specific surface characterizations. Plain polyethylene well-plates, tissue-culture-treated polyethylene well-plates and Au-coated silicon wafers were used for cellular adhesion measurements. Pins from surgical stainless-steel type 316L (iron, 16-18 % chromium, 10-12 % nickel, 2-3 % molybdenum) were used as medical steel stent substitutes for measurements of interleukin expression. The details of the deposition process are described in the chapter 7 – materials and methods.

The studied surface modifications of polyelectrolyte multilayer (PEM) coatings are summarized in Table 3.1. In the abbreviation the letters ‘S’ and ‘W’ are applied to define the strong or respectively the weak polyanion in the coating. The letters ‘P’ or ‘N’ stand for positive or negative surface charge. The following numbers describe the electrolyte concentration in the coating solution (e.g. 05 stands for 0.5 M NaCl).

Table 3.1. Surface modification by application of polyelectrolyte (PE) multilayer (PEM) coatings. PEI: polyethyleneimine; PSS: poly(styrene sulfonate); PAH: poly(allylamine hydrochloride); HA: hyaluronic acid; CHI: chitosan; The HA/CHI PEM are always dissolved in 5 mM sodium acetate (NaAc); Numbers 0, 05 and 10 in the PSS/PAH PEM abbreviations relate to the concentration of NaCl in the deposition solution (0, 0.5 and 1.0 M); The letters P or N relate to the sign of outmost surface charge of the respective coating (positive or negative). The lower index presents the number of repetitions for each PE couple.

Abbreviation:	**Buildup:**	**Terminating polyelectrolyte layer (charge):**	**NaCl or NaAc concentration in deposition solutions:**
SP0	$PEI/(PSS/PAH)_5$	PAH (+)	0 M (no NaCl)
SN0	$PEI/(PSS/PAH)_5/PSS$	PSS (-)	0 M (no NaCl)
SP05	$PEI/(PSS/PAH)_5$	PAH (+)	0.5 M NaCl
SN05	$PEI/(PSS/PAH)_5/PSS$	PSS (-)	0.5 M NaCl
SP10	$PEI/(PSS/PAH)_5$	PAH (+)	1.0 M NaCl
SN10	$PEI/(PSS/PAH)_5/PSS$	PSS (-)	1.0 M NaCl
WP	$PEI/(HA/CHI)_5$	CHI (+)	0.005 M NaAc
WN	$PEI/(HA/CHI)_5/HA$	HA (-)	0.005 M NaAc

3.1.1 Applied characterization techniques

The polyelectrolyte multilayers are thin coatings ranging from few nanometers to several micrometers and their characterization requires specific appropriate measuring methods. This paragraph illustrates the used surface characterization methods. Detailed materials and methods for all experiments are presented in chapter 7.

The **contact angle** of water is measured by contact angle goniometer analyzing the drop shape of a placed sessile drop of water on the substrate surface. The process begins by placing a small droplet of liquid (e.g., water) on the surface of the material being tested. A high-resolution camera then captures the profile of the droplet, showing its shape and the angle it forms with the surface. This angle, known as the contact angle, is measured using software that analyzes the captured image. The drop contour and the projection of the surface baseline is analyzed by applying the Young's equation. The contact angle is a measure for the degree of hydrophobicity

of the surface and can be used to characterize the surface energy. The used device was a contact angle measuring system OCA 15E from DataPhysics Instruments, Germany.

The alternating deposition of charged PEs on surfaces inverses the charge and alters the degree of charge on the surface. One method to reveal changes related to surface charge is the **electrophoretic mobility zeta potential measurement** technique based on light scattering measurements of particle movement in solution under application of an electrical field. The zeta potential takes into account the water and ion layers on the surface and is directly related to the surface charge, which is described by the Grahame equation. Non-sedimenting particles are coated with the PEM. By application of an electrical field to a particle suspension, the particles flow with a specific velocity towards the anode or the cathode. The speed and direction of the movement is used to measure the size of the particles and the zeta-potential at the surface. The used device was Zetasizer Nano ZS from Malvern Instruments, Germany.

Atomic force microscopy (AFM) is a powerful technique, which is often utilized to reveal the micro- to nanoscopic topography of surfaces. A sharp probe attached to a flexible cantilever scans the surface of the sample. As the probe moves across the surface, it bends trailing the topography of the surface in vertical direction. A laser beam is focused on the back of the cantilever and reflects onto a photodetector. The deflection of the laser beam, caused by the bending of the cantilever, is measured by the photodetector. The AFM system uses the deflection data to generate a topographic image of the surface in small scales that are not detectable by optical microscopy. In these images the z-direction is usually amplified to clearly show the topography (e.g., x-/y-direction is plotted in 1 µm scale and z-direction in 10 nm scale).

The physical interaction of the AFM-probe with the surface enables other techniques such as the force spectroscopy, which can be used to measure the mechanical elasticity of surfaces. The cantilever, which holds the AFM-probe, acts as a spring. When pushing the AFM-probe on top of the surface, both the surface and the cantilever will yield under the pressure. The surface will indent and the cantilever will bend outwards. By measuring the indentation and knowing the specific spring constant of the cantilever the mechanical elasticity (Young's modulus) of the surface can be calculated. The used device was NanoWizard I from JPK Instruments, Bruker, Germany.

Quartz-Crystal-Microbalance (QCM) can be used to measure the adsorption of mass on surfaces. The process begins with a thin quartz crystal disk that oscillates at its resonance frequency is applied by alternating voltage. The holding cell can be flooded with a molecule or protein solution, which enables the molecules to adsorb on the surface. When a material adsorbs

onto the surface of the quartz crystal, it increases the mass of the crystal, leading to a proportional decrease in resonance frequency. This frequency shift can be measured and is directly related to the mass change on the sensor crystal surface. This technique enables the measurement of thin PE layers, which commonly have a weight of a few nanograms per square centimeter.

The advanced quartz-crystal-microbalance with **dissipation monitoring** (QCM-D) provides a useful additional measurement of energy loss (dissipation) of the sensor crystal oscillation. To measure the dissipation, the applied voltage to the piezo crystal is momentarily stopped. The crystal continues to resonate for a short amount of time (fractions of nanoseconds) and finally arrests in its oscillation. If the adsorbed film (e.g., PEM or proteins) is not entirely stiff and has certain viscoelastic properties, the speed of dampening the oscillation is increased. The energy is adsorbed by the storage (shear elasticity) and loss (shear viscosity) moduli of the film and decreases the time the sensor crystal needs to stop oscillating. This technique allows for the calculation of elastic and viscous properties, more precisely the shear elasticity and the shear viscosity of thin films in nanometer scale. The used device was Quartz Crystal Microbalance with Dissipation monitoring (QCM-D) from QSense AB, Sweden.

Neutron reflectivity (NR) is a neutron scattering technique for measurements of thickness, structure and chemical composition of one or several thin layers at the surface or interface.

Neutron beams properties are changed, when reflected on the surface of a thin film coated substrate. The change in beam intensity can be measured and analyzed to reveal properties of the thin film. One part of the beam is reflected at the surface of the coating, the other part of the beam travels through the thin film and is reflected at the interface between coating and substrate. The additional travel time through a medium with different density reduces the light beams speed. The reflected beams have a wave shift, which can cause interferences of reflected light. These interferences can be precisely surveyed by adjustments of the angle of incidence. The obtained reflectivity curves are analyzed by application of a model to fit parameters such as film thickness, scattering length density and roughness. Neutron reflectivity was measured at the Swiss Spallation Neutron Source SINQ, Paul Scherrer Institute, Villigen PSI, Switzerland.

3.2 Surfaces modified by polyelectrolyte multilayers from poly(styrene sulfonate)/ poly(allylamine hydrochloride) (PSS/PAH) and hyaluronic acid/chitosan (HA/CHI) at constant electrolyte concentration in the deposition solutions

The physical-chemical properties of the applied PEs in solution are important for the properties of the prepared PEM coating. PEM coatings from synthetic PE couple PSS/PAH and natural PE couple HA/CHI and were prepared. The PEM were deposited at constant electrolyte concentrations – 0.5 M NaCl for the couple PSS/PAH and 0.005 M Sodium Acetate (NaAc) for the couple HA/CHI. QCM-D experiments were performed to follow the build-up process of the studied PEM. The PSS/PAH coating showed a linear mass increase (growth) behavior. In the lower bilayer regime (up to 5.5 bilayers) the HA/CHI showed a linear growth. These findings coincide with results published in the literature [Detzel *et al.* 2011].

3.2.1 Contact angle of water on PEM from poly(styrene sulfonate)/poly(allylamine hydrochloride) (PSS/PAH) and hyaluronic acid/chitosan (HA/CHI)

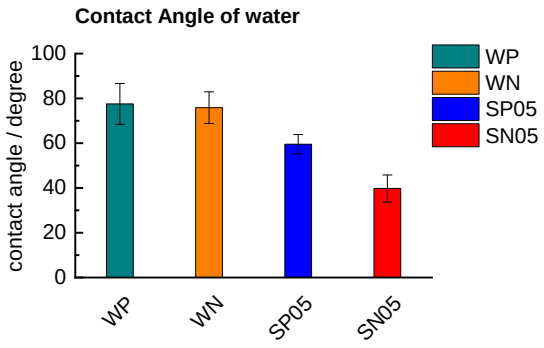

Fig. 3.1: Contact angle of water droplets on Si-wafers coated with PEM after 72 h drying in nitrogen atmosphere [Rudt 2016]. See table 3.1 on page 38 for abbreviations.

PEM-coated Si-wafer surfaces were dried for 72 hours in a nitrogen atmosphere before measurements. The contact angle of water was measured on these PEM-coated Si-wafers (figure 3.1). The WP and WN surfaces are slightly hydrophilic, with contact angles around 80 °. The SP05 and SN05 surfaces are more hydrophilic, with contact angles of around 60 ° and 40 °, respectively. The contact angle of water on the negatively finished PAH-terminated SN05 PEM is 20 ° smaller, likely due to the coating's composition of one weak and one strong polyelectrolyte. The termination with PSS, the strong polyelectrolyte, likely results in higher surface energy and therefore a smaller contact angle of water.

The thickness of SP05/SN05 PEM and WP/WN PEM is equally high at five bilayers. The exponential growth of WP/WN films is observed only at higher bilayer numbers. The positive WP and negative WN multilayers exhibit similar hydrophobicity to SP05 coating, which terminates with a weak polyelectrolyte (PAH) layer. In WP/WN coatings, both negative and positive terminations are achieved with a weak polyelectrolyte, resulting in higher water affinity compared to SP05/SN05 coatings. No difference in water contact angle is observed between HA

and CHI-terminated coatings (figure 3.1), likely due to both terminating polyelectrolytes being weak and the inclusion of hygroscopic hyaluronic acid.

The differences in water contact angle between SP05/SN05 and WP/WN indicate that the weak natural polyelectrolyte pair (WP and WN) shows higher values with no difference between negative or positive terminating layers. In contrast, the synthetic polyelectrolyte pair (SP05 and SN05) is more hydrophilic and shows a difference between terminating layers with the weak (PAH) or strong (PSS) polyelectrolyte termination.

3.2.2 Zeta potential of PEM from poly(styrene sulfonate)/poly(allylamine hydrochloride) (PSS/PAH) and hyaluronic acid/chitosan (HA/CHI)

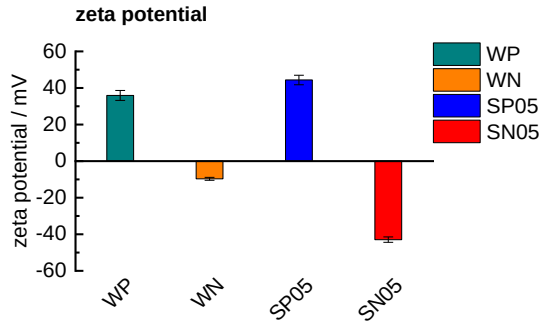

Fig. 3.2. Zeta potential of PEM coated surfaces. PEMs SP05 and SN05 were prepared from PSS/PAH in 0.5 M NaCl, the PEMs WP and WN were prepared from HA/CHI in 5 mM NaAc. All zeta potential measurements were measured in 10 mM NaCl solution [Rudt 2016]. See table 3.1 on page 38 for abbreviations.

The zeta-potential was measured on small, non-sedimenting silicon particles modified with PEM. The data is summarized in figure 3.2. Positively charged surfaces terminated with CHI or PAH exhibit similarly high zeta potentials of approximately +40 mV. In contrast, negatively charged surfaces display a distinct difference in zeta potential between HA and PSS terminations. The weakly negatively charged WN PEM has a zeta potential around -5 mV, which is about five times lower than the strongly negatively charged SN05 PEM, with a zeta potential of approximately -40 mV. The difference in zeta potential between PSS/PAH and HA/CHI modified surfaces is noticeable only on negatively terminated coatings. Here, the zeta potential of the PSS-terminated coating is significantly higher than that of the HA-terminated coating. No significant difference is observed between positive terminations with CHI and PAH. This can be attributed to PSS being a strong polyelectrolyte, which significantly influences the internal electrostatic equilibrium during multilayer construction, thereby affecting the resulting surface potential. In contrast, multilayers built from two weak polyelectrolytes, such as HA/CHI, exhibit a lower negative zeta potential.

3.2.3 Surface roughness of PEM from poly(styrene sulfonate)/poly(allylamine hydrochloride) (PSS/PAH) and hyaluronic acid/chitosan (HA/CHI)

Surfaces coated with PEM from PSS/PAH and HA/CHI were characterized using atomic force microscopy in contact mode within a liquid environment. Figure 3.3 displays representative topographic images. It was observed that surfaces modified with PSS/PAH and HA/CHI exhibit distinct surface topographies between both systems, which is independent of the terminating polyelectrolyte layer. There is a noticeable difference between surfaces modified with PSS/PAH and HA/CHI, but no difference between positive or negative terminations.

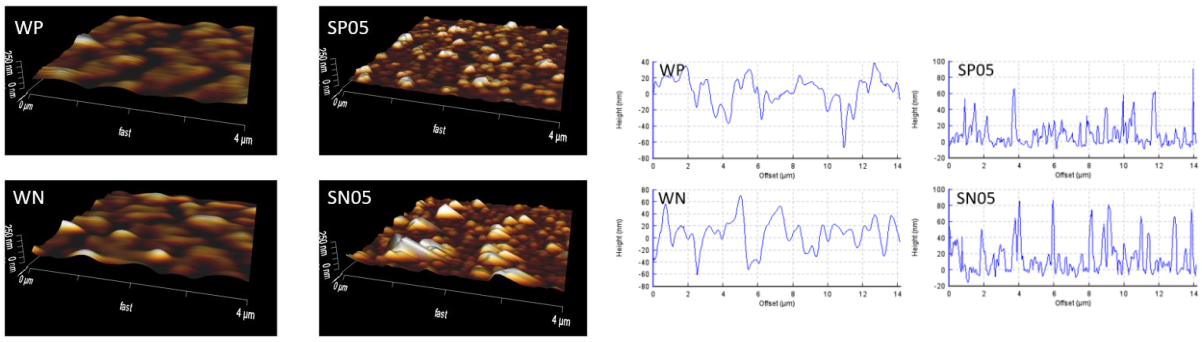

Fig. 3.3. Left images) 3D-presentation of contact images of PEM coatings in liquid environment of an area of 4 µm^2; Right images) Profile images showing difference in roughness between different PEM coatings [Rudt 2016]. See table 3.1 on page 38 for abbreviations.

Figure 3.3 shows the height of the peaks observed in the AFM images along a line at the surface. A pronounced difference in the profiles between SP05/SN05 coatings and WP/WN coatings is evident. The peaks of SP05/SN05 coatings appear sharper and more numerous compared to the smoother peaks of WP/WN coatings. Although 'sharp' and 'smooth' are relative terms due to the large vertical/horizontal ratio, a clear visible difference in surface roughness is apparent between the SP05/SN05 and WP/WN coatings, as well as in the 3D projections.

To clarify the differences in surface roughness, numeric values were evaluated using the most common roughness definitions: average roughness (R_a), root mean squared roughness (R_q), and peak-to-valley roughness (R_t). However, since these standard definitions couldn't distinguish between the roughness of SP05/SN05 and WP/WN coatings, a custom 'peak-count' method was devised to clearly highlight the differences in surface roughness.

$$R_{peak\ count} = \frac{\sum n_p}{l} \qquad \text{(eq. 19)}$$

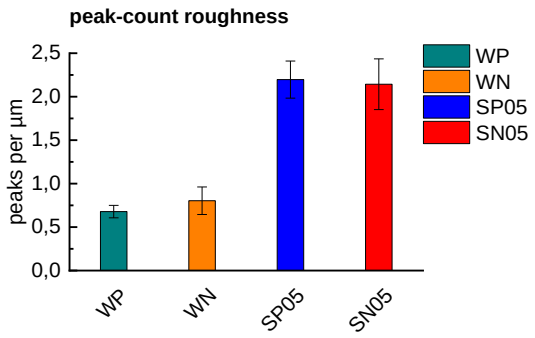

Fig. 3.4. Roughness of PEM samples calculated according to 'peak-count' definition [Rudt 2016]. See table 3.1 on page 38 for abbreviations.

The calculated values from common roughness measurements showed no clear difference between the tested samples, despite the well-pronounced differences visible in the profile images between SP05/SN05 and WP/WN in figure 3.3. To better quantify these results, a custom roughness definition with focus on number of profile elements per length was applied (eq. 5). This method involves counting the number of peaks above or valleys below the zero line (the height at which average roughness is minimal) over a measured distance. Here, R represents the calculated peak-count roughness, n_p is the number of peaks, and l is the analyzed distance in the profile images. The 'peak-count' roughness definition revealed a clear difference in roughness between the tested PEM-modified surfaces. Peak- count roughness is shown in figure 3.4.

3.2.4 Mechanical stiffness of PEM from poly(styrene sulfonate)/poly(allylamine hydrochloride) (PSS/PAH) and hyaluronic acid/chitosan (HA/CHI)

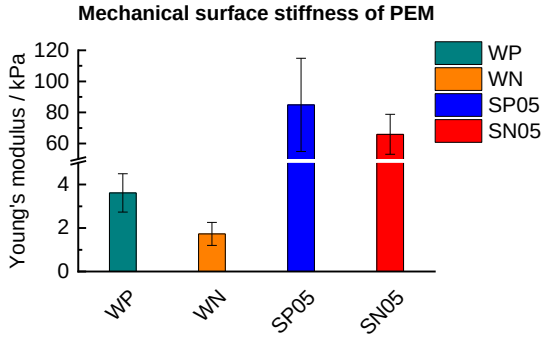

Fig. 3.5. Young's modulus of PEM coatings measured by AFM and fitted with Hertz equation [Rudt 2016]. See table 3.1 on page 38 for abbreviations.

The elastic modulus (Young's modulus) of the completed coatings was measured using atomic force spectroscopy. A distinct difference between the Young's moduli of SP05/SN05 and WP/WN films was observed (figure 3.5). The SP05 film has a Young's modulus of 85 kPa and the SN05 film 65 kPa, whereas the WP and WN coatings have much lower Young's moduli of 4 kPa and 2 kPa, respectively. The Young's modulus of PSS/PAH coatings is significantly higher than that of HA/CHI. This can be attributed to the strong polyelectrolyte PSS, which greatly enhances the internal electrostatic bonds of the polyelectrolytes, thereby increasing the mechanical stiffness of the entire coating. In contrast, the WP/WN coatings, composed of two weak polyelectrolytes, have weaker internal connections, resulting in less stiff films.

3.3 Surfaces modified by polyelectrolyte multilayers from poly(styrene sulfonate)/poly(allylamine hydrochloride) (PSS/PAH) prepared at different electrolyte concentration in the coating solution

The PEM from PSS/PAH were further diversified by changing the electrolyte concentration in the deposition solution, which affects the polyelectrolyte radius of gyration in the solution and the properties of formed coatings. These films were characterized by measurements of water contact angle and zeta potential and by measurements of mass deposition, shear stress, shear viscosity by QCM-D.

The prepared PEMs from PSS/PAH differ in electrolyte concentration in the deposition solutions of polyelectrolytes. Electrolyte concentrations are known to affect thickness increment per deposition cycle, the permeability and the stability of multilayers [Dubas & Schlenoff 2001]. The thickness of PEM depends on the electrolyte concentration and is related to the dependence of PE conformation in solution on the electrolyte concentration. The conformation of polyelectrolyte chains is governed by electrostatic repulsion of charges on the polymer chain. This can be described by changes in Bjerrum length, which describes the distance between two interacting charges where the electrostatic energy is equal to thermal energy. The self-repulsion of the poly-ion chain leads to an increase of persistence length and in radius of gyration. The repulsion is weakened by addition of electrolytes such as NaCl to the PE deposition solution. Polyelectrolytes from deposition solutions with increased counter ion (electrolyte) concentrations therefore adsorb in a state with smaller radius of gyration and require less space per chain on the surface, which leads to a larger volume of segments and consequently to a thicker layer [Schönhoff 2003].

3.3.1 Contact angle of water on PEMs from poly(styrene sulfonate)/poly(allylamine hydrochloride) (PSS/PAH) prepared at different electrolyte concentration in the coating solution

The contact angle of water on PEM surfaces depends on the surface energy of the coating, as well as on residue water in multilayer. Due to different counter ion concentrations in PSS and PAH solutions, the formed multilayers had variable capacities of water retention due to swelling states of the completed PEM. The contact angle was measured on two different points in drying time to observe this effect. The first measurement was conducted immediately after deposition of PSS/PAH coatings and subsequent drying with nitrogen until no water was visible (figure 3.6-A). In this state, the PEMs are still swollen to a certain degree after exposition to watery

environment during the deposition process. The second measurement was conducted after an extensive drying period of 72 h in nitrogen atmosphere at room temperature of 22 °C (figure 3.6-B). It is observed that the water contact angle changes and depends on the terminating layer for all tested PEMs, as well as the electrolyte concentration of the deposition solution in the case of PAH-terminated PEMs.

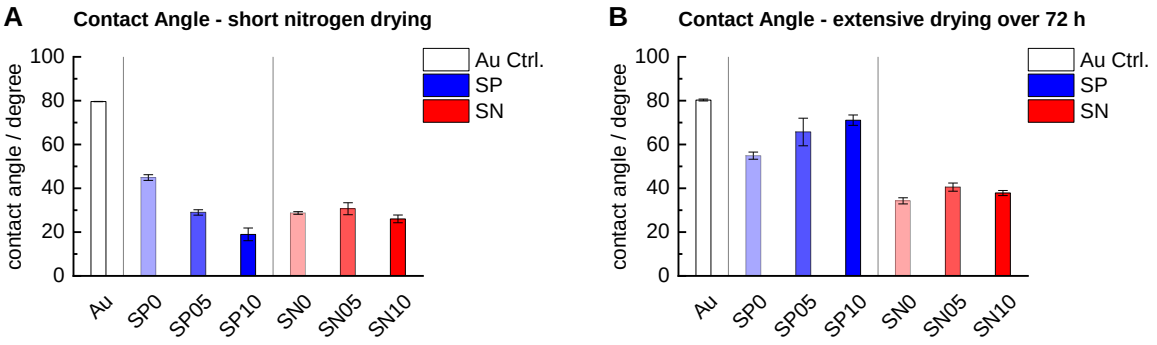

Fig. 3.6. Contact angle of water on PEM coated substrates. White bar shows contact angle on clean Au surface. Blue and red bars show contact angles on positively (PAH) and negatively (PSS) terminating PEMs from deposition solutions with NaCl concentrations of 0, 0.5 and 1.0 M respectively. **(A)** Contact angle immediately measured after PEM deposition and nitrogen drying. **(B)** Contact angle on the same samples after extensive drying over 72 h in nitrogen atmosphere [Rudt *et al.* 2021]. See table 3.1 on page 38 for abbreviations.

The effect of electrolyte concentrations in the deposition solution on the water contact angle on PEM films was already observed in [Warszynski & Kolasinska 2005]. Our measurements of water contact angle on PEMs from PSS/PAH after drying for 72 h in nitrogen atmosphere are in agreement with their results. In 2007, Hänni-Ciunel *et al.* stated that by exposing PEMs to environment with high air humidity the films are swelling and changing their surface energy, which is reflected by a decreasing contact angle of water [Hänni-Ciunel *et al.* 2007]. The contact angle of all PEMs was rising after the extended drying period.

The extensive drying period affected the contact angle of the PEM coatings differently. The contact angle of PSS-terminated PEMs increased uniformly, regardless of the NaCl concentration in the deposition solution. In contrast, the contact angle of PAH-terminated PEMs highly depends on the NaCl concentration. PAH-terminated PEMs from solutions with higher NaCl concentrations showed a greater increase in the contact angle of water in correlation with the NaCl concentration. The extreme case was observed with the SP10 coating, which had the

lowest contact angle immediately after PEM deposition but the highest contact angle after extensive drying. PAH-terminated PEMs from solutions with lower electrolyte concentrations exhibited smaller changes in the contact angle after drying. This aspect is noteworthy because, while literature often examines the contact angle of water on fully dried PEM surfaces, PEMs in contact with biological systems are exposed to wet conditions, altering surface properties based on the coating and terminating polyelectrolyte used.

One possible explanation for the different drying behavior between PSS- and PAH-terminated layers is the so called 'odd-even effect' which was first introduced in 2002 by [Schwarz & Schönhoff 2002] and partially explained in [Benbow *et al.* 2019]. By formation of PEM from a weak polyelectrolyte (PAH) and a strong polyelectrolyte (PSS), the multilayer grows in a zig-zag partern (as seen in figure 3.8) with a trend of incremmental linear growth. Most probably the multilayers internal water is intensly released on finalizing coating steps with the strong polyelectrolyte (such as PSS), which leads to a less bulky coating. Upon the subsequent coating step with the weaker polyelectrolyte (such as PAH), the internal electrostatic structure favours a higher capacity for counter ions and amplifies incorporation of internal water.

The odd-even effect fits as explanation to our findings as the PAH-terminated coatings show are more pronounced drying in comparison to the PSS-terminated coatings, assuming that internal water directly affects surfaces affinity towards water in contact with the surface. Additionally, it was observed that the concentration of electrolytes in the deposition solution further enhances this effect. Higher electrolyte concentrations in the deposition solution amplify the drying of PAH-terminated PEMs, thereby reducing the surface's affinity for water.

3.3.2 Zeta potential of PEMs from poly(styrene sulfonate)/poly(allylamine hydrochloride) (PSS/PAH) with variation of electrolyte (NaCl) concentration in the deposition solutions

The zeta potential was measured on PEM-coated SiO_2 particles in aqueous solution after each PE deposition step (figure 3.7). Initially, the zeta potential of SP0 and SN0 surfaces slightly deviates from that of SP05, SN05, and SP10, SN10. This deviation can be attributed to the absence of electrolytes in the deposition solution, resulting in less flexible PE chains that struggle to fully adsorb to the surface. After a few additional coating steps, the surface becomes saturated, allowing for complete coverage with an additional PE layer. Starting with the first PAH deposition, all PEM surfaces exhibit similar zeta potential in subsequent PE depositions.

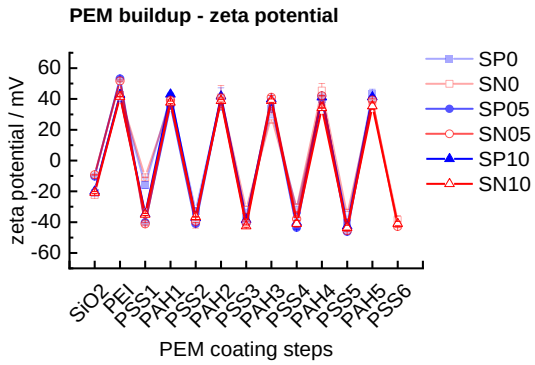

Fig. 3.7. Zeta potential of PEM deposition steps on silica particles [Rudt *et al.* 2021]. See table 3.1 on page 38 for abbreviations.

Once the initial layers are applied, the zeta potential stabilizes at +40 mV and -40 mV for positively and negatively charged SP/SN-PEMs, respectively, regardless of the electrolyte concentration in the deposition solutions. In the final coating steps, no dependence of zeta potential on the electrolyte concentration in the deposition solution is observed.

3.3.3 QCM-D frequency of PEMs from poly(styrene sulfonate)/poly(allylamine hydrochloride) (PSS/PAH) with variation of electrolyte (NaCl) concentration in the deposition solutions

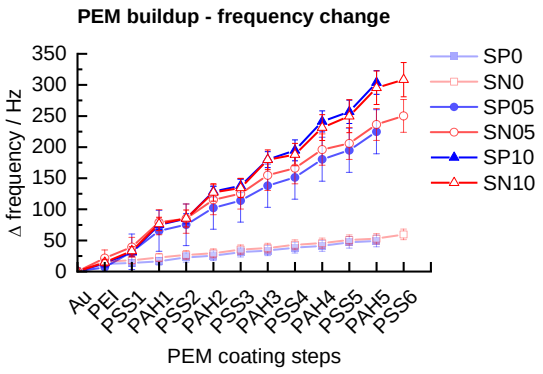

Fig. 3.8. Frequency change by adsorbed polyelectrolyte layers upon PEM buildup [Rudt *et al.* 2021]. See table 3.1 on page 38 for abbreviations.

Quartz Crystal Microbalance with Dissipation Monitoring (QCM-D) was used to measure the frequency shift upon adsorption of polyelectrolyte layers, which is proportional to the adsorbed mass. QCM-D was applied to characterize the PEM buildup process, with the frequency shift at overtone 5 (25 MHz) being recorded. The rates of mass deposition of PEs depend on the NaCl concentration in the deposition solutions, showing an incremental linear growth in studied PEMs from PSS/PAH (figure 3.8).

The growth behavior of PSS/PAH coatings, as shown in the quartz crystal microbalance measurements in figure 3.8, depends on the electrolyte concentration in the deposition solution. Each individual PE layer and the total amount of the formed PEM from 0 M NaCl show the lowest frequency shift, while PEM from 1 M NaCl in the deposition solution shows the highest frequency shift, corresponding to the deposited mass. This confirms that the NaCl concentration in deposition solutions is a solid factor for adjusting the buildup properties of PEM.

3.3.4 QCM-D viscosity and elasticity of PEMs from poly(styrene sulfonate)/poly(allylamine hydrochloride) (PSS/PAH) with variation of electrolyte concentration in the deposition solutions

The mechanical properties of surfaces modified with PEM from poly(styrene sulfonate)/poly(allylamine hydrochloride) (PSS/PAH) with variation of electrolyte (NaCl) concentration in the deposition solutions were characterized using the QCM frequency shift and dissipation data. The shear elasticity and the shear viscosity of the layers were calculated using a fitting routine based on the Voigt model. Results are summarized in figure 3.9.

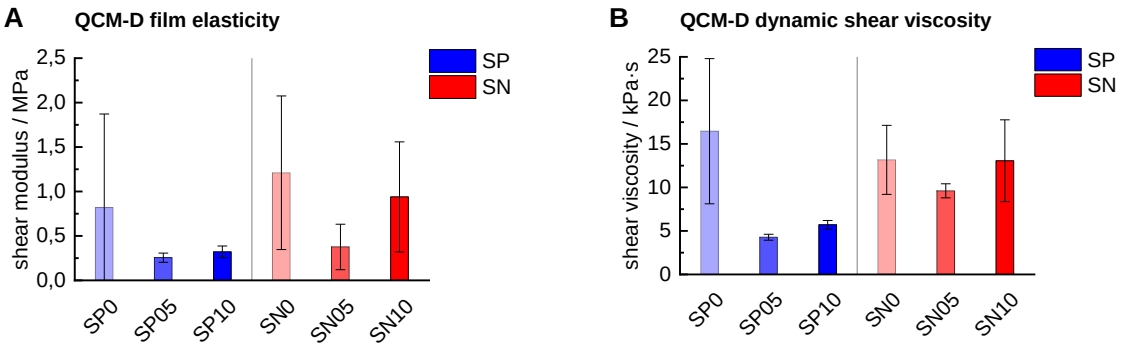

Fig. 3.9. Film elasticity (A) and film viscosity of PEM prepared from PSS/PAH at different electrolyte concentrations in the deposition solution. SP0, SP05, SP10 – positively charged PEM from strong polyelectrolytes at NaCl concentration in the deposition solution of 0, 0.5 and 1.0 M; SN0, SN05, SN10 - negatively charged PEM from strong polyelectrolytes at NaCl concentration in the deposition solution of 0, 0.5 and 1.0 M. See table 3.1 on page 38 for abbreviations.

Both the shear modulus and the dynamic shear viscosity exhibit a similar trend, with a slight increase in values for PEMs from higher electrolyte concentration deposition solutions. The exceptions are the PEMs from 0 M NaCl solutions (SP0 and SN0), which show high values and high variation. This may be because viscoelasticity measurements by QCM-D require a certain film thickness and are operating at the edge of their limitations, making it difficult to accurately measure the extremely thin (~10 nm) PEM multilayers from deposition solutions without electrolytes. In subsequent measurements, where additional proteins were adsorbed onto the SP0/SN0 coated surfaces (chapter 4.8), the added mass resulted in much smaller variation and more reasonable values.

It can be assumed that PEMs from higher electrolyte concentration deposition solutions are capable of storing more ‘reversible’ energy and absorbing more ‘non-reversible’ energy through the oscillation of the QCM-D sensor crystal. These PEMs adsorb a greater mass and quantity of polyelectrolyte chains, leading to increased elasticity due to the higher number of stretchable

and rotatable molecules, as well as additional electrostatic interactions between charged groups. The increased viscosity can be attributed to the higher mass of polyelectrolytes, which, similar to a tempering process in polymers, may exhibit polymer relaxation under pressure. In contrast, PEMs from lower electrolyte concentration deposition solutions have a firm interaction between polyelectrolytes without additional interactions with electrolytes (counterion NaCl) within the PEM. This results in a stiffer and more rigid multilayer with less steric freedom, limiting the absorption of reversible and non-reversible energy.

3.3.5 Thickness and water content of PEMs from poly(styrene sulfonate)/poly(allylamine hydrochloride) (PSS/PAH) with variation of electrolyte concentration in the deposition solutions

The PEM coatings on modified surfaces are exposed to a watery environment during all surface characterization and biological experiments. A key property of these films is their capacity to retain intrinsic water when exposed to a watery environment, which could influence cellular protein adsorption and cellular recognition mechanisms. The water content of thin films was measured using neutron reflectivity (NR).

Reflectivity experiments were conducted at the Swiss Spallation Neutron Source SINQ at the Paul Scherrer Institute in Villigen, Switzerland. The surfaces of polished silicon blocks were modified with PEM coatings made from poly(sodium styrene) and poly(allylamine hydrochloride), with variations in electrolyte content in the deposition solutions. Neutron reflectometry was used to reveal information about the composition at the solid/liquid interfaces.

3.3.5.1 Thickness and scattering length density of PEMs from poly(styrene sulfonate)/ poly(allylamine hydrochloride) (PSS/PAH) with variation of electrolyte concentration in the deposition solutions

The NR measurements were performed in a solid/liquid experimental cell. A Si monocrystal covered with PEM was fixed on a Teflon trough, which was filled with heavy water (D_2O). The fitting procedure was performed by the NCNR online reflectivity calculator, which was supplied by [Maranville 2017]. Measured reflectivity curves are shown in figure 4.17 (chapter 4.3).

The readout from the fitting procedure is film thickness, scattering length density (SLD) and roughness at the interfaces between film and substrate and at the interface between film and D_2O. The film thickness and SLD values are shown in figure 3.10.

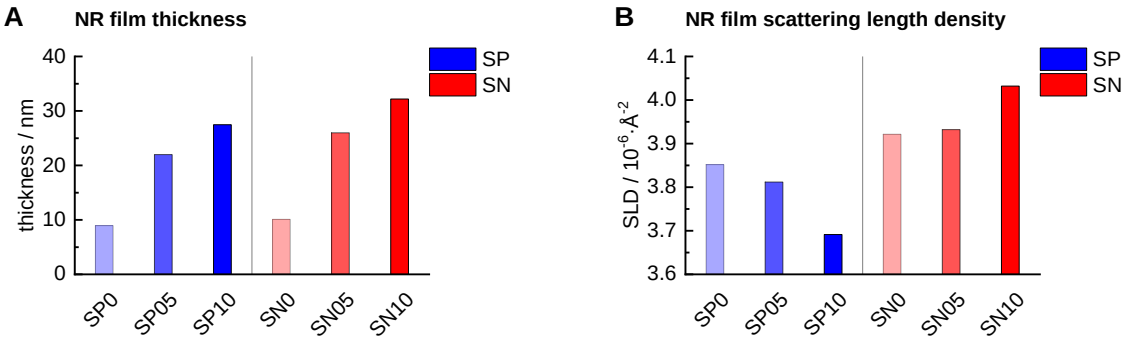

Fig. 3.10. Characteristic film thickness (A) and scattering length density (B) of PEM prepared from PSS/PAH at different electrolyte concentrations in the deposition solution. SP0, SP05, SP10 – positively charged and SN0, SN05, SN10 - negatively charged PEM from deposition solution at concentrations of 0, 0.5 and 1.0 M NaCl. See table 3.1 on page 38 for abbreviations.

The PEM film thickness (figure 3.10-A) ranges from thinnest to thickest as follows: SP0 < SN0 < SP05 < SN05 < SP10 < SN10. As observed in QCM-D experiments, increasing the electrolyte content in the deposition solution results in thicker films with greater adsorbed mass. The negatively charged films (SN) are consistently thicker due to an additional deposited layer of PSS.

The scattering length density (SLD, shown in figure 3.10-B) varies across the tested PEM films. SP0 and SN0 exhibit similar SLD values, but as the electrolyte content in the deposition solution increases, the SLD values for SP and SN films diverge incrementally. With higher electrolyte concentrations, the SLD of positively charged SP films decreases, while the SLD of negatively charged SN films increases. Among all samples, SP10 has the lowest SLD value, and SN10 has the highest.

3.3.5.2 Water content of PEMs from poly(styrene sulfonate)/poly(allylamine hydrochloride) (PSS/PAH) with variation of electrolyte concentration in the deposition solutions

Scattering length density is directly correlated to film density and can be used to calculate the water content of thin films in watery environment.

The measured SLD values of PEM films are a sum of the volume ratio of dry PEM (ϕ_{water}) with its specific SLD (ρ_{water}) and the volume ratio of water (ϕ_{water}) with its specific SLD (ρ_{water}).

This can be expressed as:

$$1 = \phi_{water} + \phi_{dry\ PEM}$$

$$\rho_{wet\ PEM} = (1 - \phi_{water}) \cdot \rho_{dry\ PEM} + \phi_{water} \cdot \rho_{water}$$

As such, by measuring the SLD of wet film and knowing the SLD of dry film, the volume ratio of intrinsic water can be calculated:

$$\phi_{water} = \frac{\rho_{wet\ PEM} - \rho_{dry\ PEM}}{\rho_{water} - \rho_{dry\ PEM}}$$

Before measurements, the tested PEMs were exposed to a D_2O environment, allowing all H_2O content to be replaced by D_2O driven by diffusion. The scattering light density was measured on D_2O soaked PEM films. SLD values of dry PEM films were calculated according to [Carrière *et al.* 2004]. The water content of PEM films is plotted in figure 3.11.

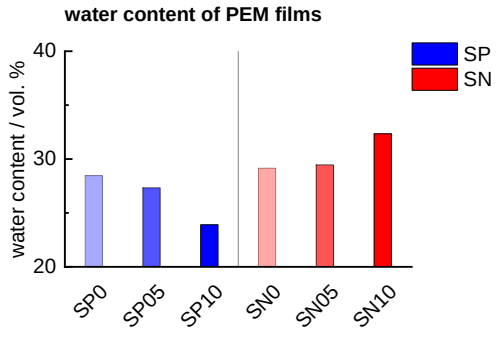

Fig. 3.11. Characteristic volume fraction of water in PEM films prepared from PSS/PAH at different electrolyte concentrations in the deposition solution. SP0, SP05, SP10 – positively charged and SN0, SN05, SN10 - negatively charged PEM from deposition solution at concentrations of 0, 0.5 and 1.0 M NaCl. See table 3.1 on page 38 for abbreviations.

The tested PEMs have different water volume fractions, ranging from 24.0% to 31.1%. There is an observed dependence of water content on the electrolyte concentration in the deposition solution. The terminating layer determines whether an increase in electrolyte concentration increases or decreases the water content of the multilayers. Negatively charged SN films consistently show higher water content compared to positively charged SP coatings. An increase in electrolyte concentration in the deposition solution increases the water content of negatively charged PEMs and decreases the water content of positively charged PEMs.

The odd-even effect describes the influence of the terminating layer on the mobility of hydration water and the water fraction bound in multilayers [Schönhoff et al. 2007]. This effect is evident in multilayers constructed from one strong and one weak polyelectrolyte, such as PSS and PAH. A linear increase in the amplitude of the odd-even effect with the number of layers was discovered in [Schönhoff et al. 2007; Schwarz & Schönhoff 2002]. It is speculated that the odd-even effect is associated with the swelling and de-swelling of PEMs, leading to variations in the water fraction within the multilayer.

In our findings, the odd-even effect is observed on all tested PEM films. The negatively charged SN-films always show higher water content in comparison to the positively charged SP-counterparts. An interesting find is that the amplitude of the odd-even effect is magnified by increase of electrolyte concentration in the deposition solutions. The difference in water volume fraction between SP0 and SN0 films is only 0.7 % water content, whereas the difference between water contents of SP05 and SN05 films is 2.1 % and of SP10 and SN10 films it is 8.4 %. It is speculated that the odd-even effect is based on swelling and de-swelling of the PEM films. The SP10 and SN10 films are the thickest (by NR) and bulkiest (by QCM-D) tested PEM coatings. The amplification of the odd-even effect might be explained by the higher capability of these films to swell and de-swell due to higher quantities of swelling PEs.

3.3.6 Cytotoxicity of PEM from poly(styrene sulfonate)/poly(allylamine hydrochloride) (PSS/PAH) and hyaluronic acid/chitosan (HA/CHI)

A main goal of this work is to identify and correlate physico-chemical surface properties of surfaces with the biological response of human cells. Surface modifications by polyelectrolyte multilayers were utilized to diversify the properties of surfaces. The possibility that the used polyelectrolytes might biologically affect cells had to be excluded. Therefore, a study of cytotoxicity was conducted to exclude potentially toxic effects of surface chemistry on cells, which could alter cellular behavior by biological intervention.

The experiments were designed according to guidelines from ISO standard 10993-5. An extraction of potentially toxic substances was performed on uncoated and PEM coated substrates by 24 h incubation with DMEM cell culture medium (Dulbecco's Modified Eagle Medium). The extracts were diluted with fresh cell culture medium and added to confluent L929 cells in well plates. Extracts of toxic latex and un-toxic polypropylene served as controls. Extraction medium volume to substrate surface ratio was adjusted according to ISO standard 10993-12. After 24 h incubation time the cell growth inhibition was measured by resazurin assay.

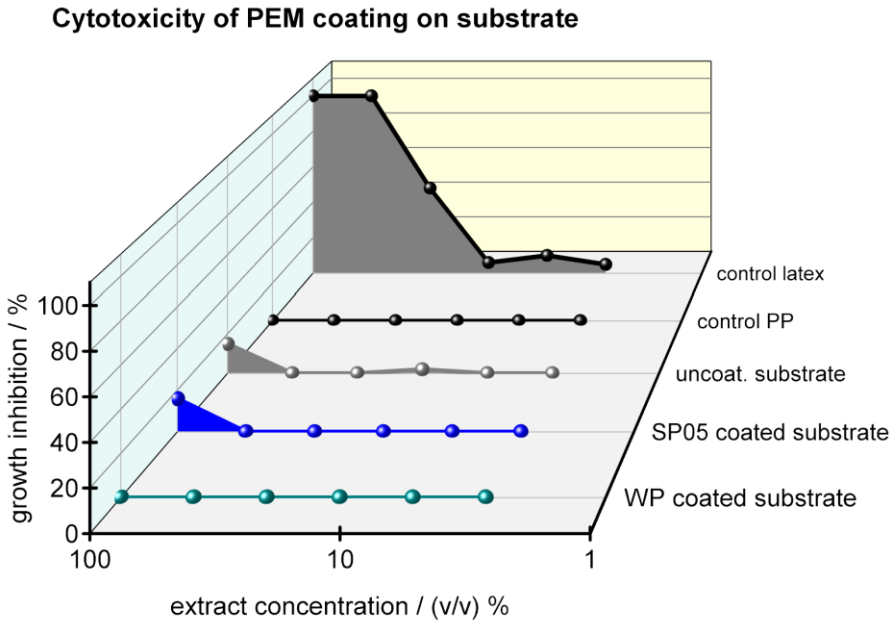

Fig. 3.12. Cytotoxicity of extracts from PEM from poly(styrene sulfonate)/poly(allylamine hydrochloride) (SP05) and hyaluronic acid/chitosan (WP).

Figure 3.12 shows the L929 cell growth inhibition by incubation with extracts from completed PEM coatings. The toxic latex control shows total growth inhibition over several dilution steps and the polypropylene control shows no growth inhibition. The extracts of the uncoated substrate and SP05 coated substrate show 15 % and 16 % growth inhibition on measurements with 100 % extraction medium. All further dilutions show no growth inhibitions. The extract of WP coated substrate shows no growth inhibition. According to ISO standard 10993 values of less than 20 % growth inhibition can be viewed as non-toxic. In our findings, the tested PEM coatings either do not change the cytotoxicity of the uncoated substrate or improve upon it.

This observation is expected as the PE in PEM coatings are very strongly complexed and are not easily dissolved in solution. However, the question remained: what would happen if PE from a PEM coating dissolved and contaminated the cell culture medium? To address this, a second set of experiments was conducted, focusing not on extracts of completed PEM coatings, but on pure PE deposition solutions and complexes of PEM in solution. The results are shown in figure 3.13.

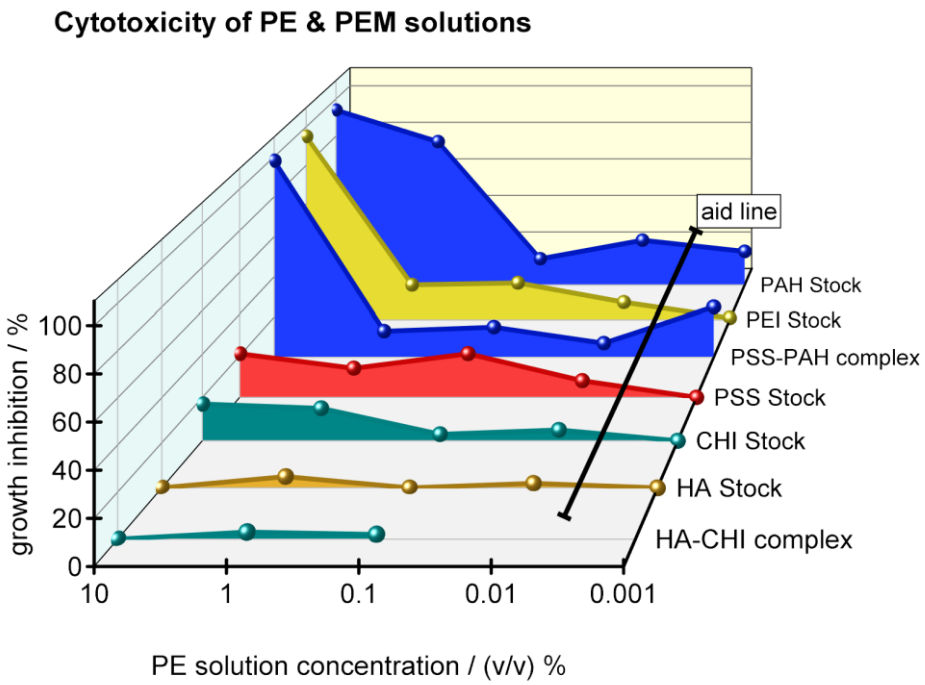

Fig. 3.13. Cytotoxicity of polyelectrolyte (PE) solutions with poly(styrene sulfonate); poly(allylamine hydrochloride), hyaluronic acid, chitosan and complexes of these PE in solution. The black aid line indicates concentrations of PE if a PEM coating would be completely dissolved and would release all bound PE in a PEM coating to the testing volume.

Figure 3.13 shows the measured cytotoxicity of PE stock solutions and solutions of complexes from pairs of PEs. The standard PE stock solution concentrations are 2 mg/mL for PEI, PSS, and PAH, and 1 mg/mL for HA and CHI. These stock solutions were diluted with cell culture medium to 10 % (v/v). Experiments with higher percentages of PE stock solutions were not conducted, as the lack of nutrients would hinder cell growth. The 10 % (v/v) concentrated stock solution in cell culture medium shows high growth inhibition for PAH and PEI polyelectrolytes, which are known to be cytotoxic at high concentrations. All other tested PEs show less than 20 % growth inhibition.

At 10 % (v/v) stock concentration, a high growth inhibition was observed for PSS-PAH complexes in solution. However, this result is a false negative because high concentrations of PSS-PAH complexes cause opaqueness in the testing solution, interfering with the later analysis of the resazurin assay by spectroscopy. After two 1/10 dilution steps, all tested solutions showed less than 20 % growth inhibition, which is considered non-toxic. The aid line in Figure 3.13 indicates the concentration of PE if a PEM coating was completely dissolved and released into the specific volume of the testing medium. At this specific surface/volume ratio, no PE solution can be considered toxic.

In conclusion, while some PEs (such as PEI and PAH) are cytotoxic at high concentrations, they show no cytotoxicity when complexed in the form of PEM. Under physiological conditions, it is unlikely for a PEM coating to dissolve rapidly. Even if this were to occur, the concentrations of PE would still be too low to be show cytotoxicity.

3.4 Summary - Controlled modification of surfaces with polyelectrolyte multilayer and their characterization

A main goal of this work was to study the interactions between physico-chemical surfaces properties and biological responses of cells in contact with these surfaces. The method of choice for variation of surface properties was surface modification by Layer-by-Layer deposition of polyelectrolyte multilayers (PEM) as introduced by [Decher *et al.* 2012]. Polyelectrolyte Multilayers based on the polyelectrolyte pair poly(styrene sulfonate) (PSS) and poly(allylamine hydrochloride) (PAH) is generally the most studied polyelectrolyte pairing and is considered a standard PEM (in short SP05, SN05 coatings). These surface modifications were applied, characterized and further diversified to generate high variation of surface properties. One variation was the utilization of natural based polysaccharides for the PEM construction (WP, WN coatings). This natural PE pair of chitosan (CHI) and hyaluronic acid (HA) is interesting for biomedical application due to similarity to human proteins and enhanced biodegradability. Another surface variation was the change of electrolyte (neutral salt, NaCl) concentration in the PSS and PAH deposition solutions (SP0, SN0, SP10, SN10 coatings). This approach does neither introduce new chemicals to the system nor alter the chemical composition of PEM, but enables change of the intrinsic structural composition, which significantly affects surface properties such as stiffness and water retention capacity.

The cytotoxicity of all used polyelectrolytes was tested. Polyelectrolytes such as PAH and the adhesion agent poly(ethylene imine) (PEI) are toxic in high concentrations, however they are not toxic when complexed in multilayers. The other polyelectrolytes showed no cytotoxicity.

The finalizing layer (termination) governs the charge of the surface. SP05 is positively charged (zeta potential of +44 ± 3 mV), whereas SN05 is negatively charged (zeta potential of -43 ± 1 mV). The zeta potential of the SP/SN PEM with variation of electrolyte concentration in the deposition solutions is either +41 ± 3 mV for SP coatings or -41 ± 3 mV for SN coating. The electrolyte concentration in the deposition solution does not affect the zeta potential of the formed PEMs.

PAH and CHI terminated PEMs (SP05 and WP) show comparable positive surface potential, which is 44 ± 3 mV (SP05) and 36 ± 3 mV (WP), respectively. However, the negatively terminated PEMs show a stronger difference in zeta potential. Whereas PSS terminated PEMs have a zeta potential of -43 ± 1 mV (SN05), the HA terminated multilayers (WN) have 77 % reduced zeta potential with -10 ± 1 mV in neutral conditions. The reduced charge density not

only affects the outmost layer but contributes to the whole PEM building process, which results in weaker attraction of oppositely charged PEs and less connected and less compact multilayers.

After extensive drying SP05 shows a 62 % higher contact angle of water in comparison to SN05 (66 ± 6 ° for SP05 and 41 ± 2 ° for SN05). The contact angle of WP and WN after 72 h drying were measured as high as 78 ± 9 ° and 76 ± 7 °, respectively. Therefore, WP is 30 % and WN is 27 % more hydrophilic than SP, as well as 94 % and 90 % more hydrophilic than SN.

A pronounced dependence of water contact angle on drying time was found on SP and SN from deposition solutions with varied electrolyte concentration. The contact angle of water was measured after short nitrogen drying and after 72 h extensive drying. The short nitrogen drying reveals a constant contact angle of around 28 ° on negatively charged SN (29 ± 1 ° for SN0, 31 ± 3 ° for SN05, 26 ± 2 ° for SN10). The water contact angle on the positively charged SP shows a decrease with an increase in electrolyte concentration in the deposition solution. SP0 has the highest water contact angle with 45 ± 1 °, followed by SP05 with 29 ± 1 ° and SP10 with 19 ± 3 °. The extensive drying treatment of the PEMs releases more intrinsic water. In general, less intrinsic water should leave the PEMs more hydrophobic. The amount of removed water depends on the intrinsic water retention capacity of the multilayers. After 72 h extensive drying in nitrogen atmosphere, the water contact angle of negatively charged PEMs (SN) rises by around 10 ° (34 ± 1 ° for SN0, 41 ± 2 ° for SN05, 38 ± 1 ° for SN10). However, the positively charged PEMs (SP) do not change in a constant manner. The water contact angle on SP0 rises by 10 ° (to 55 ± 2 °). On SP05 the water contact angle rises by 37 ° (to 66 ± 6 °). The water contact angle on SP10, which was the most hydrophobic surface after short nitrogen drying, rises by 52 ° (to 71 ± 2 °), making SP10 the most hydrophilic surface after an extensive drying period.

The average roughness (10.8 ± 2.6 nm for SP05 and 13.7 ± 0.8 nm for SN05), root-mean-squared roughness (15.5 ± 3.8 nm for SP05 and 18.9 ± 1.0 nm for SN05) and the peak-to-valley roughness (171 ± 36 nm for SP05 and 185 ± 24 nm for SN05) show no clear difference between SP05 and SN05 films. The average roughness (13.9 ± 0.5 nm for WP and 16.7 ± 0.5 nm for WN), root-mean-squared roughness (17.7 ± 0.6 nm for WP and 21.6 ± 0.7 nm for WN) and the peak-to-valley roughness (160 ± 20 nm for WP and 180 ± 9 nm for WN) show no clear difference between both SP/SN and WP/WN surfaces. The self-defined peak-count roughness revealed a clear difference between SP/SN and WP/WN. The peak-count roughness of SP and SN (2.2 ± 0.2 and 2.1 ± 0.3 peaks per µm) is significantly higher by 223 % and 166 % in comparison to WP and WN (0.7 ± 0.1 and 0.8 ± 0.2 peaks per µm).

The elasticity of PEM was measured under vertical stress (Young's modulus) and horizontal stress (Shear modulus).

SP05 shows a 28 % higher Young's modulus (measured by AFM) in comparison to SN05 (84.8 ± 30.0 kPa for SP05 and 65.9 ± 12.9 kPa for SN05). The PEMs WP and WN show a significantly lower Young's modulus in comparison to SP and SN. In comparison to SP the Young's modulus of WP is reduced by 96 % (WP Young's modulus is 3.6 kPa) and Young's modulus of WN is reduced by 98 % (WN Young's modulus is 1.7 kPa). This elastic property under vertical pressure is directly based on the interconnectivity of PE chains inside the multilayers. The reduced accessibility of charged functional groups on WP/WN multilayers leads to less repulsion of charges on single polymer chains, which leads to more coiled conformations. Additionally, the reduced charges lead to weaker attraction of PE chains when building multilayers. PEMs formed from HA and CHI result in weaker connected, softer and bulkier multilayers, when compared to PEMs from PSS and PAH.

Shear modulus and shear viscosity was characterized on SP/SN films with variation in electrolyte concentration of the deposition solution. The shear elasticity of the films (shear modulus by QCM-D) is similar between SP05 and SN05 coatings (0.3 ± 0.1 MPa for SP05 and 0.4 ± 0.3 MPa for SN05). Shear viscosity of SN05 shows a 125 % higher value in comparison to SP05 (4.3 ± 0.3 g·m-1·s-1 for SP05 and 9.6 ± 0.8 g·m-1·s-1 for SN05).

The film shear elasticity by QCM-D does not correlate with the electrolyte concentration in the deposition solution. The lowest film shear modulus was measured on PEMs from deposition solutions with 0.5 M electrolyte concentration (0.2 ± 0.1 MPa for SP05 and 0.4 ± 0.3 MPa for SN05). Decreasing or increasing the electrolyte concentration in deposition solutions forms PEM films with higher film elasticity. Films from 1.0 M electrolyte concentration in the deposition solution have 0.3 ± 0.1 MPa for SP10 and 0.9 ± 0.6 MPa for SN10. Films from deposition solutions without electrolytes form the PEM films with the highest film shear elasticity (0.8 ± 1.1 MPa for SP0 and 1.2 ± 0.9 MPa for SN0).

The film viscosity by QCM-D behaves in a similar manner to film elasticity. The PEM from deposition solutions with 0.5 M electrolytes yield films with the lowest shear viscosity in the corresponding groups with the respective surface charge (with 4.3 ± 0.3 MPa for SP05 and 9.6 ± 0.8 MPa for SN05). An increase or decrease in electrolyte concentration in the deposition solution increases the film viscosity. The coatings SP10 and SN10 have 5.7 ± 0.3 MPa and 13.1 ± 4.7 MPa, respectively. The coatings from deposition solutions without electrolytes show the highest film viscosity, with 16.5 ± 8.3 MPa for SP0 and 13.2 ± 4.0 MPa for SN0.

Upon PEM build-up the adsorbed mass per PE layer was monitored by QCM-D. The most noticeable difference between PEMs with different electrolyte concentrations is the adsorbed mass of the completed coatings with 5 or 5.5 bilayers. In comparison to SP05 adsorbed mass, SP0 has 78 % less, SN0 has 73 % less, SP05 has 11 % more, SP10 has 35 % more and SN10 has 37 % more adsorbed mass. The electrolyte content of the deposition solutions directly affects the bulk of adsorbing coatings, the 0 M NaCl PEMs are the thinnest and the 10 M NaCl PEMs are the bulkiest.

The positively charged PAH always adsorbed in higher quantities than the negatively charged PSS. By matching the mass of charged PE inside a PEM, the mass of monomers and the charge per monomer, the total intrinsic charges were calculated. As negative charges compensate positive charges, and the amount of charged monomers is inequal, a positive excess charge was identified and calculated.

The excess charge of the SP/SN system is always in the positive because PAH adsorbs in higher quantities than PSS. The positive excess charge rises in correlation with the electrolyte concentration in the deposition solutions independent on the charge of the terminating layer. Coatings from deposition solutions without electrolytes yield the least positive excess charge (5.9 ± 1.1 nmol·cm^{-2} for SP0 and 5.7 ± 0.8 nmol·cm^{-2} for SN0). SP05 and SN05 yield 26.2 ± 4.1 nmol·cm^{-2} and 29.9 ± 3.2 nmol·cm^{-2}, respectively. The coatings SP10 and SN10 yield the highest positive excess charge with 42.0 ± 2.6 nmol·cm^{-2} and 40.6 ± 3.6 nmol·cm^{-2}, respectively.

The precise content of intrinsic water and thickness of SP/SN PEM with variation of electrolyte concentration in deposition solutions was analyzed from reflectivity curves and scattering length densities measured by neutron reflectometry.

The scattering light density (SLD) of the PEM showed a certain pattern. The SLD of negatively charged (SN) coatings at the same electrolyte concentration in the deposition solution was always higher than of the positively charged counterpart (SP). The difference in SLD between SP and SN was steadily increased with the electrolyte concentration of the deposition solution. The intrinsic water volume fraction of PEM films was directly calculated from the SLD values.

The positively charged SP films showed an incremental increase in SLD and, respectively the water content with the electrolyte concentration in the deposition solution. The negatively charged SN coatings showed an incremental decrease in SLD and water content with the electrolyte concentration in the deposition solution. The SP/SN films can be order from least to

most water volume fraction in order of SP10 (23.9 %) < SP05 (27.3 %) < SP0 (28.5 %) < SN0 (29.1 %) < SN05 (29.4 %) < SN10 (32.3 %).

Chapter 4 - Cell adhesion and protein adsorption on polyelectrolyte multilayer coated surfaces

The interaction between the biological tissues and material surfaces or more precisely the local interaction between the single cells and the materials physico-chemical surface properties plays an important role for the implantation processes in medicine. The adhesion, proliferation and viability of cells, seeded on the modified surfaces, were measured and are presented in this chapter. Despite the very low thickness of only few hundreds of nanometers, the PEMs are able to not only switch a surface from non-cell-adhesive to cell-adhesive or vice versa, but also enable the precise control of the degree of cell adhesion. Proteins that adsorb prior to events of cell interactions, play an important role in the cell adhesion. The change of the deposition conditions of PEMs or the type of applied PEs allow to precisely control the surface properties of the PEMs. In turn the surface properties govern the protein adsorption on the surfaces and consequently regulate the cellular behavior. Human umbilical vein endothelial cells were chosen because they closely resemble endothelial cells, which are the initial point of contact between cells and the stent implant during the stenting procedure, leading to potential in-stent restenosis.

4.1 Cell adhesion on surfaces modified with polyelectrolyte multilayers from poly(styrene sulfonate)/poly(allylamine hydrochloride) (PSS/PAH) and hyaluronic acid/chitosan (HA/CHI)

Biological *in-vitro* cell adhesion and proliferation measurements were performed to study the effect of PEM coated surfaces on the behavior of HUVECs. Cell adhesion and proliferation on PEM from PSS/PAH and HA/CHI from deposition solutions with constant 0.5 M NaCl (for PSS/PAH) or 0.005 M NaAc (for HA/CHI) concentrations were characterized. The substrates for the coatings were non-treated polystyrene multiwell plates, which also served as negative control. The coatings were positively (SP or WP) or negatively (SN or WN) charged. HUVECs were seeded on PEM coated surfaces and after 24, 48, 72 h of incubation the adhered cells were microscopically observed. The fluorescence microscopy images are presented in figure 4.1. The images are compared to optical microscopy images presented in figure 4.2. The cellular metabolic activity was measured by Resazurin assay.

The SP05 and SN05 surfaces (positively charged SP05 and negatively charged SN05) change the adhesion and proliferation of HUVEC compared to the non-treated polystyrene surfaces that were used as negative controls (multiwell plate for suspension culture, polystyrene PS). The HUVEC adhesion on SP05 and SN05 surfaces is comparable in cell amount and morphology to

measurements on the positive control of tissue culture treated polystyrene (TCT PS). HUVECs on WP and WN surfaces show very poor adhesion. On WP and WN, HUVEC are scarcely present, show a globular morphology and are very loosely attached to the surface. The cells are attached so loosely that careful staining and rinsing steps wash them off.

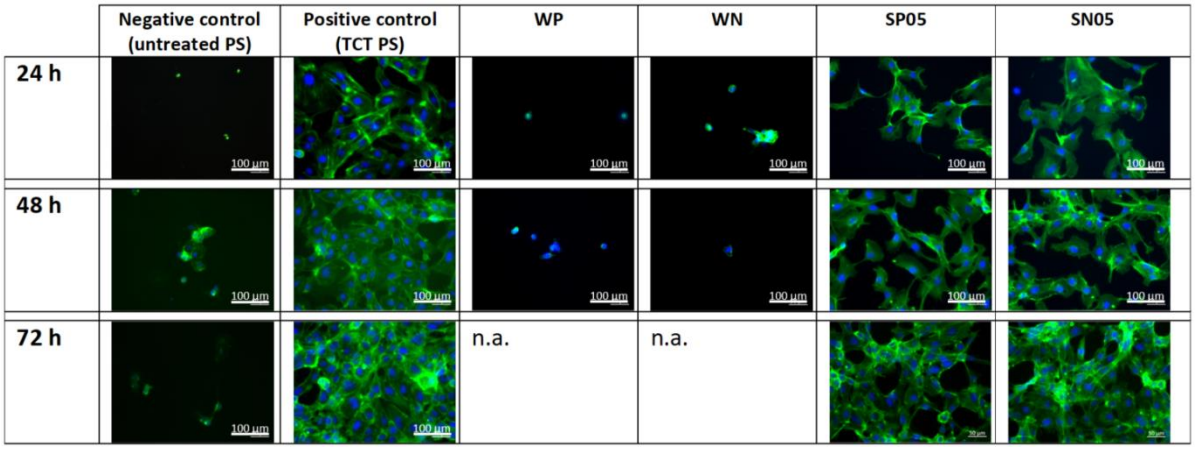

Fig. 4.1. Fluorescence microscopy images of adhered HUVECs on different PEM surfaces and controls after 24, 48, 72 h incubation. Negative control is hydrophobic untreated polystyrene, positive control is tissue-culture-treated polystyrene. Cytoskeleton is stained with fluorescent phalloidin (green) and cell nuclei are stained with Diamidino-phenylindole (DAPI, blue). See table 3.1 on page 38 for abbreviations.

The light microscopy imaging in figure 4.2 reveals additional information about adhesion of HUVEC on WP and WN surfaces. Unlike to the fluoresce imaging many cells are visible on the surface. Similarly, to observation on fluorescence images, the HUVEC morphology on WP/WN surfaces is different than morphology on positive control (TCT PS) or SP05/SN05. On WP and WN the cells do not show a spread morphology but a circular loosely attached shape. In figure 4.2 the WP and WN images after 24 h incubation show a higher number of cells than on either 24 h or 72 h. The explanation is that the HUVECs poorly adhere but are still able to weakly attach and are able to proliferate. In the images after 48 h the cells had time to proliferate and reach a higher cell number. According to the used HUVEC cultivation protocol the cell culture medium was changed for fresh medium after each two days. Immediately after the images were taken the medium was changed. In this process loosely attached HUVECs were washed off and could no longer proliferate to increase numbers for the images at 72 h. This is also an explanation why in fluorescence imaging only very few cells are observable on WP/WN surfaces. The several staining and rinsing steps require repeated washing of the wells, which removed loosely attached cells.

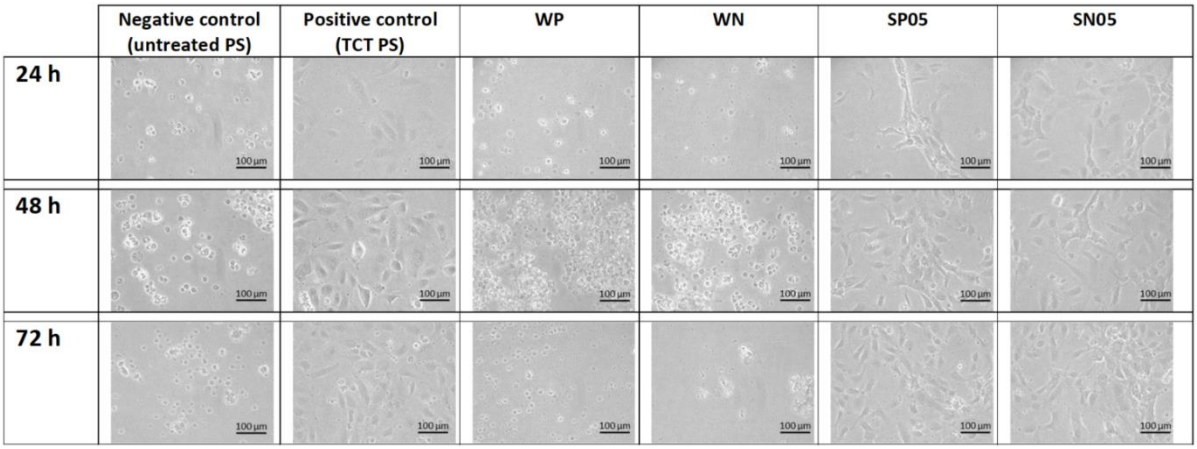

Fig. 4.2. Light microscopy images of adhered HUVECs on different PEM surfaces and controls after 24, 48, 72 h incubation. Negative control is hydrophobic untreated polystyrene, positive control is tissue-culture-treated polystyrene. See table 3.1 on page 38 for abbreviations.

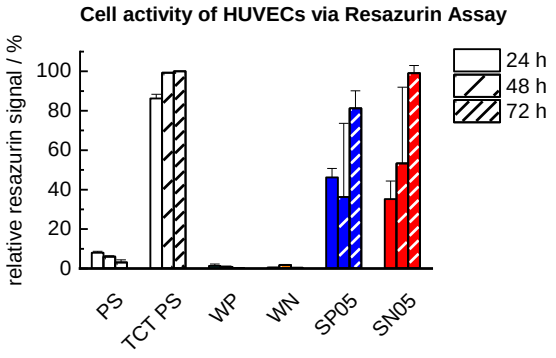

Fig. 4.3. Resazurin signals (cell viability) of HUVEC on PEM from strong and weak PE over 24, 48 and 72 h. Negative control is hydrophobic untreated polystyrene, positive control is commercially tissue culture treated polystyrene. All results are normalized to PC at 72 h (maximal metabolism ≙ 100 %). See table 3.1 on page 38 for abbreviations.

Figure 4.3 presents the data of cell viability measured by Resazurin tests. By citrate cycle Resazurin is reduced to fluorescent Resorufin, which can be spectroscopically measured. The citrate cycle is a housekeeping reaction in all living cells and representative to the cellular metabolic activity and respectively the cell viability. The results show that on SP05 and SN05 coated surfaces the cell activity is comparably strong. The initial adhesion is lower than on the positive control (PC, TCT PS) but magnitudes higher than on either the negative control (NC, untreated PS) or the WP/WN surfaces. After 72 hours the cell viability on SP and SN is comparable to numbers on tissue culture treated control surfaces. Due to poor attachment of cells, the measured viability on the surfaces NC (untreated polystyrene), as well as WP and WN is very low. It was observed that the signal decreased from ~2 to 0 % resazurin signal over the timespan of 72 h, which is hardly visible in figure 4.3. The WP/WN surfaces are not suitable for HUVEC adhesion, as even initially attached cells are dying off or are washed off over time.

The HUVEC adhesion on PEM from PSS/PAH and HA/CHI does not correlate with zeta potential of the surfaces (figure 3.2) or the contact angle of water (figure 3.1) on these surfaces. One speculation was that a lower contact angle (higher surface energy) might increase the cell

adhesion, but there is a clear difference in contact angle on the coatings SP05 and SN05 and no difference in cell adhesion on these surfaces.

The most pronounced correlation of HUVEC adhesion is observed towards mechanical elastic modulus under vertical stress (Young's modulus) of the coatings measured (figure 3.6) and the surface roughness calculated by the peak-count method (figure 3.5-d).

It was already observed and published in literature that cell types such as chondrocytes, chondrosarcoma cells and fibroblasts change their behavior depending on surface stiffness and roughness [Elbert *et al.* 1999, Richert *et al.* 2004]. Every cell-surface system is different and, in our findings, it was observed that HUVECs differently react on PEM coatings with variation in stiffness and roughness.

Our findings show that adhesion of HUVECs on PEM surfaces does not depend on either surface hydrophobicity (water contact angle) or surface charge (zeta potential). Both, the adhesion and proliferation of HUVEC show increase on rougher surfaces (according to peak-count roughness) and on stiffer surfaces (higher Young's modulus).

4.2 Protein adsorption and cell adhesion on polyelectrolyte multilayers from poly(styrene sulfonate)/poly(allylamine hydrochloride) (PSS/PAH) with variation of electrolyte concentration in the deposition solution

HUVECs showed increased adhesion on SP05 and SN05 surfaces and poor adhesion on WP and WN surfaces. However, two points were still uncertain. The studied PEM coatings consist of different PE pairs and thus had different surface chemistry. Although the surface properties were thoroughly characterized, the different surface chemistry might have an effect on cellular adhesion. Additionally, it is known that biological cells do no directly interact with surfaces but rather with proteins that adsorb from cell culture medium, before cell adhesion takes place. In the following chapter a study was conducted on a variation of PEM coatings with same surface chemistry with a thorough focus on protein adsorption from cell culture medium.

The adhesion and viability of HUVECs were studied on PEM coatings from PSS/PAH multilayers with variation of electrolyte concentration in the deposition solution. In these experiments the PEMs were not applied directly to polystyrene multiwell plates, but on substrates that were placed as inlets into the wells. The applied substrates were Au-coated Si-wafers to ensure the same substrate surface as Au-coated QCM-D sensor crystals used in

measurements of protein adsorption. The cell adhesion was measured after 48 h by fluorescence microscopy and cell number was obtained by optical quantification from these images. The cell viability was measured by Resazurin Assay. The protein adsorption was measured by incubating PEM-coated QCM-D sensor crystals with cell culture medium, which was also used for HUVEC cultivation.

4.2.1 Biological characterization of HUVECs adhesion and viability on polyelectrolyte multilayers from poly(styrene sulfonate)/poly(allylamine hydrochloride) (PSS/PAH) with variation of electrolyte concentration in the deposition solution

The tested PEMs were based on PSS/PAH multilayers with different concentrations of electrolyte (NaCl) in the deposition solution (as illustrated in Table 3.01). The number following the SP or SN abbreviation stands for the concentration of electrolyte (NaCl) in the deposition solution (0 = no NaCl; 05 = 0.5 M NaCl; 10 = 1.0 M NaCl). HUVECs were incubated for 48 h on PEM coated Au-Si-wafers. These substrates were chosen due to similarity to QCM-D Au-coated sensor crystals, which were used for protein adsorption studies. The cells were counted microscopically from averaging and extrapolating cell numbers on five spots on the substrate, measuring in triplicate.

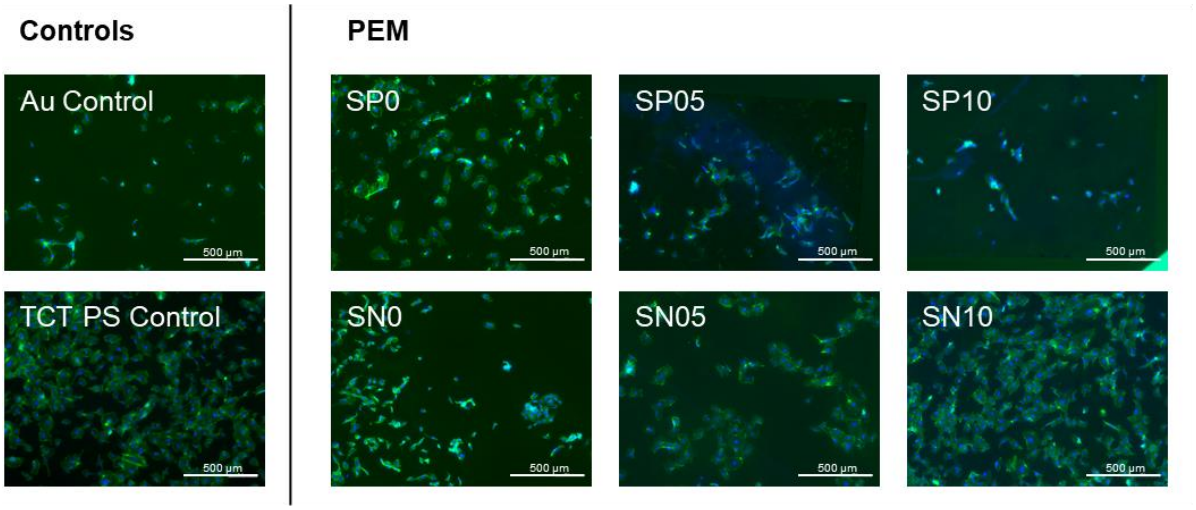

Fig. 4.4. Microscopic imaging of HUVECs after 48 h incubation on PEM coated and uncoated Au Wafers and tissue culture treated (TCT) polystyrene microtiter plate, stained with Phalloidin (cytoskeleton) and DAPI (nucleolus) [Rudt *et al.* 2021]. See table 3.1 on page 38 for abbreviations.

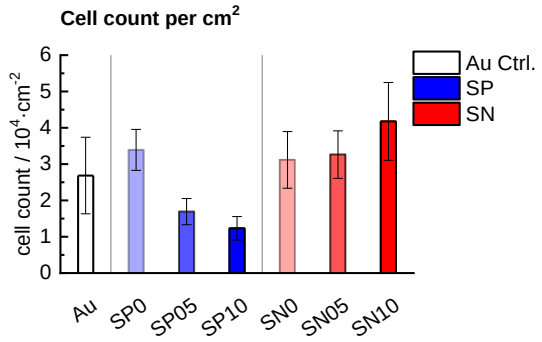

Fig. 4.5. Amount of adhered HUVEC cells on PEM coated Au-Si-wafers after 48 h incubation, calculated by averaging counts from microscopic images. Blue and red bars show number of adhered cells on positively (PAH) and negatively (PSS) terminating PEMs from deposition solutions with NaCl concentrations of 0 M, 0.5 M and 1.0 M respectively [Rudt *et al.* 2021]. See table 3.1 on page 38 for abbreviations.

Figure 4.4 presents adhered HUVECs on the PEM-coated Au-Si-wafers and figure 4.5 shows the corresponding cell number of adhered cells on the surfaces. On positively charged PAH-terminated PEMs (SP), the number of adhered cells decreases with increase of NaCl concentration in the deposition solution. On negatively charged PSS-terminated PEMs (SN), the number of adhered cells shows no significant change with the increase of NaCl concentration in the deposition solution. Results of cell viability assay (figure 4.6-A) show similar trend of cell activity on PEM substrates. Increase of the electrolyte concentration in the PEM deposition solutions leads to decrease of the cell activity on PAH-terminated PEMs. The cellular activity on PSS-terminated PEMs is equally high and does not change with a variation of electrolyte concentration in the deposition solution.

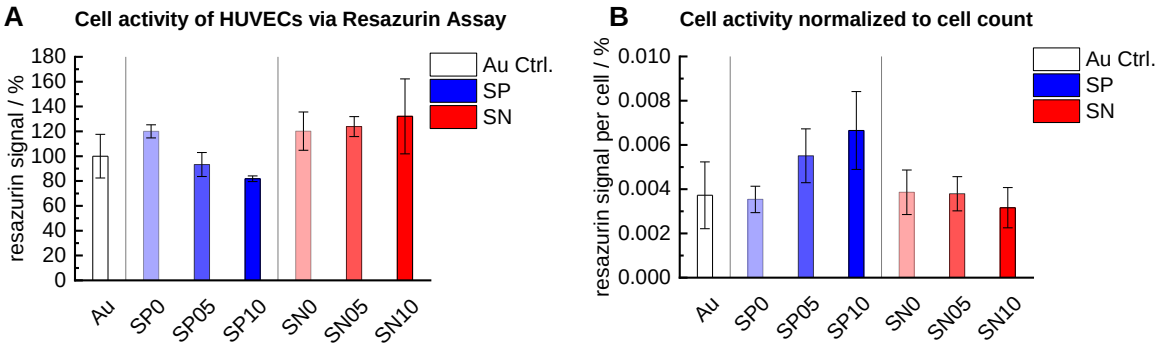

Fig. 4.6. (A) Cell viability by resazurin signal normalized to the value of uncoated Au control. **(B)** Cell viability by resazurin signals normalized to the number of adhered cells. Resazurin signals of HUVECs after 48 h incubation on PEM coated substrates: white bar shows signal of HUVECs activity on uncoated Au control, blue bars show signal on PAH-terminated PEMs, red bars show signal on PSS-terminated PEMs. Tested PEMs varied in NaCl concentration in the deposition of 0 M, 0.5 M and 1.0 M [Rudt *et al.* 2021]. See table 3.1 on page 38 for abbreviations.

The cellular activity normalized to the number of cells is shown in figure 4.6-B. This calculation presents the degree of metabolic activity per single cell on tested PEM coatings. The cells are equally active on the bare Au surface and PSS-terminated PEMs, which also do not show an effect of the NaCl concentration in the deposition solution. In the case of PAH-terminated PEMs, the activity of the singular cells depends strongly on the electrolyte concentration in the deposition solution. An increase of electrolyte concentration in deposition solutions during PEM build-up, leads to increased activity per cell on these surfaces. This effect might be explained unattached to surface properties of the substrates, as the highest cell activity per cell is measured on samples that at the same time show the smallest number of adhered cells (see figure 4.5). HUVECs are in need of cell-cell interactions and are easily irritated if neighbor cells are not present. If no contacting cells are nearby, by increasing the metabolism the HUVECs might mobilize energy reserves to migrate and find other cells in a struggle for survival. This could be one explanation of increased cellular activity on surfaces at lower cell counts.

The number of adhered cells cannot be explained by zeta potential of PEM surfaces (from figure 3.8). Zeta potential of surfaces shows either +40 or -40 mV independent of NaCl concentration in the PEM deposition solutions. However, cellular adhesion shows a certain dependence on PEM surfaces from deposition solutions with different NaCl concentrations. The contact angle was measured in swollen state and dry state of PEMs (presented in figure 3.10). For biological experiments, the PEMs are always in contact with water-based solutions (cell culture medium). Thus, the contact angle after short nitrogen drying might be more relevant to cellular sensing in the water-based cell culture medium. The contact angle in swollen state to some extend correlates with the number of adhered cells. PSS-terminated PEMs show a contact angle independent on NaCl concentration of the deposition solution. Similarly, the number of adhered cells does not significantly change on these surfaces. The PAH-terminated PEMs show a decreasing contact angle with increase in NaCl concentration in the deposition solutions. The number of adhered cells also decrease with increase in NaCl concentration of the deposition solution. However, total number of adhered cells is higher on PSS-terminated surfaces than on PAH-terminated surfaces. This cannot be explained by the values of the contact angle or respectively the degrees of surface energy on these surfaces.

4.2.2 QCM-D measurement of protein adsorption on polyelectrolyte multilayers from poly(styrene sulfonate)/poly(allylamine hydrochloride) (PSS/PAH) with variation of electrolyte concentration in the deposition solution

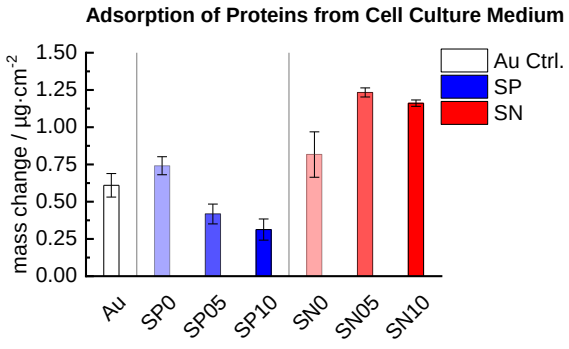

Fig. 4.7. Adsorbed protein layer on PEM coated substrates, measurement by QCM-D and mass calculation via Sauerbrey. White bar shows mass of proteins on clean Au surface. Blue and red bars show mass increase on PAH- and PSS-terminating PEMs from deposition solutions with NaCl concentrations of 0, 0.5 and 1 M respectively. See table 3.1 on page 38 for abbreviations.

The protein adsorption, which always takes place before any cell interaction, needs to be taken into account, when studying cell behavior on surfaces. PEM coated surfaces were incubated with HUVEC cell growth medium for one hour while simultaneously monitored by QCM-D. Components from the cell culture medium adsorb on top of each sample after incubation. The QCM-D technique was utilized to measure adsorption of components (mostly proteins) from the cell culture medium on the surfaces of PEMs prepared with different NaCl concentration in the deposition solution (figure 4.7). The amount of adsorbed proteins, practically in the limits of the experimental error, does not depend on the NaCl concentration in the PEM forming solutions for PSS-terminated samples (SN). Contrary, the amount of absorbed proteins clearly depends on the NaCl concentration in the PEM deposition solutions for PAH-terminated samples (SP). On SP coated surfaces, the amount of adsorbed proteins decreases with the increase of the NaCl concentration in the PEM deposition solutions.

4.2.3 The effect of HUVEC culture medium protein adsorption on the adhesion behavior of HUVECs

The cellular behavior (adhesion, activity) of HUVEC was correlated to the measured surface properties of PSS/PAH PEM coatings from deposition solutions with variation in electrolyte concentration. The number of adhered cells on PEM coated surfaces (presented in figure 4.5) proportionally correlates with the amount of cell culture medium protein adsorption (figure 4.8). This finding is confirmed by observed clear correlation of total cellular activity with the amount of protein adsorption (shown in figure 4.9).

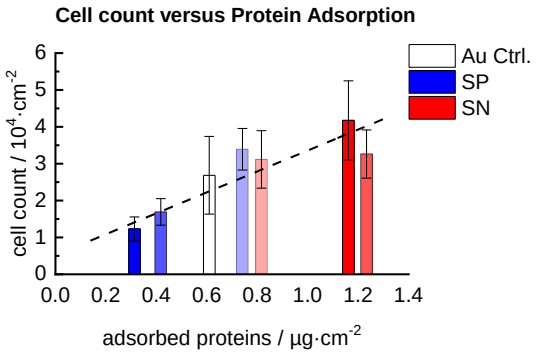

Fig. 4.8. Plot of **cell count** versus amount of adsorbed proteins after incubation in cell culture medium. The line is only a guide for the eye.

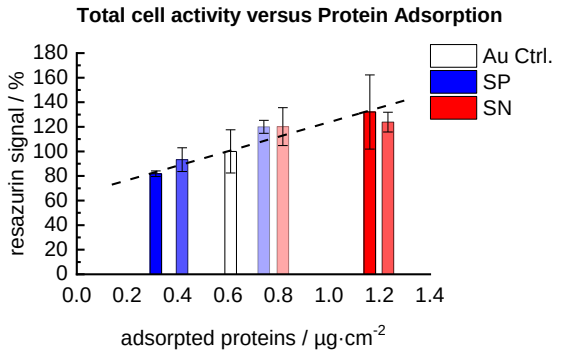

Fig. 4.9. Plot of **cell activity** versus amount of adsorbed proteins after incubation in cell culture medium. The line is only a guide for the eye.

The number of adhered cells increases nearly linear with the increased amount of adsorbed protein. This indicates that properties of modified surfaces might not directly affect cell adhesion but instead affect the protein adsorption, which in turn governs the cellular adhesion.

An important observation was that the amount of proteins strongly correlates with the number of adhering biological cells. This was confirmed through independent biological experiments: one involving microscopic cell counting and the other a colorimetric cell activity assay. The trend is consistent – more proteins on the surface lead to higher cell numbers and increased cell activity. Both biological readouts show a strong correlation with the amount of adsorbed protein, although the degree of the effect of protein on cell adhesion varies between the methods. This variation becomes evident when applying a ratio to the biological readouts. By dividing the total cellular activity (Resazurin Assay) of a sample by the number of adhered cells (microscopic analysis), we obtain the metabolic activity per single cell. Plotting this ratio against the amount of adsorbed proteins reveals an interesting observation.

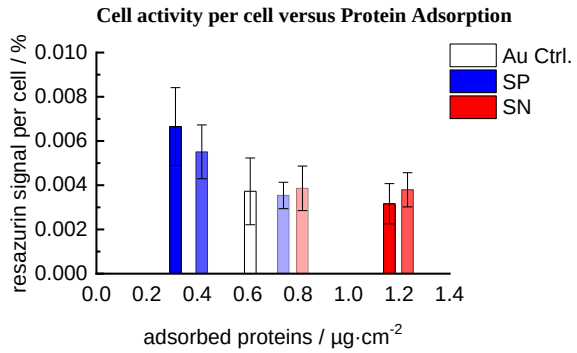

Fig. 4.10. Plot of cell activity normalized to cell count versus amount of adsorbed proteins. See table 3.1 on page 38 for abbreviations.

The cell activity normalized to the number of cells over the amount of adsorbed proteins is presented in figure 4.10. It indicates that cells show an increase in cellular activity under a specific limit of adsorbed proteins of around 0.6 µg/cm^2. The reasons might be that the activity of the cells increases because of the low amount of adsorbed cell culture medium proteins or because of the lack of neighboring cells (low cell count on these surfaces). Hypothetically, these reasons might interconnect. The cells might adhere in lesser quantities on surfaces with less adsorbed protein and therefore experience the lack of neighboring cells, which leads to an increased metabolism.

Results show that the number of adhered cells and their activity correlates with the amount of adsorbed proteins (or other components of the cell culture medium) on these surfaces. Also, the normalized activity reveals a certain dependance/ or threshold on the amount of proteins on surfaces.

4.2.4 Analysis of protein adsorption on polyelectrolyte multilayers from poly(styrene sulfonate)/poly(allylamine hydrochloride) (PSS/PAH) with variation of electrolyte concentration in the deposition solution

It was observed that protein adsorption differs on surfaces modified with PEM from deposition solutions with variation in electrolyte concentration. The question remains of why proteins adsorb differently on these surfaces. Specific protein adsorption is mainly governed by electrostatic interaction of complementary functional groups between protein and surface (e.g., positive charge on negative charge). However, all tested positively charged PEM surfaces (SP) and all negatively charged PEM surfaces (SN) show a constant zeta potential of either +40 mV or -40 mV (see figure 3.8). Therefore, this cannot be the only driving factor for the protein adsorption.

The adsorbed proteins from HUVEC cell culture medium consist mostly of fetal calf serum, but also other surface-active substances such as heparin. Any charged molecules from the medium can also act as electrolytes and may interact with the charged surfaces of the PEM. The protein adsorption on the bare gold surface used as control shows a moderate protein adsorption (figure 4.7), however, the protein adsorption on PEMs depends on NaCl concentration in the deposition solutions and the charge or the terminating PEs. On negatively charged PSS-terminated coatings, cell culture medium components adsorb on PEMs with increasing NaCl concentration in the deposition solutions, showing minor dependence. On positively charged PAH-terminated coatings, the protein adsorption is lower but shows dependence on the NaCl concentration in the deposition solution. To explain this adsorption, further experiments with simple BSA protein solution were conducted and analyzed.

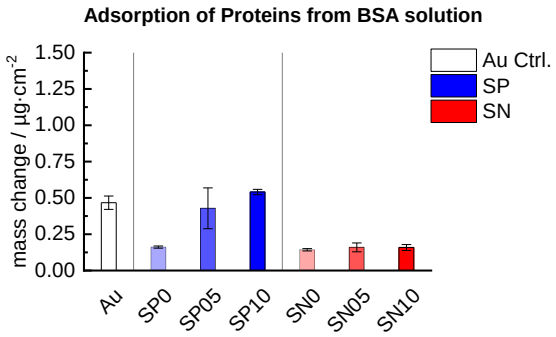

Fig. 4.11. Adsorbed mass of BSA from pure 1 mg/mL BSA solution on PEM coated substrates. White bar shows mass of proteins on clean Au surface. Blue and red bars show adsorbed masses on PAH- and PSS-terminating PEMs from deposition solutions with NaCl concentrations of 0, 0.5 and 1 M respectively [Rudt *et al.* 2021]. See table 3.1 on page 38 for abbreviations.

Bovine serum albumin (BSA) is the main protein in the fetal calf serum (FCS) and has an isoelectric point at pH(I) ≈ 5. Thus, in physiological conditions and in the cell culture medium (pH = 7.4) it is negatively charged. The isoelectric point of the complete HUVEC medium was measured by light scattering, the result was pH(I) = 3.5 ± 0.5. Generally, in cell culture conditions (pH = 7.4) the majority of proteins must be negatively charged. The expectation would be that the negatively charged FCS components adsorb stronger on positively charged surface, however, a control experiment with 1 mg/mL pure BSA solution in TRIS buffer (pH = 7.4) showed much different features (figure 4.11) compared to protein adsorption from HUVEC cell culture medium (figure 4.7).

The BSA adsorption on negatively charged PSS-terminated surfaces is minor. Most probably, this is due to repulsion of negatively charged BSA molecules at these conditions. The adsorption is higher on positively charged PAH-terminated PEMs and shows a dependence on the electrolyte concentration in the deposition solutions.

The adsorption of BSA or the adsorption of protein components from cell culture medium cannot be fully understood and explained by sole comparison to the zeta potential of the surface or its surface energy (related to contact angle of water). Another property of the PEMs that changes with the electrolyte concentration in deposition solution is the excess charge in the whole film. This concerns not only the surface charge that is related to the zeta-potential, but also the number of free charges in the intrinsic volume of the film. The calculation and analysis of intrinsic excess charge was described and explained by [Zan *et al.* 2012].

Next to entropic and hydrophobic interaction, the electrostatic interaction is the main driving force of PEM formation. Essentially, the charged PE in the PEM form complexes and compensate one another's charge. Mismatches in number of positive and negative charges (excess charges) can be made visible with QCM-D by measurements of adsorbing total mass of the polyelectrolytes and consideration of charges per adsorbing PE molecule. Excess charges are formed by PEs that are not fully compensated by the oppositely charged PEs. Instead, these excess-charged PEs remain compensated by counter ions. The added charge per layer can be calculated using the mass of adsorbed PE (Δm) and the mass of corresponding monomer mass (M_{PE}). The positive excess charge (Σ) is calculated by adding all total positive charges and by subtracting all total negative charges. A positive number of Σ means that less negative charges are present than positive charges, equaling to an increase in positive excess charge. The net excess of positive polyelectrolyte charge per area (Σ), is described by eq. 20, as published in [Zan *et al.* 2012].

$$\Sigma = \sum_{iPEI}^{N} \frac{\Delta m^i}{M_{PEI}} + \sum_{iPAH}^{N} \frac{\Delta m^i}{M_{PAH}} - \sum_{iPSS}^{N} \frac{\Delta m^i}{M_{PSS}} \qquad \text{(eq. 20)}$$

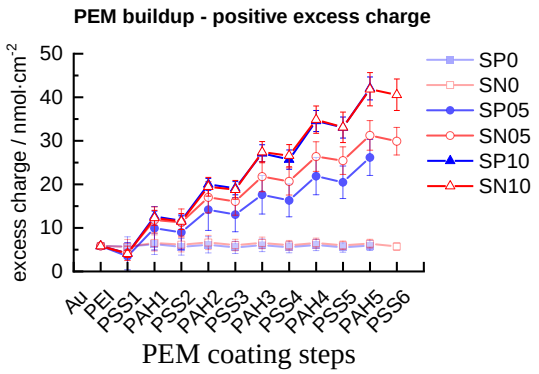

Fig. 4.12. Excess charge per area Σ, calculated from QCM-data. PEMs shown were prepared from deposition solutions with 0 M (squares), 0.5 M (circles) and 1.0 M (triangles) NaCl concentrations [Rudt *et al.* 2021]. See table 3.1 on page 38 for abbreviations.

The excess charge of PEM was calculated from QCM-D data by summing up total intrinsic positive and subtracting negative charges, which would compensate positive charges (figure 4.12). No excess charge forms in the case of PEM prepared from solutions without electrolytes (SP0, SN0). Both polyelectrolytes fully compensate each other. The net excess charge is mostly positive in PEMs from deposition solutions containing higher electrolyte concentrations. An increase in electrolyte NaCl concentration in the deposition solution nets a higher positive excess charge of the completed PEM.

Considering both, the zeta potential and the positive excess charge, the BSA adsorption on multilayers (figure 4.11) can be explained as follows. On negatively charged PEMs, the surface charge is the more dominant force and repels negatively charged BSA molecules, which leads to low adsorption. On positively charged PEMs, the BSA is attracted to the surfaces by the surface charge and is enabled to interact with the surface.

At the surface another effect comes into play, which was discovered in studies of exponential growth of PEMs might contribute to the explanation [Dubas & Schlenoff 1999, Kolasińka *et al.* 2005, Lösche *et al.* 1998, Schönhoff 2003]. It describes that intrinsically located polyelectrolyte chains are pulled towards the PEM surface when the PEM is surrounded by oppositely charged polyelectrolyte solution. If the chains are mobile enough, they diffuse from inside towards the surface of the multilayer and there can affect adsorption of the following polyelectrolyte layers.

In our studied system, the excess charge equals PAH charges that are not compensated by PSS charges. These PAH charges remain compensated by Cl^- counterions. By not binding/complexing to PSS chains, the PAH chains are less restricted and more mobile. In PEMs from higher NaCl concentration in the deposition solution, PAH chains have more mobility and are able to diffuse towards the surface, approaching the adsorbing BSA molecules. On the surface BSA adsorbs on top of the surface PE layers, as well as diffused parts of intrinsic PAH

chains. Therefore, on positively charged PEMs from higher electrolyte concentrated deposition solutions more BSA is able to adsorb onto the surface.

In regard of the adsorption of cell culture medium proteins (figure 4.7) the effect of PEM surfaces differs from BSA adsorption results. In this case, the positively charged components of the medium are more surface-active and interact with the surfaces. Heparin is a cell culture medium component that has a strong negative charge and therefore more affinity to adsorb on positively charged PEM surfaces than FCS. The amount of cell culture medium used for testing was 200 µL, which contained an amount of ~18 µg heparin. This would be enough to cover the whole testing surface of 1 cm^2 by ~15 fold of the highest measured total mass of adsorbed proteins. It is reasonable to assume that heparin is more surface-active and predominant than FCS. It is likely that heparin does not adsorb in its pure form but rather as a complex with FCS. Consequently, when complexed with heparin, FCS undergoes a charge inversion. On PSS-terminated PEM, the surface charge pulls heparin-FCS complexes towards the surface until coverage is reached. On PAH-terminated PEM, two kinds of repulsion affect the heparin-FCS complex adsorption. At first, the surface repels positively charged heparin. Secondly, intrinsic PAH molecules that are diffusing towards the cell culture medium solution may also contribute to repelling of heparin. This could explain why on PAH terminated PEMs with high positive excess charge the heparin adsorption is restricted the most.

4.2.5 Cell adhesion and viability dependence on the viscoelastic properties of the PEM coatings from poly(styrene sulfonate)/poly(allylamine hydrochloride) (PSS/PAH) with variation of electrolyte concentration in the deposition solution

As observed in the previous chapters, the cellular adhesion and proliferation is different on PEM coatings from PSS/PAH and HA/CHI, which might depend on surface mechanical elasticity in vertical direction (Young's modulus by AFM force microscopy in figure 3.6). This part focus on the interaction with the horizontally acting shear elasticity and viscosity. The studied PEM coatings are based on PSS/PAH from deposition solutions with varied electrolyte concentration (0 M, 0.5 M, 1 M NaCl) to keep surfaces with same surface chemistry and varied viscoelastic properties. The coatings were characterized by QCM-D with dissipation monitoring to determine elastic modulus (shear modulus) and shear viscosity of the film surfaces. The viscoelastic properties are characterized before and after exposition of PEM surfaces to cell culture medium to observe the effect of protein adsorption on the viscoelastic properties. Finally, the viscoelastic

properties are correlated with the adhesion and metabolic activity of HUVECs to determine the effect of viscoelastic surface properties on cellular behavior.

4.2.5.1 Effect of protein adsorption on viscoelastic properties of the PEM coatings from poly(styrene sulfonate)/poly(allylamine hydrochloride) (PSS/PAH) with variation of electrolyte concentration in the deposition solution

The film elasticity and film viscosity of PEM films after protein adsorption were measured by QCM-D according to measurements of plain PEM in chapter 3.3.4. At first, the aim was to measure properties of the standalone protein layer on top of the PEM multilayer. But due to native viscoelastic properties of the underlying PEM film and interactions between proteins and PEM, it was not possible to distinguish the influence of either the protein film or the underlying PEM film on the measured results. Thus, the protein-PEM film was regarded as an interrelated film, instead of two independent films. Likewise, it is most probable to assume that, upon protein absorption, the underlying PEM will not keep its native viscoelastic properties but change them when engaging interactions with the adsorbing proteins.

The film elasticity and film viscosity of the combined protein-PEM film was measured and calculated. The results are summarized in figure 4.14. For clearer comparison of viscoelastic film properties, the film shear elastic modulus and the shear viscosity are plotted before and after protein adsorption in figure 4.13. For more focus on only the film properties after protein adsorption, the properties of PEM-protein complex film are plotted in figure 4.14.

When comparing viscoelastic properties of the plain PEM films and PEM films after deposition of protein, following observations can be made. The mechanical properties of the surfaces coated with different PEM are changed after the protein deposition from HUVEC cell culture medium compared to the plain PEM measurements (in figure 4.13).

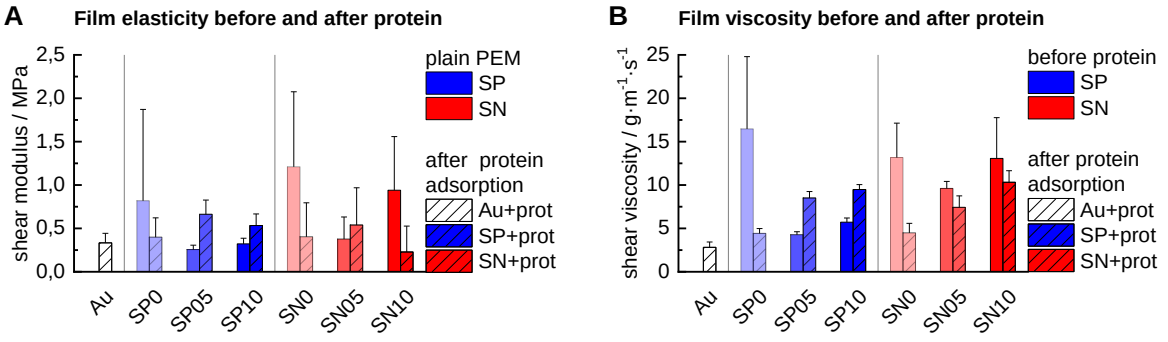

Fig. 4-13. Film elasticity/ shear modulus (**A**) and film dynamic shear viscosity (**B**) of PEM films for comparison purpose **before and after protein deposition** from HUVEC cell culture medium. SP0, SP05, SP10 – positively charged PEM from strong polyelectrolytes at NaCl concentration in the deposition solution of 0, 0.5 and 1.0 M; SN0, SN05, SN10 - negatively charged PEM from strong polyelectrolytes at NaCl concentration in the deposition solution of 0, 0.5 and 1.0 M, Au control surface after protein deposition. See table 3.1 on page 38 for abbreviations.

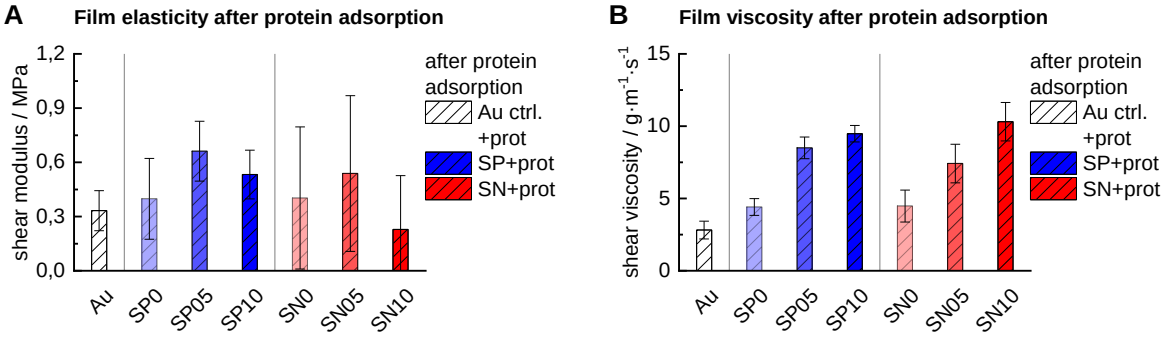

Fig. 4.14. Film elasticity/ shear modulus (**A**) and film dynamic shear viscosity (**B**) of **PEM-Protein films after protein deposition** from HUVEC cell culture medium. SP0, SP05, SP10 – positively charged PEM from strong polyelectrolytes at NaCl concentration in the deposition solution of 0, 0.5 and 1.0 M; SN0, SN05, SN10 - negatively charged PEM from strong polyelectrolytes at NaCl concentration in the deposition solution of 0, 0.5 and 1.0 M, Au control surface after protein deposition. See table 3.1 on page 38 for abbreviations.

Regarding the film elasticity (figure 4.13-A), after protein adsorption the measured values of all studied PEMs are equally high with no significant difference between the different underlying PEM surfaces. One explanation might be that the adsorbed proteins equilibrate the tensions of the native coating on all coatings or mask the underlying elasticity. Similarly, to measurements of plain PEM elasticities, it is possible that the used technique operates at the border of its limitations and a stable measurement of elasticity at two-digit nano-scale is not reliable. Hence, the variation of the measurements is high and results are not significantly different.

However, film viscosity measurements (figure 4.13-B) show an interesting finding. The variations are low and the tested films show a clear trend. On both terminations, positively

charged SP and negatively charged SN, the film viscosity increases with the electrolyte concentration in the deposition solutions of PEMs.

The PEMs deposited from deposition solutions with higher electrolyte concentrations contain more adsorbed mass (see figure 3.9) and therefore have more free charges (figure 4.12). In deposition solutions, the high electrolyte content shields the charges of PE in solution and leads to a more coiled conformation upon adsorption in comparison to PE in low electrolyte content solutions, which have pronounced equally charged groups that repel each other and lead to a more linear conformation.

Upon adsorption, the PE from high electrolyte solutions partly keep their coiled or linear structure. This leads to a multilayer of coiled PE chains, which maintain available space within the coils and the possibility of intrinsically bind opposite charge molecules such as proteins. One assumption is that adsorbing proteins on these coiled PEMs are not only able to adsorb on the outmost surface, but also penetrate inside the multilayer, where they can occupy and interlink the spare charges of the PEs. This leads to an effect of strengthening the intrinsic PE interactions comparable to crosslinking by electrostatic interaction and consequently results in higher interconnectivity and higher viscosity of the films.

4.2.5.2 Cell adhesion and viability dependence on the viscoelastic properties of the PEM coatings from poly(styrene sulfonate)/poly(allylamine hydrochloride) (PSS/PAH) with variation of electrolyte concentration in the deposition solution

The number of adhered cells, cellular activity, and cellular activity normalized to cell count were plotted over the shear modulus and the dynamic shear viscosity of PEM films after protein adsorption from HUVEC cell culture medium to determine correlations between cellular behavior and viscoelastic surface properties. Figure 4.15 presents the cellular behavior over the shear modulus and figure 4.16 presents the cellular behavior over the shear viscosity. For clarification, positively charged surfaces (SP) and negatively charged surfaces (SN) were plotted separately.

The shear modulus shows no distinct effect on cellular behavior. Several explanations for this observation are probable. (1) It might be that the amount of proteins and surface viscosity are more important in cellular mechanical sensing and therefore the cellular behavior is primary changed by them, instead of surface elasticity. (2) The surface elasticity might be important for cellular behavior but the change of surface elasticity by variation of electrolyte concentration in the deposition solutions of PEM does not achieve a strong enough change to trigger a different

cellular response. In the studied range of elasticity, biological cells might still recognize surfaces as equally stiff/soft. (3) The measured film elasticity by QCM-D with dissipation monitoring yielded data with high variation. The methods of measuring viscoelastic properties in this nanoscale range are very rare and complicated. For these measurements the QCM-D is the method of choice, but still, it might be not sufficient to yield precise data of mechanical properties in the studied system. One possibility to increase the accuracy of the readings would be to increase the PEM thickness, but this would simultaneously change the mechanical properties at the surface and would not be less comparable to PEM at 5-5.5 bilayers.

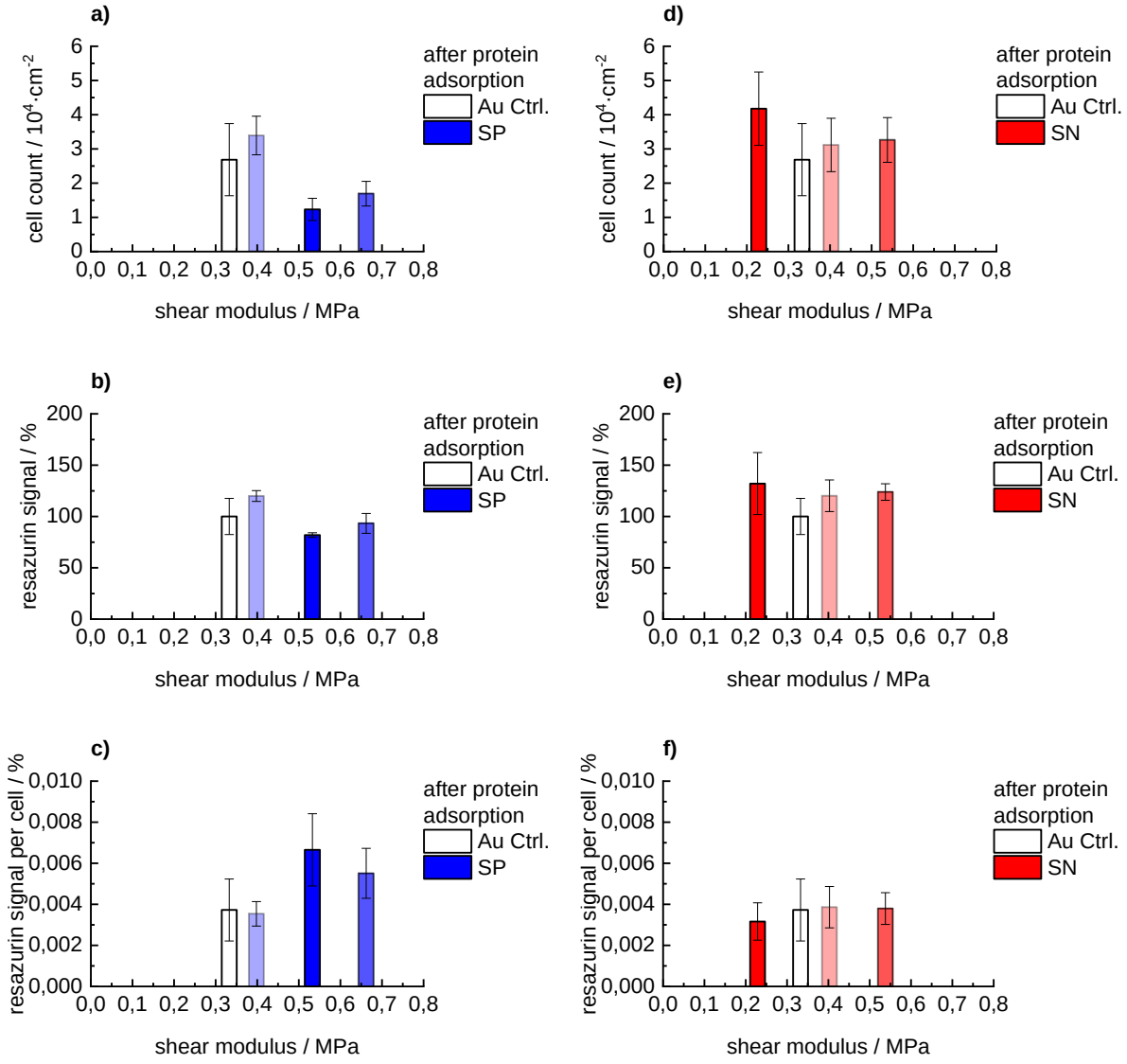

Fig. 4.15. Number of adhered cells (a, d), cell activity (b, e) and activity per cell (c, f) versus surface elasticity of PEM after incubation in cell culture medium, on Au QCM crystal (control) and on with PEM modified surfaces, left) positively charged PEM, right) negatively charged PEM. See table 3.1 on page 38 for abbreviations.

The film shear viscosity measurements by QCM-D yielded more accurate results with low variations. The HUVECs show a clearly different reaction depending on the surface viscosity of the different PEM layers. One interesting observation is that the cells tend to sense surface viscosity in relation with the surface charge. This is why in this experiment positively and negatively charged PEM surfaces are separately considered. Correlations between cellular behavior and surface shear viscosity are shown in figure 4.16.

It is observed that cell adhesion is linearly decreased by increase of surface viscosity when the surface is positively charged by SP modifications (figure 4.16-a). The opposite trend is observed on negatively charged surfaces (SN), where cells adhere in higher numbers when the surface shear viscosity increases (figure 4.16-d). The same observation can be made regarding the cellular activity (figure 4.16-b,e). However there, the slope of decline of cell activity over surface viscosity is less pronounced.

A second interesting observation can be made when looking at the cellular activity per cell over the surface viscosity (figure 4.16-c,f). The cellular activity per cell shows clear increase with increase on positively charged surfaces. On the negatively charged surfaces the cell activity per cell is not changed by surface viscosity.

It is reasonable to assume that cell adhesion and activity change depending on surface charge combined with surface shear viscosity. The cellular sensing mechanisms might not only recognize surface shear viscosity, but also either directly the underlying surface charge or the type and concentration of adsorbed proteins on these surfaces. In the previous experiments the surface charge did not show a clear effect on the cellular behavior, however when taking into consideration the surface viscosity a pronounced effect is observable.

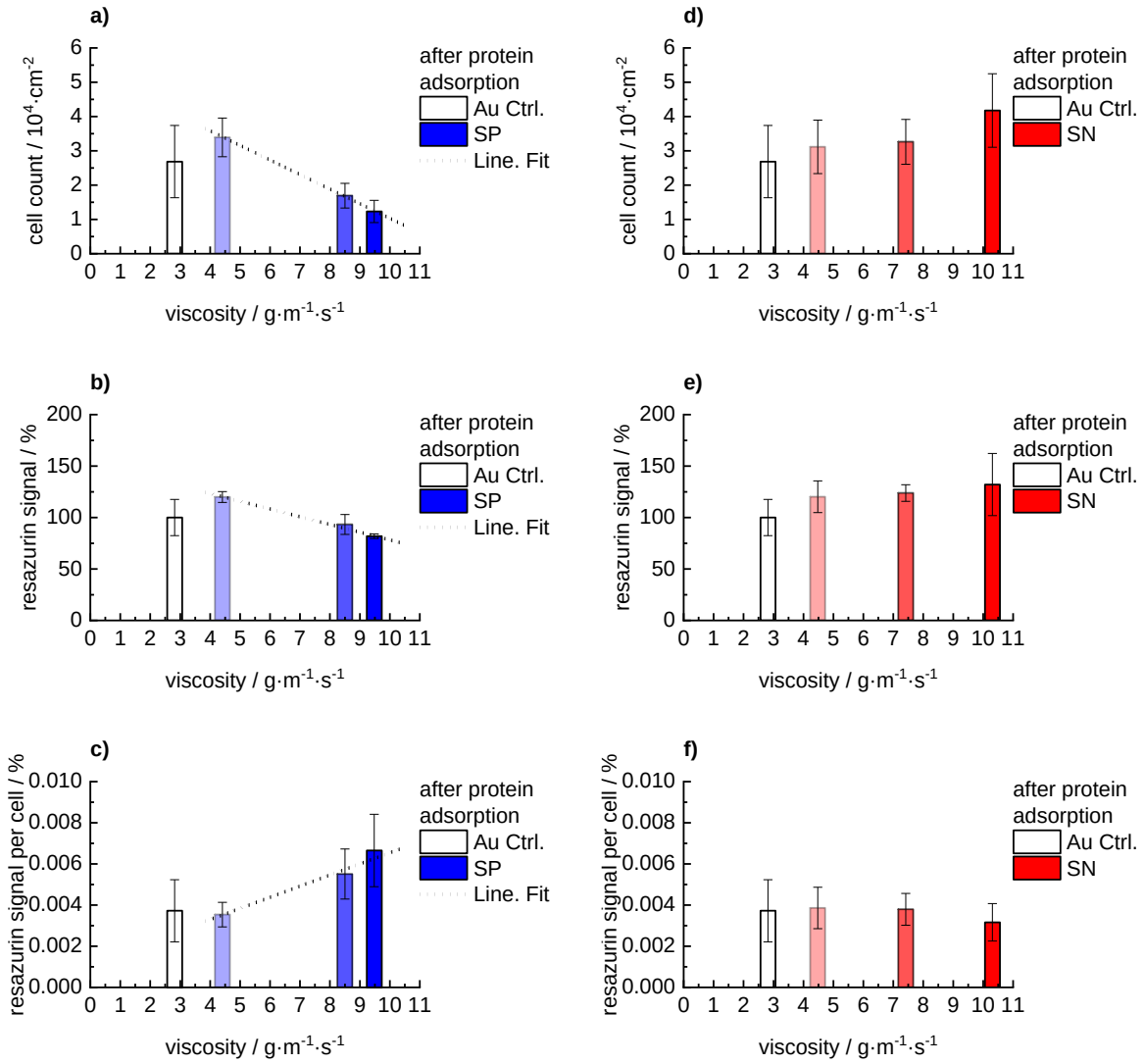

Fig. 4.16. Plot of number of adhered cells (a, d), total cell activity (b, e) and activity per cell (c, f) versus surface viscosity of PEM after incubation in cell culture medium, in the case of Au QCM crystal control the viscosity of protein-film, left) positively charged PEM, right) negatively charged PEM. The lines are a guide for the eye. See table 3.1 on page 38 for abbreviations.

4.3 Effect of protein adsorption on thickness and water content of the PEM coatings from poly(styrene sulfonate)/poly(allylamine hydrochloride) (PSS/PAH) with variation of electrolyte concentration in the deposition solution

In chapter 3.3.5 plain PEM films are characterized using neutron reflectometry. This chapter focuses on characterizing the protein layers on top of PEM film via neutron reflectometry. Surfaces modified with PEM from poly(sodium 4-styrenesulfonate)/poly(allylamine hydrochloride) (PSS/PAH) with variation of electrolyte (NaCl) concentration in the deposition solutions were incubated for one hour with 1 mg/mL BSA in TRIS solution (pH = 7.4) prior to measurements. The reflectivity curves are shown in figure 4.17.

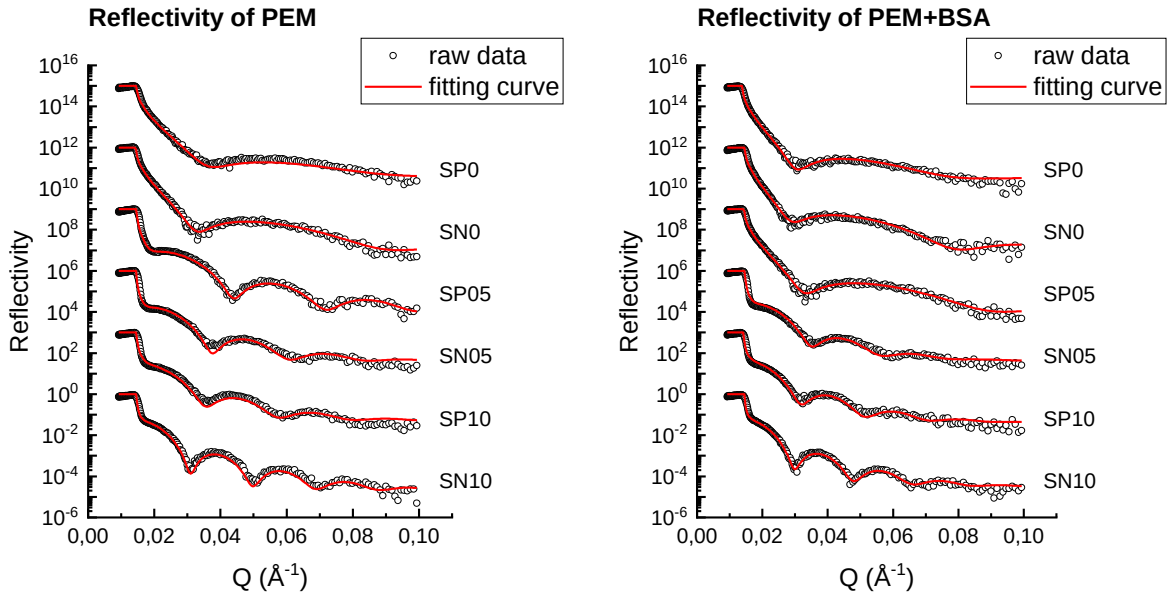

Fig. 4.17. Reflectivity curves of PEM prepared from PSS/PAH at different electrolyte concentrations in the deposition solution. SP0, SP05, SP10 – positively charged and SN0, SN05, SN10 - negatively charged PEM from deposition solution at concentrations of 0, 0.5 and 1.0 M NaCl. Left figure shows reflectivity curves of plain PEM films, right figure shows reflectivity curves of PEM-BSA films. Empty circles, data points; full line, fitting curve. All measurements were performed against D_2O. See table 3.1 on page 38 for abbreviations.

For plain PEM films a single layer model was applied for fitting procedure. The SLD of Si substrate and D_2O was fixed at a constant value. Roughness of the interfaces was set to values between 0.1-0.2 nm. Thickness and SLD of the PEM film was determined by a fitting procedure.

Si slab	
PEM film	SLD = fitting parameter thickness = fitting parameter
D_2O	

For the PEM-BSA films three different approaches for modelling were conducted. The SLD of Si substrate and D_2O was fixed at a constant value. Roughness of the interfaces was set to values between 0.1-0.2 nm. Thickness and SLD of the PEM film were determined by a fitting procedure.

The first model regarded the PEM film and the BSA film as separate layers. Under the assumption that BSA adsorption does not influence the PEM film, the PEM film parameters were set as fixed values from previous measurements of plain PEM films.

The second model regarded PEM and BSA films as separate layers. There the PEM film parameters were set to variable, as BSA adsorption might influence thickness of the PEM film by interacting with intrinsic electrostatic interactions, or water content. BSA might also penetrate inside the PEM film changing the SLD value.

The third model regarded PEM and BSA films as a single film. The SLD and thickness values of the PEM-BSA film were fitted.

	Two-layer model with fixed PEM parameters:	Two-layer model with variable PEM parameters:	One-layer PEM-BSA model:
Si slab			
PEM film	SLD = fixed thickness = fixed	SLD = variable thickness = variable	PEM-BSA fitted as single layer: SLD = variable thickness = variable
BSA film	SLD = variable thickness = variable	SLD = variable thickness = variable	
D_2O			

The models were calculated and evaluated by the deviation (x^2) of the fitting curve towards the raw data.

The fitting curve of the two-layer model with fixed PEM parameters showed the least agreement with the data points of reflectivity curves. From this observation, it can be assumed that the PEM film properties notably change when an additional layer of proteins adsorbs on top.

The fitting curves of the two-layer model with variable PEM parameters and the one-layer model showed similarly high agreement with the data set. Therefore, the simplest model, which was the one-layer PEM-BSA model was accepted as best fit.

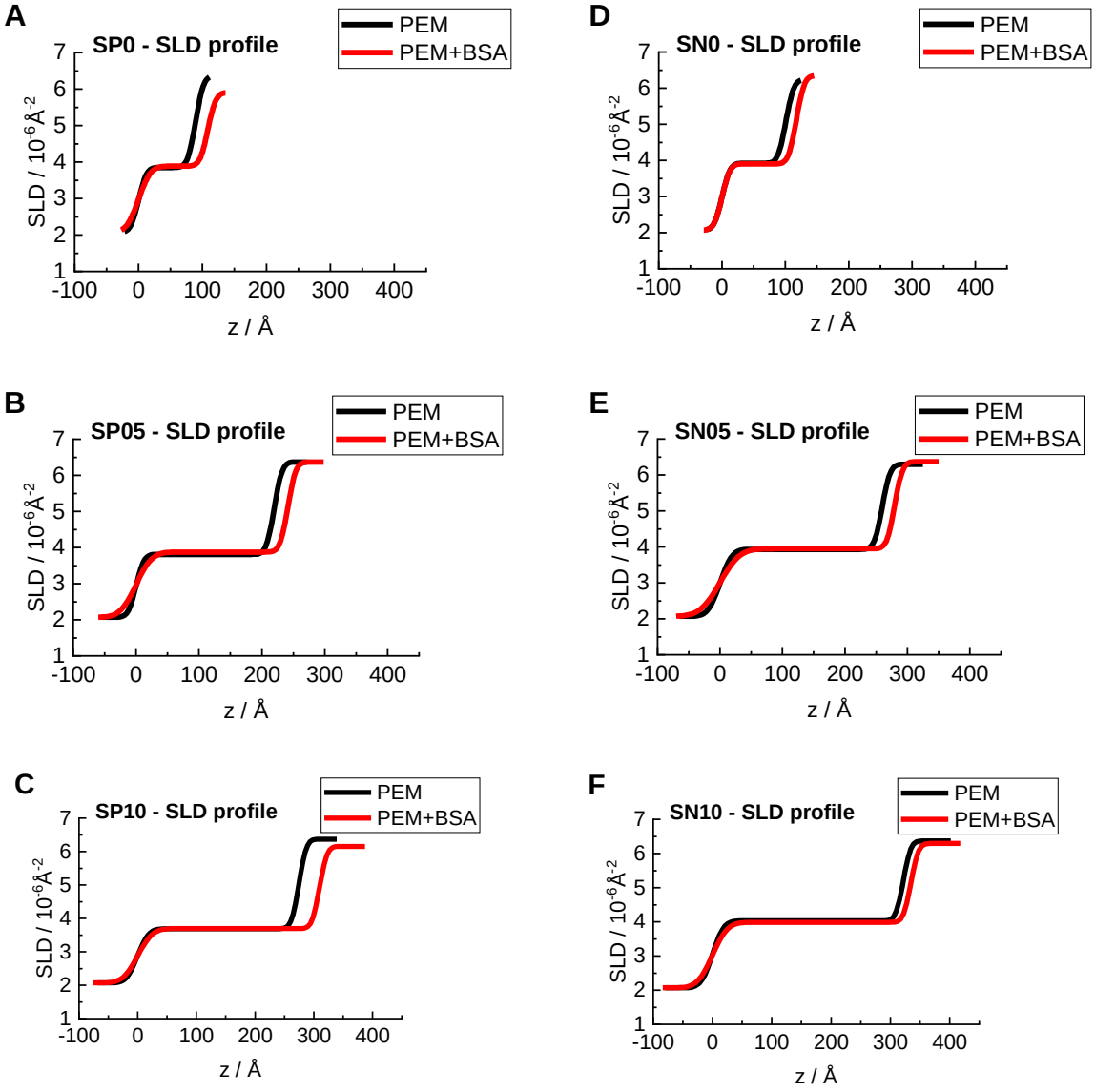

Fig. 4.18. Scattering-length density profiles in a one-layer model evaluated from reflectivity curves of PEM prepared from PSS/PAH at different electrolyte concentrations in the deposition solution after incubation with 1 mg/mL BSA solution for one hour. SP0 (A), SP05 (B), SP10 (C) – positively charged and SN0 (D), SN05 (E), SN10 (F) - negatively charged PEM from deposition solution at concentrations of 0, 0.5 and 1.0 M NaCl; Black curves show results of plain PEM films, red curves show results of PEM films after deposition of BSA solution. See table 3.1 on page 38 for abbreviations.

Scattering-length density profiles of one-layer model of PEM-BSA films in comparison with plain PEM films are shown in figure 4.18. The extracted film thickness and SLD values are presented in figure 4.19. On all tested PEM films, the thickness always increases after protein adsorption from BSA solution. Figure 4.20 highlights the addition of thickness by the BSA adsorption by subtraction of PEM film thickness from PEM-BSA thickness.

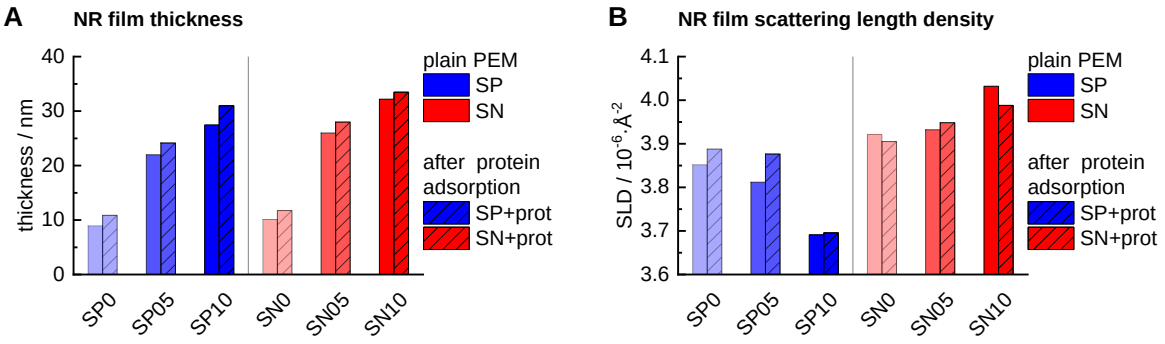

Fig. 4.19. Film thickness (**A**) and scattering length density (**B**) of PEM films for comparison purpose **before and after protein deposition** from BSA solution. SP0, SP05, SP10 – positively charged PEM from strong polyelectrolytes at NaCl concentration in the deposition solution of 0, 0.5 and 1.0 M; SN0, SN05, SN10 - negatively charged PEM from strong polyelectrolytes at NaCl concentration in the deposition solution of 0, 0.5 and 1.0 M. See table 3.1 on page 38 for abbreviations.

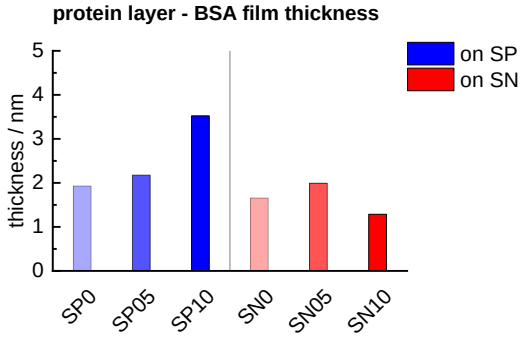

Fig. 4.20. Protein film thickness on PEM prepared from PSS/PAH at different electrolyte concentrations in the deposition solution. SP0, SP05, SP10 – positively charged and SN0, SN05, SN10 - negatively charged PEM from deposition solution at concentrations of 0, 0.5 and 1.0 M NaCl. See table 3.1 on page 38 for abbreviations.

As show in figure 4.20 the highest increase of thickness after BSA adsorption is observed on film SP10 film followed by SP05 film. All other films (SP0, SN0, SN05, SN10) show equally high thickness increase. The trend of thickness increase after BSA adsorption is in agreement with the trend of increased mass after BSA adsorption by QCM-D measurements (figure 4.11), which confirms this observation by two independent methods. One hypothesis is that intrinsic positive charged polymer chains diffuse towards the surface of the film and enable additional

binding of BSA. If all BSA molecules would penetrate inside the film, no significant increase in thickness would have been observed. Consequently, an increased layer or 'fuzzy' layer [Decher 1997] of BSA on top of SP10 surface is plausible. The change of SLD by adsorption of BSA proteins shows little change and no clear dependence on the composition of PEM films.

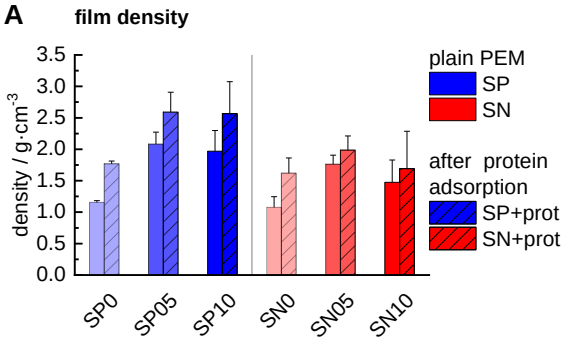

Fig. 4.21. Film density obtained from NR film thickness and QCM-D deposited mass measurements of PEM films for comparison purpose **before and after protein deposition** from BSA solution. SP0, SP05, SP10 – positively charged PEM from strong polyelectrolytes at NaCl concentration in the deposition solution of 0, 0.5 and 1.0 M; SN0, SN05, SN10 - negatively charged PEM from strong polyelectrolytes at NaCl concentration in the deposition solution of 0, 0.5 and 1.0 M. See table 3.1 on page 38 for abbreviations.

The NR revealed thickness of soaked PEM films with D_2O. It can be assumed that the thickness of PEM films remains consistent whether immersed in D_2O or H_2O. The QCM-D mass measurements revealed mass of H_2O-soaked PEM films. Using the obtained NR film thickness with the QCM-D mass measurements enabled the calculation of H_2O-soaked film density of PEM films before and after protein adsorption from BSA solution (figure 4.21). One clear observation is that BSA adsorption increases the film density on all tested coating, independent on thickness or mass changes by the protein adsorption. The mass of soaked PEM was measured in H_2O immersion, which means that a wet film density is a sum of fractions of dry PEM and water (density ≈ 1 g/cm3).

Dry BSA protein has not much different density than water [Singh *et al.* 2005]. In Singh *et al.* (2005) it was also observed that BSA density decreases with an increase in salt concentration in solution. The BSA used for NR and QCM experiments was dissolved in TRIS buffer. If the present electrolytes in solution would be removed, the BSA would be expected to change conformation and become denser.

The adsorption effect on density could be explained as following. Upon adsorption on PEM, the BSA binds to charged PE groups, reducing the interactions with TRIS, which then is released into solution. Assuming the BSA only binds to PEM on outer binding spots the intrinsic TRIS molecules would be released and the BSA would change conformation and become denser, which consequently increases the total density of the PEM-BSA complex.

Previous SLD measurements of PEM films revealed that the odd-even effect affects the intrinsic water content on positively and negatively charged PEM films. The positively charged PEM films (SP) show a decrease and negatively charged PEM films (SN) show an increase of water content with an increase in electrolyte concentration in deposition solutions. The highest difference of thickness change after BSA adsorption is between the films SP0 and SP10 (2 nm on SP0 and 3.5 nm on SP10), which is an increase by 75 %. However, the mass increase upon BSA adsorption on these surfaces is increased by 240 % (0.16 µg/cm2 on SP0 and 0.54 µg/cm2 on SP10). The density of SP10 is the among the highest of the tested PEM films and it is further increased by BSA adsorption. This observation led to the conclusion that BSA penetration into the multilayer is intensified on positively charged PEM from deposition solution with high electrolyte concentrations (SP10, to a lesser degree SP05), while it mostly adsorbs on top of PEM surfaces that are negatively charged (SN0, SN05, SN10) or have low positive excess charge (SP0).

4.4 Summary of cell adhesion and protein adsorption on PEM coatings from poly(styrene sulfonate)/poly(allylamine hydrochloride) (PSS/PAH) with variation of electrolyte concentration in the deposition solution

The number of adhered cells and cellular activity of Human Umbilical Vein Endothelial Cells (HUVEC) were measured after incubation of 24, 48 and 72 h on polyelectrolyte multilayer surfaces from poly(styrene sulfonate)/poly(allylamine hydrochloride) (SP05, SN05 coatings) and hyaluronic acid/chitosan (WP, WN coatings).

HUVECs show high affinity towards SP05 and SN05 surfaces, the cell adhesion and viability are high and comparable to the positive control (tissue culture treated polystyrene). About 93 % more cells adhere on SN05 in comparison to SP05 ($1.7 \pm 0.4 \cdot 10^5$ cells·cm^{-2} for SP05 and $3.3 \pm 0.7 \cdot 10^5$ cells·cm^{-2} for SN05). The total cell activity on SN05 is by 33 % higher in comparison to total cell activity on SP05 (relative activity normalized to control: 93 ± 10 % for SP05 and 124 ± 8 % for SN05). The cell activity per cell of HUVEC is higher on SP05 in comparison to SN05 ($5.5 \pm 1.2 \cdot 10^{-3}$ % for SP05 and $3.8 \pm 0.8 \cdot 10^{-3}$ % for SN05).

Contrary, the surfaces of WP and WN show extremely low cell adhesion and proliferation. Hardly any cells manage to adhere to the WP and WN surfaces. After 72 h the remaining adhered cells perish. In comparison to SP05 the cell viability after 24 h is reduced by 97 % (WP) and by 99 % (WN). Compared to SP05 the cell viability after 72 h is reduced by 100 % on both, WP and WN. Therefore, WP and WN show adverse surface properties for HUVEC cell adhesion, as well as proliferation. This observation reveals a useful cell adhesion control tool for controlled cell adhesion. Almost any surface can be coated with PEMs from PSS/PAH or HA/CHI to switch HUVEC adhesion on or off by demand.

The strong cell adhesion on SP/SN surfaces and the weak adhesion of WP/WN surfaces can neither be explained by the zeta potential nor by surface energy (contact angle of water). The most pronounced correlation of HUVEC adhesion is observed towards mechanical elastic modulus under vertical stress (Young's) modulus and the surface roughness evaluated by the peak-count method. The SP/SN surfaces are approximately 3-fold rougher and 25-fold stiffer than WP/WN coatings. Therefore, it can be assumed that in the borders of the observed system a higher HUVEC adhesion affinity is caused by rougher and stiffer surfaces.

HUVECs were incubated for 48 h on polyelectrolyte multilayer surfaces from poly(styrene sulfonate)/poly(allylamine hydrochloride) with variations in electrolyte concentration in the deposition solution (SP0, SN0, SP05, SN05, SP10 and SN10 coatings). Cell adhesion is different

on the tested coatings. The cell adhesion changes in dependance on the surface charge, as well as the electrolyte concentration in the deposition solutions. On positively charged coatings the cell count after 48 h is highest on SP0 with $3.4 \pm 0.6 \cdot 10^5$ cells·cm^{-2}. The SP coatings with higher electrolyte concentration in the deposition solution show an incrementally lower cell adhesion ($1.7 \pm 0.4\ 10^5$ cells·cm^{-2} for SP05 and $1.2 \pm 0.3 \cdot 10^5$ cells·cm^{-2} for SP10). On negatively charged SN coatings the cell adhesion is higher than on positively charged SP coatings and incrementally increased with the electrolyte concentration in the deposition solutions ($3.1 \pm 0.8 \cdot 10^5$ cells·cm^{-2} for SN0, $3.3 \pm 0.7 \cdot 10^5$ cells·cm^{-2} for SN05 and $4.2 \pm 1.1 \cdot 10^5$ cells·cm^{-2} for SN10). This observation is highly interesting, as it shows that surfaces might not only be switched from adhesive to anti-adhesive or vice versa by application of PEM surface modification, but the degree of cell adhesion might be controlled by simple addition of a neutral salt to deposition solution used for PEM buildup.

The measured cell activity on tested PEM coatings showed very similar trend to microscopic cell counting. The total cell activity is highest on positively charged SP0 and is incrementally lowered on positively charged SP PEMs with electrolyte concentration in the deposition solution. On negatively charged SN coatings the total cell activity is equally high independent on electrolyte concentration in the deposition solution and is generally higher than on positively charged SP coatings. The ratio between cell count and total cell activity reveals the cell activity per cell. When applying this ratio to the measurements a visible difference between the coatings is observed. The cell activity per cell is equally high on coatings SP0, SN0, SN05 and SN10. However, it is increased by 53 % on SP05 and by 85 % on SP10. The HUVECs show an increased metabolism on the coatings SP05 and SP10, which might be caused by the denser surfaces (measured by NR and QCM-D) or by the decreased amount of adsorbed proteins from cell culture medium.

Protein adsorption on surfaces always takes place before any interaction with biological cells is realized. Types and density of proteins on surfaces directly affect cellular behavior, additionally, adsorbing protein interact with and change nano-scaled surface properties such as elastic and viscous surface properties. Therefore, protein adsorption on modified surfaces was extensively characterized.

The investigated proteins were a single protein solution of BSA in tris buffer and a more complex protein mixture in optimized HUVEC cultivation medium, containing FCS, epidermal growth factors, heparin, hydrocortisone and an endothelial growth supplement of an aqueous bovine hypothalamus extract.

Incubating of PEM coated surfaces with BSA solution revealed a dependence of protein adsorption on the charge of terminating layer in combined with the electrolyte concentration in the deposition solution. The highest amount of adsorbed BSA was found on the coatings SP05 and SP10, with 0.43 ± 0.14 μg·cm^{-2} and 0.54 ± 0.43 μg·cm^{-2}, respectively. On all other tested surfaces (SP0, SN0, SN05, SN10) the BSA adsorption was decreased by 63-67 % in comparison with adsorption on SP05. SP0 shows 0.16 ± 0.01 μg·cm^{-2}, SN0 shows 0.14 ± 0.01 μg·cm^{-2}, SN05 shows 0.16 ± 0.03 μg·cm^{-2} and SN10 shows 0.16 ± 0.02 μg·cm^{-2} of adsorbed BSA. The different adsorption of BSA on PEM surfaces could be explained by a combination of attraction from positively charged surfaces and an interaction with intrinsic positively charged polymer chains inside the PEM. A calculation of intrinsic excess charge revealed that all PEM have intrinsic positive excess charge, due to increased adsorption of PAH in the course of PEM buildup. The intrinsic positive excess charge is lowest on SP0 and SN0 and highest on SP10 and SN10. The adsorption of BSA on negatively charged PEM is hindered, due to repulsion between negative surface charge and negatively charged BSA. However, on positively charged surfaces BSA is attracted towards the surface and interacts with the surface. Positively charged SP10 has the highest positive excess charge, as well as the highest BSA adsorption. It is assumed that BSA not only interacts with polyelectrolytes at the surface, but also with loose positively charged intrinsic chains, which leads to an amplification of BSA adsorption.

Measurements of film thickness by NR and film mass by QCM-D revealed the density of PEM films. Incubation of plain films with BSA solution leads to an increase in PEM-BSA film density. BSA protein in solution containing electrolytes (TRIS buffer) is known to have similar density to water. Adsorption of BSA in native state could not explain an increase in PEM-BSA film density. However, BSA proteins are known to increase in density by changing conformation, if electrolytes in solution are reduced. One explanation for the increase in density of PEM films after BSA adsorption might be that, when BSA adsorbs, it binds to active groups on the surface of PEM, which releases the BSA-bound TRIS molecules. Adsorbed BSA might then change conformation and become denser, as well as interconnecting loose PE molecules at the surface of PEM, which might cause an increase of density in the PEM-BSA film as a whole.

Incubating of PEM with HUVEC cell culture medium showed a different adsorption behavior in comparison to adsorption with pure BSA solution. Proteins from the complex protein mixture adsorb in dependance of surface charge as well as electrolyte concentration in the PEM deposition solutions. On positively charged PEMs (SP) the highest adsorbed mass was measured on SP0 with 0.74 ± 0.06 μg·cm^{-2}. The positively charged PEMs with higher electrolyte concentration showed an incrementally lower protein adsorption (0.42 ± 0.07 μg·cm^{-2} for SP05

and 0.31 ± 0.07 µg·cm^{-2} for SP10). The protein adsorption on negatively charged PEMs (SN) was higher than on positively charged PEMs (SP) and showed no clear dependance on electrolyte concentration in the deposition solution. On positively charged surfaces protein adsorption on SN0 was the highest with 0.82 ± 0.15 µg·cm^{-2} followed by SP10 with 1.16 ± 0.02 µg·cm^{-2} and SN05 with 1.23 ± 0.03 µg·cm^{-2}. The adsorption of proteins from HUVEC medium can be explained by taking into consideration other surface-active ingredients of the medium such as Heparin, which features a strong negative charge. Positively charged albumin proteins might interact with negatively charged Heparin, which leads to switched trend of adsorption compared to pure BSA solution. This observation is important, as it highlights that different protein or even the addition of other surface-active ingredients might heavily affect the adsorption on surfaces.

The adsorption of proteins changes the film shear elasticity (shear modulus) and shear viscosity of the PEM coatings. After protein adsorption from HUVEC cell culture medium the film elasticity of all tested coatings equilibrates to around 0.5 MPa without significant difference in between the tested PEMs. The film viscosity changes in a specific manner. Film viscosity of PEM-protein complexes shows a dependency on the electrolyte concentration in the deposition solution but no dependency on surface charge. PEMs from deposition solutions without electrolytes show the lowest film viscosity (4.4 ± 0.6 g·m^{-1}·s^{-1} for SP0 and 4.5 ± 1.1 g·m^{-1}·s^{-1} for SN0), which is increased by PEMs from deposition solutions with intermediate electrolyte concentration (8.5 ± 0.8 g·m^{-1}·s^{-1} for SP05 and 7.4 ± 1.3 g·m^{-1}·s^{-1} for SN05) and further increased by PEMs from deposition solutions with high electrolyte concentrations (9.5 ± 0.6 g·m^{-1}·s^{-1} for SP10 and 10.3 ± 1.3 g·m^{-1}·s^{-1} for SN10). This might be explained by structural conformation of PE chains in PEMs from deposition solution with high electrolyte concentration. On build-up of these PEMs, more mass of PE adsorbs, leading to higher flexibility of chains as well as potentially more intrinsic free space due to their coiled conformation. Adsorbing proteins might not only bind on the surface, but also penetrate inside the PEM films interacting with intrinsic chains and interconnecting them, which consequently results in higher viscosity of the whole film.

Chapter 5 - Characterization of immune response to surfaces via measurements of reduction of pro-inflammatory interleukin expression by HUVECs in contact with PEM coated surfaces

The initiation of immune response towards surfaces of substrate materials with PEM modified surfaces was studied by *in-vitro* measurements of NF-κB pathway activation and pro-inflammatory interleukin expression. A focused setup of experiments was conducted by pressing modified surfaces on top of human endothelial cells (HUVEC) and measuring the extent of pro-inflammatory messenger molecule secretion by the cells. This chapter presents the effect of PEM-modified surfaces on the expression of pro-inflammatory interleukins by HUVEC cells.

In general, when foreign materials such as cardiovascular stents are implanted, the tissue host cells are triggered by injury from the operation and by the physical presence of the foreign body. The injured host cells express pro-inflammatory messenger proteins such as tumor-necrosis-factor alpha (TNFα) to alert the neighboring cells. The cells in direct contact with the foreign implant material are stressed biologically by TNFα and physically by contact with foreign surfaces, which induces the secretion of further pro-inflammatory signaling proteins such as cytokines, chemokines (interleukin family) and the development of adhesive membrane proteins (CAMs, selectins) on the cell surface. At the injury site, the concentration gradient of signaling molecules is at its peak and gradually diminishes with increasing distance. Immune cells such as leukocytes are able to sense the molecular signals and purposefully move towards the point of injury by attaching to blood vessel walls and advancing inside the tissue at the point of injury (leukocyte rolling). There the immune cells induce further immunological processes such as inflammation and foreign body reaction.

If the expressed signaling by host cells (such as endothelial cells) would be reduced by the PEM coating of the implant material, then ultimately the attraction of leukocytes and the subsequent pathways leading to inflammation and foreign body reactions would be reduced.

In clinical conditions, stressed host cells such as endothelial cells express the tumor necrosis factor alpha (TNFα), which, among other functions, is stimulating the nuclear factor kappa-light-chain-enhancer pathway (NF-κB-pathway). The transcription factor NF-κB is activated (by TNFα and other stimuli such as signals from integrins) and translocated into the nucleolus, where it induces the transcription of genes coding for pro-inflammatory signaling proteins. The

inactivation or reduction of activation of the NF-κB would reduce subsequent inflammatory and immunological reactions.

The NF-κB-pathway is complex and yet not fully understood, new general understanding of involved proteins is published in biochemical research every second year. Many involved signaling molecules can act as pro- or anti-inflammatory in dependance of progress of the pathway and cross-participation of other signaling molecules. A high interconnectivity between a multitude of signaling molecules is evident. The TNFα is not the only, but one among various triggers for the NF-κB pathway. There are cellular sensor mechanisms that recognize the foreign bodies surface as not-native tissue and co-activate the NF-κB pathway or enhance the NF-κB pathway. As in all major biological reactions, feedback loops exist, that are able to deactivate and cancel the NF-κB pathway, if stimulation was falsely triggered or the stimulation impulse decreases. In this work, the generally accepted facts about NF-κB pathway are focused.

In the example of cardiovascular stenting, injured host cells (endothelial cells of the blood vessel) secret TNFα, which initially activates the NF-κB pathway and leads to translocation of phosphorylated NF-κB (p-NF-κB) into the nucleolus, where it induces the transcription of genes for pro-inflammatory proteins. The biomaterial (here medical steel stent) has specific surface properties, which contribute to triggering the host cells responses. Additionally, the stent applies pressure by its spring effect on the surrounding host cells of the vessel wall, which further enhances the effect of the surface properties. Initially, in the stenting operation the stent is expanded by inflating a balloon with a pressure of 10 bar to widen the blood vessel. After this step is finished, the balloon is deflated and the guide-wire is removed. The stent remains in place and widens the blood vessel by its materials spring property. The tissue adapts and relaxes over time, which leaves a significantly reduced pressure of the stent surface on the host cells. In our experiments the pressure is simulated by the bearing pressure of the substrate steel pins (~ 300 Pa), which are placed on top of the cells. The physical stress on the host cells acts as a co-trigger in addition to TNFα on the NF-κB pathway, which then is activated with more intensity. The co-triggering of both, the biological signaling protein TNFα and the physical application of pressure by stent material surface with specific surface properties on the cells, is clearly visible in our findings. If only one trigger is applied to the cells, the amount of secreted pro-inflammatory proteins is severely reduced. When both triggers are applied, the secretion of pro-inflammatory proteins is amplified.

The NF-κB pathway was measured at three points of progress. The three target molecules were (1) the activated form of NF-κB, (2) mRNAs coding for pro-inflammatory interleukins and (3) the secreted interleukin proteins. The simplified scheme in figure 5.1 illustrates the expected numbers and residual times of target molecules. After initial stimulation, the activation of NF-κB leads to phosphorylation and translocation of the transcription factor. The numbers of NF-κB are low and the residual time is short (10 min). After NF-κB induces transcription of genes inside the nucleus it inactivates and leaves the nucleolus. Transcription of genes yields high numbers of mRNA, which reside for a long period of time (4-8 h). Post-transcriptory modulation, as opposing force, might lead to disassembly of mRNA. This causes that not all of mRNA-molecules are translated into proteins. The number of proteins is lower than that of mRNA, however expressed proteins reside for are long time in cell culture medium (> 24 h). Scheme of experimental setups for measurement of these target molecules is illustrated in figure 5.2.

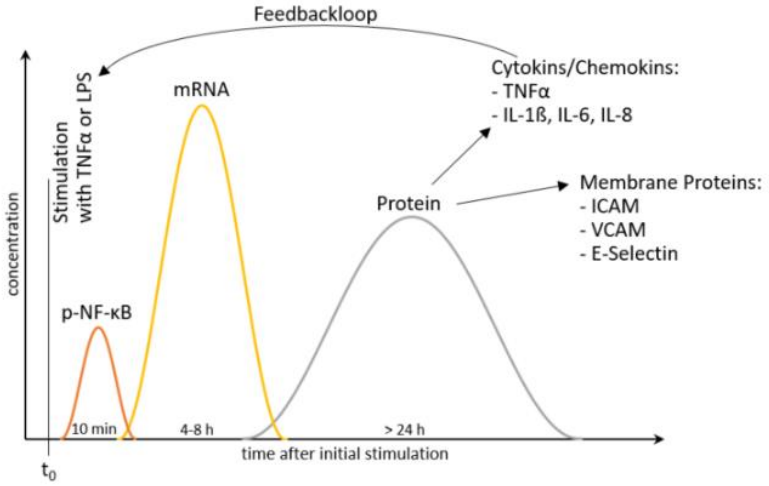

Fig. 5.1. Scheme of NF-κB-activation depending on the concentrations of up- and downstream products from the point of stimulation to the formation of pro-inflammatory proteins.

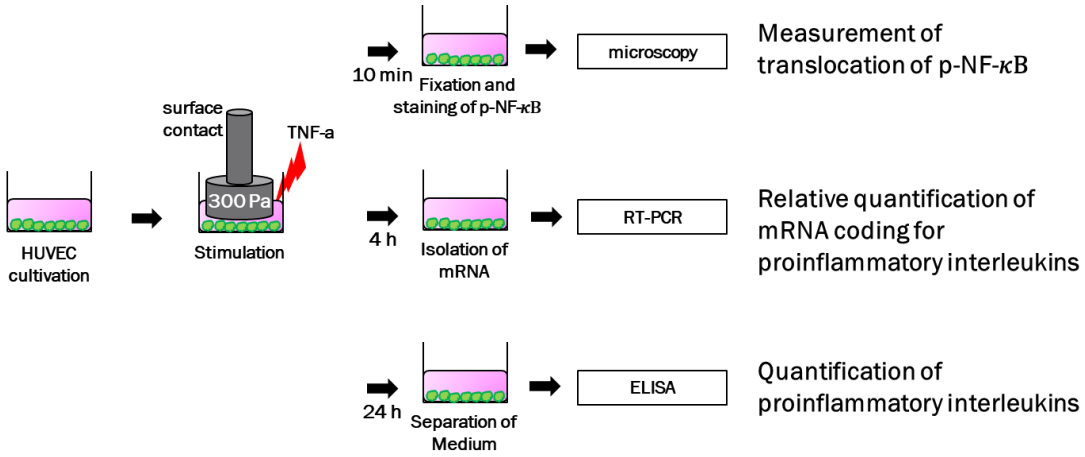

Fig. 5.2. Scheme of experimental setup measuring the NF-κB pathway at different progressions. The activation (phosphorylation) and translocation of the transcription factor NF-κB was measured by staining and fluorescent microscopy. The subsequent production of mRNA transcribing for pro-inflammatory interleukins was measured by rt-PCR. The formed and secreted pro-inflammatory interleukin proteins were measured by quantitative ELISA.

As first step, HUVECs were cultivated to confluence. The stimulation was performed by simultaneous addition of TNFα-containing cell culture medium and by bringing in contact of PEM-coated and uncoated medical steel substrates. For the measurements of NF-κB the substrates were removed after 10 min, the cells were fixed, stained and analyzed by fluorescence microscopy. For measurements of mRNA expression, the substrates were removed after 4 h, the mRNA of the cells was isolated and measured by real time Polymerase Chain Reaction (rt-PCR). For measurements of interleukin protein expression, the cell culture medium containing the expressed messenger molecules was separated from cells after 24 h and measured by quantitative sandwich ELISA.

5.1 Activation and translocation of nuclear factor kappa B (NF-κB)

The immunological reaction of cells *in-vitro* is related to expression of the Nuclear Factor kappa B (NF-κB). It is identified as a factor in the nucleolus of B cells that binds to the enhancer of the kappa light chain of immunoglobulin. It has been shown to be present in the cytoplasm of every cell in its inactive state and is conserved in all animals from Drosophila to man. It is translocated to the nucleolus only when activated, where it regulates the expression of over 300 immune-, growth- and inflammation-genes. Five different NF-κB family members are known. Two different NF-κB activation pathways have been identified, a canonical pathway and a non-canonical pathway. Thus, the quantification of the NF-κB in the cells gives information about the immunological reaction of the cells. The up- and down-stream activity of NF-κB is

mandatory for all inflammatory and immunological processes. An inactivation of NF-κB would reduce or inhibit the immune response of cells against foreign bodies.

After starting the NF-κB cascades of HUVEC by simultaneous activation with TNFα and pressing of PEM-coated steel surfaces on top of the cells for a certain amount of time, the cells were fixed with formaldehyde. The NF-κB was stained with a labeled antibody, nuclei were stained by DAPI and cytosol was stained by phalloidin. The location of NF-κB was optically analyzed on fluorescence images.

The microscopic images were performed on HUVECs adhered on tissue culture treated well plates as preliminary experiment. As evaluation of the data, a ratio between NF-κB inside the cytosol to the NF-κB inside the nucleolus can be applied. A pronounced difference in location is visible when comparing the combined images of all three colors (figure 5.3). Before TNFα treatment the transcription factor residues outside the nucleolus, resulting in a blue nucleolus encircled by red transcription factor NF-κB. After 10 min of TNFα treatment (40 ng/mL in cell culture medium), the triggered NF-κB pathway leads to a phosphorylation and translocation of the transcription factor NF-κB inside the nucleolus. The position of the translocated NF-κB (red labeled) then overlaps with the position of the nucleolus (blue labeled), which results in a combined color at the position of the nucleolus (purple).

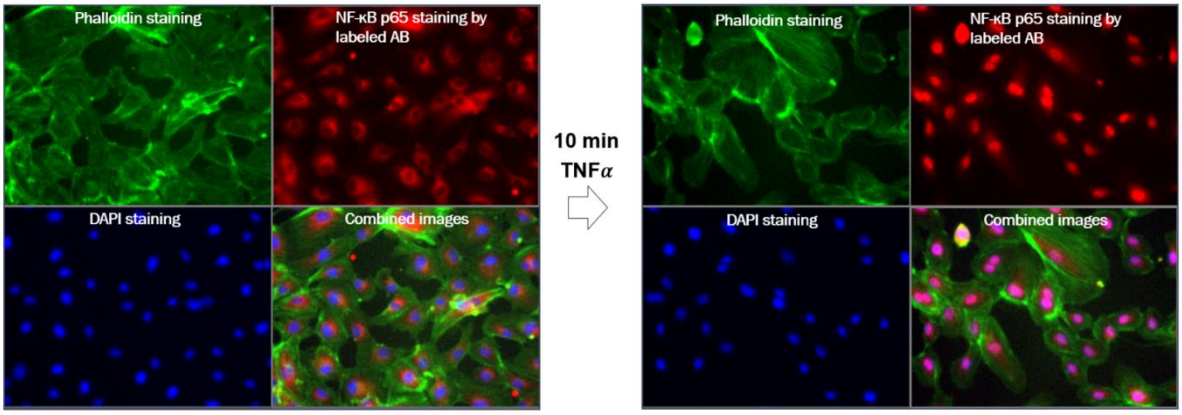

Fig. 5.3. Fluorescence labeled NF-κB in inactivated (left) and activated HUVEC (right). The image shows different fluorescence intensities of HUVEC on transparent tissue culture treated well plate. The transcription factor NF-κB (red labeled) is activated and translocated from the cytosol (green labeled) into the nuclei (blue labeled). In the right bottom corners (left image and right image) show the combined image of overlapping all three colors.

However, this procedure could not be applied for tests with PEM modified substrates. It was not possible to say which cells were really in contact with the substrates and should be analyzed by

performing a ratio between NF-κB inside and outside the nucleolus. Therefore, all cells were analyzed which resulted in very high variation of values and no statistically certain results. Most probably, deformed cells were in contact with the substrate, which could be not analyzed due to overlap of nuclei and cytosol.

Another approach to measure the active form of NF-κB was by in-cell ELISA with application of antibodies specifically targeting only the active phosphorylated form of NF-κB. Simultaneously, the cells were biologically activated with TNFα and mechanically activated by steel substrates. Afterwards the cellular metabolism was fixed by formaldehyde and the cells were opened by surfactant solutions. Still, it was not possible to receive accurate reproducible results from this approach. Possible reasons could be that the short time window of 10 min significantly affects the measurement, and that antibodies falsely cross-bind on the inactive form of NF-kB. The results showed high signals all over PEM-coated or PEM-uncoated samples, including all controls.

5.2 Pro-inflammatory interleukin mRNA expression of HUVEC in contact with PEM-modified surfaces

Other techniques had to be applied focusing target molecules further downstream in the process of NF-κB pathway that enabled measurements that are more accurate and had a wider time window for measurements. In the course of the NF-κB pathway, the translocation of the transcription factor is the first step, followed by downstream processes in transcription of genes to mRNA and the translation into proteins, which finalizes in the synthesis of pro-inflammatory proteins (for details see figure 5.1). The mRNA coding for pro-inflammatory interleukins can be measured by rt-PCR technique. This approach indirectly reveals the degree of NF-κB activation and gives further insight. The rt-PCR approach featured several advantages in comparison of directly measuring NF-κB. The messenger RNAs are generated in higher quantities and are present for longer amounts of time before they are translated into proteins. This enables measurements with higher accuracy and less disturbance by measurement delays.

Two interleukins (IL-1ß and IL-6) and a chemokine (IL-8) were selected for further testing due to significant contribution of examples of real-life cell-surface interactions such as in-stent restenosis (see chapter 2.5.4).

The messenger RNAs coding for these pro-inflammatory interleukins were measured relative to a housekeeping gene which was GAPDH by rt-PCR. A fixed amount of the housekeeping gene is present in every cell. By normalizing IL-signal to the housekeeping gene-signal, the total signal per cell could be evaluated. In the course of the experiment, HUVECs were biologically activated by TNFα and, simultaneously, the cells were mechanically treated by pressure/contact to PEM coated substrates.

For the evaluation the delta-delta-C_t method was used [Livak & Schmittgen 2001]. All cells were activated with TNFα as initiator. A control group was solely treated by pressure and contact with substrates, without the activation by TNFα. One group of cells was simultaneously activated by TNFα and brought in contact with PEM-coated substrates. The relative expression ratio was calculated by ratio between results of both groups.

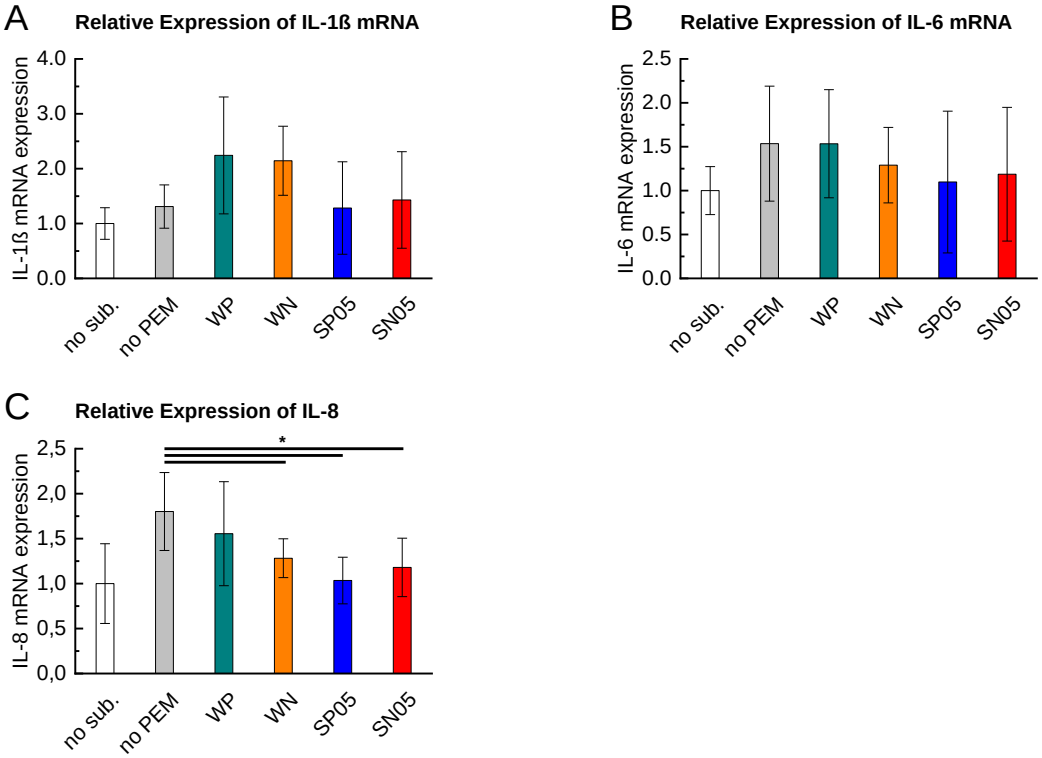

Fig. 5.4. Relative expression of mRNA coding for IL-1ß (a), IL-6 (b), IL-8 (c) normalized to signal from HUVECs without contact to steel substrates (no sub.). White column represents relative expression of IL by cells without contact to substrates, grey column by contact with uncoated substrates, colored columns by PEM coated substrates, respectively. Significant difference of PEM-coated substrates in comparison with uncoated substrates was identified by ANOVA with a significance level of 0.05. See table 3.1 on page 38 for abbreviations.

Figure 5.4 presents the relative expression of mRNA coding for IL-1ß, IL-6 and IL-8 after stimulation with PEM-coated substrates. The cells that are in contact with non-coated bare steel substrates (grey column) always have an increased relative IL-expression when compared with

cells that are not in contact with substrates (white column). The pressure/contact of the samples amplifies the expression of interleukins. The colored columns stand for steel substrates coated with SP05, SN05 and WP, WN films. Interleukins IL-1ß and IL-6 show no significant change between contact to uncoated substrate and on PEM-coated substrate.

Interleukin IL-8 is the main interleukin that governs the leukocyte attraction. The rt-PCR results (figure 5.4-C) show a significant reduction in relative expression by coatings WN, SP05, SN05 when compared to non-coated substrates. The effect is most pronounced by the SP05 coating, which reduces the relative expression to the level of the positive control, which was measured on cells without contact to substrates. The SP05 coating effectively cancels the effect of steel substrates on HUVEC to a degree as if there was no contact with the substrates. The expression of IL-8 is significantly reduced by WN, SP05 and SN05 PEM-modification of surfaces.

5.3 Pro-inflammatory interleukin expression of HUVEC in contact with PEM-modified surfaces

The results of mRNA expression had to be confirmed by another method. The rt-PCR technique measures the expression of messenger RNAs as a marker for expression of certain interleukins. However, the number of expressed mRNA does not directly correspond to the number of expressed proteins, as cellular post-transcriptional modification processes might inhibit mRNA translation into proteins. The expressed mRNA might be recognized as falsely expressed and deactivated/ dismantled.

A sandwich ELISA was applied to measure the amount of secreted interleukins by HUVEC into cell culture medium. The targets were fully secreted IL-1ß, IL-6 and IL-8 interleukins released by HUVEC into the cell culture medium.

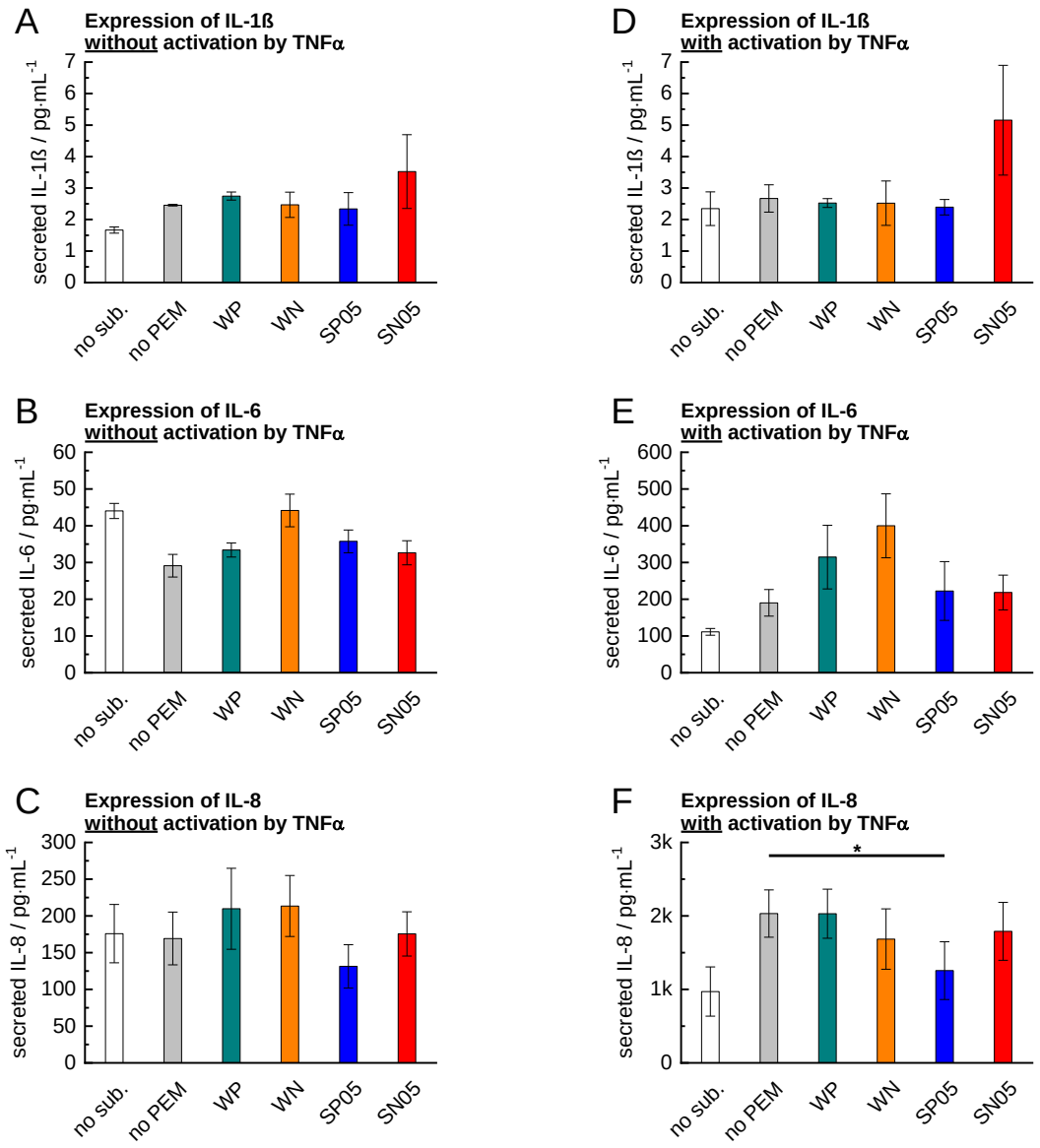

Please note the different scales of the y-axes.

Fig. 5.5. Left side (A, B, C): Expression IL-1ß (A), IL-6 (B), IL-8 (C) secreted from HUVECs in contact and under pressure with PEM-coated surfaces **without** activation by TNFα; Right side (D, E, F): Expression of IL-1ß (D), IL-6 (E), IL-8 (F) secreted from HUVECs in contact and under pressure with PEM-coated surfaces **with simultaneous activation** by TNFα. See table 3.1 on page 38 for abbreviations.

HUVECs were incubated on tissue culture treated well plates. The cells were activated by addition of TNFα and/or put in contact with PEM-coated steel substrates. After 24 h the cell culture medium was separated and transferred to the ELISA assay. The design of the sandwich ELISA was based on two antibodies specific for the respective interleukins.

Figure 5.5 presents the expression of interleukins by HUVEC when in contact with PEM-coated steel substrates. The left side (figure 5.5-A, B, C) presents the expression of interleukins without activation by TNFα. The right side (figure 5.5-D, E, F) shows the expression of interleukins with simultaneous activation by TNFα.

The first observation is the big difference in expression rates between the interleukins. The highest expression by sole contact with PEM-coated surface of IL-1ß is 3 $pg \cdot mL^{-1}$, while for IL-6 it is 40 $pg \cdot mL^{-1}$ and for IL-8 it is 200 $pg \cdot mL^{-1}$. The simultaneous activation by TNFα and contact with PEM-coated surfaces the highest expression of IL-1ß is 5 $pg \cdot mL^{-1}$, while for IL-6 it is 400 $pg \cdot mL^{-1}$ and for IL-8 it is 2000 $pg \cdot mL^{-1}$.

Interleukin IL-1ß is expressed in low quantities by HUVEC. The expression rate does not change by activation with TNFα, by contact with substrate surfaces, or by both stimuli. This observation might also explain the high variation in results of mRNA expression by rt-PCR.

Interleukin IL-6 shows a higher expression than IL-1ß. Interestingly, the activation by only contact to surfaces, reduces the interleukin expression in comparison to HUVECs without contact. The simultaneous trigger of biological TNFα and contact to substrate surfaces amplifies the expression of IL-6 by approximately ten-fold. Samples in contact with substrates always express more IL-6 than the controls without contact to substrates. This indicates that IL-6 expression is directly amplified by the simultaneous biological and physical triggers by surfaces. In figure 5.5-E it is shown that the surface coatings WP and WN increase the IL-6 expression by approximately two-fold in comparison to the uncoated steel substrate. The coatings SP05 and SN05 do not change the expression in comparison to the uncoated steel substrate. It is observed that the tested PEM coatings either increase or do not alter the IL-6 expression when compared to plain steel surfaces.

Interleukin IL-8 shows an even higher expression than IL-1ß and IL-6. The basic level expressed by untreated HUVEC is around 175 $pg \cdot mL^{-1}$, which is not increased by contact with plain steel surfaces. WP and WN coated surface contact increases the IL-8 expression to 200 $pg \cdot mL^{-1}$, while SN05 surfaces do not alter it and SP05 surfaces reduce it to 125 $pg \cdot mL^{-1}$. The simultaneous surface contact and TNFα stimulation increases the total expression by approximately ten-fold, similar to the case of IL-6 (figure 5.5-F). The highest expression is observed on cells in contact with uncoated steel surfaces. The WP-coated surface does not change the expression, while WN and SN05 slightly decrease the IL-8 expression and SP05 significantly decreases the IL-8 expression in comparison to uncoated steel surfaces. Therefore, the observation of IL-8 mRNA

expression-reducing effect by certain PEM surfaces is confirmed. The surface modification by SP05 significantly reduces IL-8 expression on transcriptional and translational level.

5.4 Analysis of the effect of surface properties on interleukin expression

In the previous part, it was shown that surface contact with PEM-modified surfaces is able to significantly alter interleukin expression of activated HUVEC compared to surface contact with uncoated steel surfaces. A pronounced reduction of expression of IL-8 on certain PEM coated surfaces was observed. IL-8 is a mandatory messenger protein responsible for attraction of immune cells to the site of injury. The relations between physico-chemical properties of the surfaces and the interleukin expression are important for understanding of the immune response towards surfaces and for potential optimization of the immunosuppressive surface modifications.

The measurements of interleukin expression by cells in contact with surfaces on transcriptional level yielded the most accurate results. A correlation between the expression of mRNA coding for interleukin IL-8 and properties of the surfaces was evaluated. In figure 5.6 the expression of interleukin IL-8 mRNA is plotted against contact angle, zeta potential, surface roughness and surface elasticity.

No clear correlation between contact angle water and interleukin expression is observed. Cells in contact with SN05 and WN surfaces show a similar amount of IL-8 mRNA expression, although the contact angle is vastly different, 40 degree and 80 degrees respectively. The zeta potential shows a weak correlation with interleukin expression. The SN05 and WN surfaces are negatively charged (-40 mV and -10 mV zeta potential, respectively) and show the similar IL-8 mRNA expression. The positive charged coatings SP05 and WP both have a zeta potential of +40 mV, but show different effects on IL-8 mRNA expression.

The strongest correlations are observed between IL-8 mRNA expression and peak-count roughness and surface elasticity (Young's modulus). Rougher and stiffer surfaces might cause decrease of IL-8 mRNA expression.

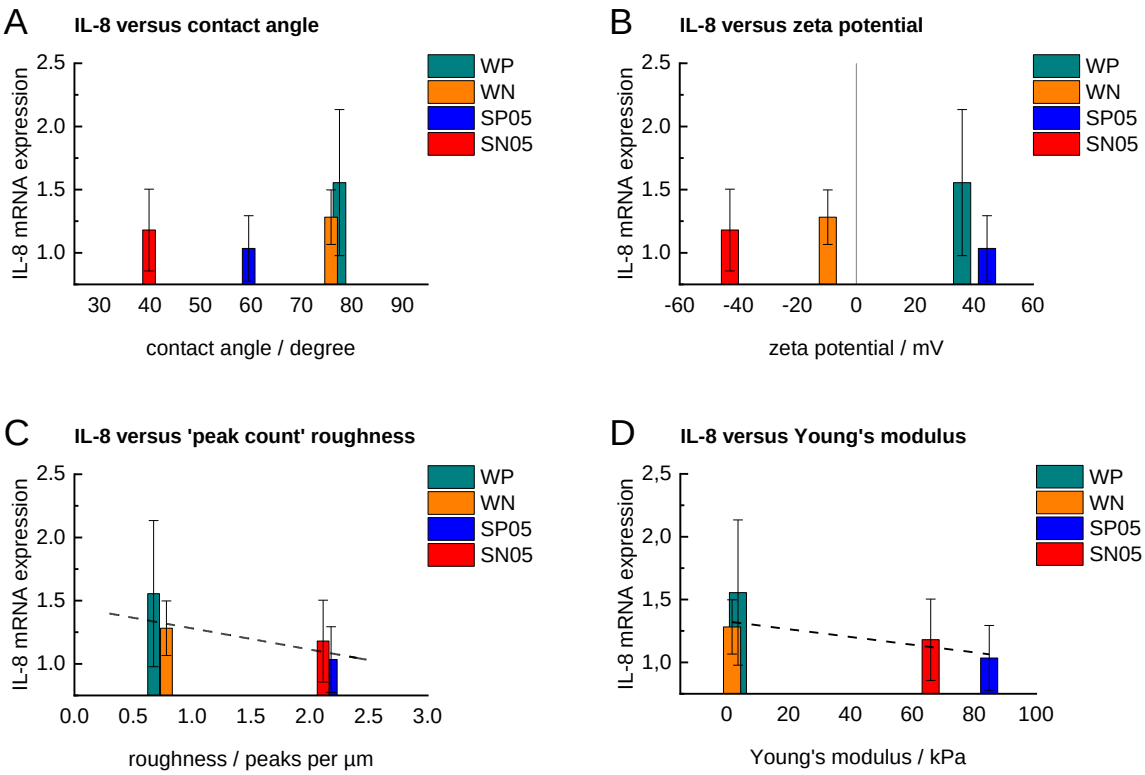

Fig. 5.6. Cellular relative expression of mRNA coding for interleukin IL-8 versus contact angle (A), zeta potential (B), peak-count roughness (C) and Young's modulus (D) of SP05, SN05, WP and WN coated surfaces. The controls are either Au QCM crystals for protein adsorption or corresponding non-coated steel pins for IL-8 mRNA expression. Lines are guides for the eye. See table 3.1 on page 38 for abbreviations.

The protein adsorption, cell adhesion and cell activity of HUVEC on SP05 and SN05 modified surface is different and might influence the expression. In figure 5.7, the IL-8 mRNA expression is plotted over the amount of adsorbed proteins from HUVEC cell culture medium, measured by QCM-D. No clear correlation is observed towards the protein adsorption.

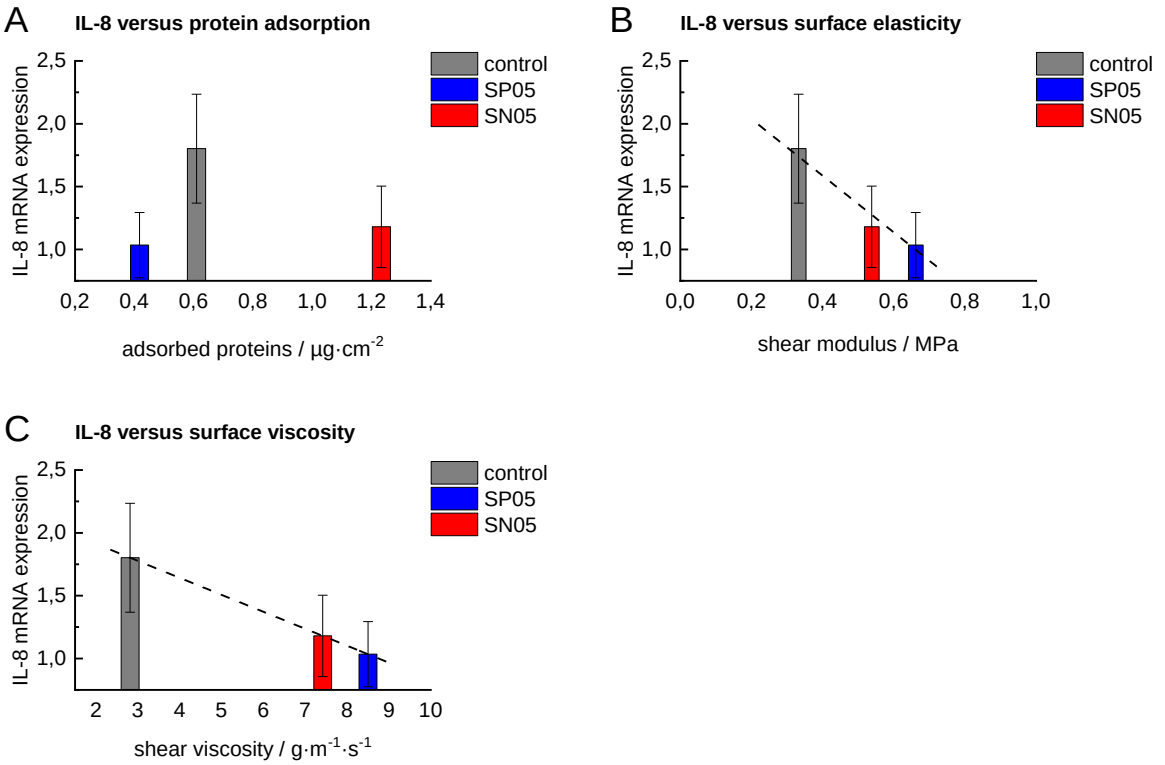

Fig. 5.7. Cellular relative expression of mRNA coding for interleukin IL-8 versus protein adsorption (d), surface elasticity (shear modulus) (e) and surface shear viscosity (f). The controls are either Au QCM crystals for protein adsorption, surface elasticity and surface viscosity and corresponding non-coated steel surfaces for IL-8 mRNA expression. Lines are guides for the eye. See table 3.1 on page 38 for abbreviations.

Surface elasticity (shear modulus) and surface viscosity (dynamic shear viscosity) of plain PEM surfaces show no correlation to IL-8 mRNA expression. However, if regarding the changed surface elasticity and viscosity by protein adsorption, a clear correlation to both becomes apparent. In figure 5.7-B,C the IL-8 mRNA expression is plotted over the shear modulus and the shear viscosity of PEM after incubation with HUVEC medium. A linear correlation is observed on both properties. A decrease of shear modulus after protein adsorption and a decrease in shear viscosity after protein adsorption of surfaces linearly reduce the IL-8 mRNA expression.

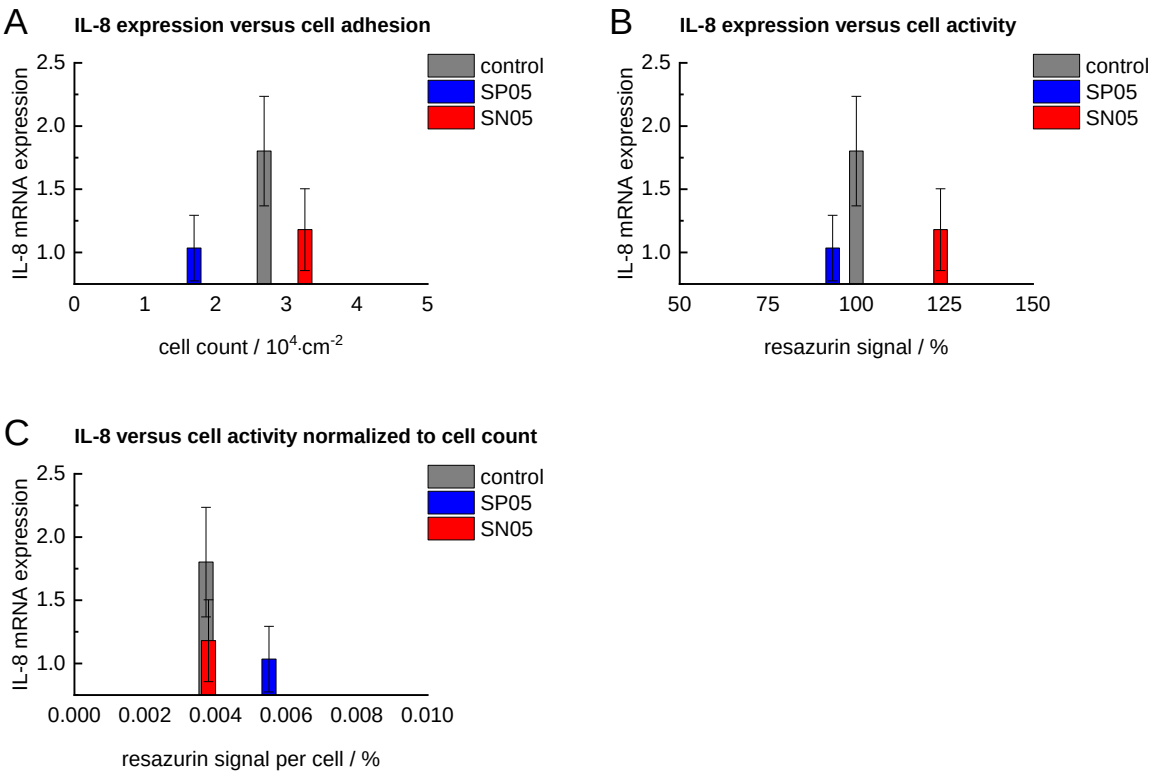

Fig. 5.8: Cellular expression of mRNA coding for expression of interleukin IL-8 (IL-8 mRNA) versus cell count (a), total cell activity (b) and cell activity per single cell (c). All results are normalized to the expression of mRNA on SP05 surfaces. The controls are Au-coated Si-wafers (for adhesion) and uncoated steel surfaces (for interleukin expression). See table 3.1 on page 38 for abbreviations.

The activation of immune response might be influenced by cellular adherence and activity. Figure 5.8 shows the expression of IL-8 mRNA plotted over number of cells, cellular activity and cellular activity per cell on PEM-modified surfaces. The number of adhered cells (figure 5.8-A) and cellular activity (figure 5.8-B) show no correlation to IL-8 mRNA expression, the signals of IL-8 mRNA on SP05 and SN05 are equally low, but show vastly different number of adhered cells and cellular activity. The cellular activity normalized to cell number (figure 5.8-C) might exponentially correlate with the IL-8 mRNA expression.

5.5 Summary – Characterization of immune response to surfaces via measurements of reduction of pro-inflammatory interleukin expression by HUVECs in contact with PEM coated surfaces

The precursor reactions of immune response by HUVEC towards surfaces modified with PEM coatings from poly(styrene sulfonate)/poly(allylamine hydrochloride) and hyaluronic acid/chitosan was characterized. The main pathway of immunological, inflammatory and foreign body reaction is the NF-κB pathway. In the progress of the pathway the transcription factor NF-κB is activated and translocated into the nucleolus inducing the transcription of genes coding for pro-inflammatory messenger molecules such as the interleukin family. The activation of NF-κB pathway was conducted by simultaneous biological stimulation with TNFα and by contact-pressure of PEM coated surfaces on top of the cells. The pro-inflammatory interleukins IL-1ß, IL-6 and IL-8 expression was measured on transcriptional (mRNA) by rt-PCR and translational (protein) level by quantitative ELISA.

Interleukin IL-1ß is expressed in very low quantities by HUVEC and no dependence on stimuli is observed. Neither TNFα-activation, nor contact with surfaces or both stimuli significantly affect the expression on both, transcriptional and translational level.

Interleukin IL-6 is expressed in higher quantities and the expression is amplified by ten-fold by the contact of substrate surfaces. Surfaces modified with SP05 and SN05 might reduce the IL-6 mRNA expression, however this could not confirmed on translational level. The SP05 and SN05 surfaces do not alter the IL-6 protein expression in comparison to uncoated steel surfaces. The surface modifications by WP and WN do not change the IL-6 mRNA expression, but even increase the IL-6 protein expression compared to uncoated steel surfaces.

Interleukin IL-8 is expressed in the highest quantities and the expression is amplified by ten-fold by contact with substrate surfaces. On transcriptional level the IL-8 mRNA expression is significantly reduced by contact to surfaces modified with WP, SP05 and SN05 in comparison to contact with plain steel surfaces. The significant reduction of IL-8 by contact with SP05 is confirmed by measurements of IL-8 protein expression. Therefore, the surface coating of SP05 is identified as the most promising surface modification to reduce IL-8 expression.

The expression of IL-8 mRNA is focused for analysis of correlation with surface properties. Neither the contact angle of water, nor the zeta potential show a distinct correlation. The strongest correlations are observed between IL-8 mRNA expression and peak-count roughness

of the surfaces and surface elasticity (Young's modulus). Rougher and stiffer surfaces reduce the IL-8 mRNA expression.

No direct correlation of IL-8 mRNA expression with the cell adhesion, cell activity or the amount of adsorbed proteins on surfaces is observed. The surface elasticity (shear modulus) and surface viscosity of plain PEM film do not correlate with IL-8 mRNA expression. However, when applying elasticity and viscosity levels changed by protein adsorption, a linear correlation becomes apparent. The surfaces need to have reduced surface elasticity and reduced surface viscosity after protein adsorption from cell culture medium in order to reduce the expression of IL-8 mRNA expression.

Chapter 6 – Achievements

The main goal of this work was the study of the effect of physico-chemical surfaces properties on behavior of biological cells such as adhesion, activity and immune response towards surfaces. Variations in surface properties such as surface charge, hydrophobicity, stiffness, roughness and viscoelastic properties were constructed by surface modification with polyelectrolyte multilayer coatings. A large part of this work is the characterization of protein adsorption on surfaces, as surface properties severely change in physiological conditions before any cell interactions take place. Following milestones and achievements have been reached in the course of this work.

1. Surfaces were precisely modified by polyelectrolyte multilayer (PEM) coatings. Variations in surface properties were reached by alteration of the used polyelectrolytes, negative or positive terminations and alteration of coating conditions. One PEM system was based on the synthetic strong polyanion and weak polycation and one PEM system was based on a weak polyanion and a weak polycation from natural origin. Further variation of the surfaces was conducted by alteration of electrolyte content in the deposition solutions during the coating process. The utilized PEM coatings are not harmful towards biological cells, which was confirmed by cytotoxic assay. A non-toxic, precise and robust system to alter surface properties was established.

2. Surface characterization techniques were specifically tailored and used to measure properties of the modified surfaces. The characterized surface properties included zeta potential, water contact angle, surface viscosity, surface elasticity (shear modulus and Young's modulus) and surface roughness. The modified surfaces were characterized and showed different characteristics in surface properties.

3. Protein adsorption on modified surfaces was measured. The adsorption of proteins from simple BSA solution as well as complex HUVEC cell culture medium was studied. Results showed variation in amount of proteins on different modified surfaces, as well as changes in shear viscosity and shear modulus of the surface. The protein adsorption behavior was explained by charge of the surfaces and intrinsic excess charge of PEM films.

4. The protein adsorption process was described and explained by contributions of surface charge and intrinsic excess charge. Negatively charged albumin is mostly repelled by negative surface charge and attracted by positive surface charge. Increasing intrinsic positive

excess charge of the PEM modified surfaces further amplifies BSA adsorption by enabling the diffusion of intrinsic mobile chains towards the surface. The adsorption of proteins from complex HUVEC medium differs from that of pure BSA solution. More proteins adsorb on negatively charged surfaces. Components of the HUVEC medium include albumins as well as strongly positively charged molecules, such as heparin, which act as a mediator between albumins and the surface. On negatively charged surfaces albumin-heparin complexes are attracted until coverage is reached, the surface charge is the predominant force. On positively charged surfaces both the surface charge as well as the positive excess charge contribute to the repulsion, hence on surface with high intrinsic positive excess charge the albumin-heparin complexes are increasingly repelled and the protein adsorption is lowered.

5. Measurements by neutron reflectometry revealed precise thickness and scattering length density of plain PEM films and PEM films altered by protein adsorption. Considering adsorbed mass, it was possible to calculate PEM film density and water content, as well as the protein layer thickness and protein layer density. A certain thickness of protein layer is observed on all tested PEM film surfaces. Notably, the protein layer thickness is incrementally increased on positively charged surfaces with higher intrinsic positive excess charge. The PEM film density and water content follow records from literature. The odd-even effect, which describes differences in water retention capacity of positively and negatively terminated PEM films was observed. An increase in electrolyte content of the deposition solution further amplified the odd-even effect.

6. Human umbilical vein endothelial cell adhesion experiments were conducted on modified surfaces. The modification of surfaces by application of PEM enables to precisely control the extent cell adhesion and switch a surface from adhesive to non-adhesive or vice versa. Alteration of coating conditions (the electrolyte concentration of the deposition solutions) enabled a precise control of the degree of cell adhesion and cell activity.

7. The cell adhesion was correlated to surface properties of modified samples. Surface Young's modulus and peak-count roughness correlate with cell adhesion. An increase in stiffness and roughness increases the adhesion of cells. Cell adhesion strongly correlates with the amount of adsorbed proteins from cell culture medium. A higher amount of adsorbed proteins on surfaces leads to higher numbers of adhered cells. When considering isolated PEM film dissipation, surface viscosity and zeta potential, these parameters show no effect on cell adhesion. However, when taking into consideration zeta potential combined with surface

viscosity, a trend is observable. Cells show more affinity towards negatively charged surfaces with increasing shear viscosity and towards positively charged surfaces with decreasing shear viscosity. The water content of PEM films directly correlates with the number of adhering cells.

8. A set of experiments was established to simulate the precursor reaction of the immune response after implantation of foreign material into the human tissue. Viable human endothelial cells were cultivated brought in contact with modified substrate surfaces. The immune response towards surfaces of implants is induced by activation of the nuclear factor kappa B pathway with subsequent cellular secretion of pro-inflammatory interleukins. The NfkB-pathway was measured at three points of evolution: (1) the activation of the transcription factor NfkB, (2) the expressed mRNA transcribing for pro-inflammatory interleukins and (3) the translated and secreted interleukins.

   The activation of NfkB was successfully monitored on positive and negative controls, however the timeframe of the life period of the active form was too short to yield significantly different results on modified sample surfaces. The transcription of genes for pro-inflammatory interleukins was successfully measured on controls and modified surfaces. A significant decrease in expression was observed by certain PEM modified surfaces, which was confirmed by measurements of secreted pro-inflammatory proteins. A certain set surface properties was identified, that contact-induces the reduction of the expression of pro-inflammatory interleukins on transcriptional and translational level.

9. The pro-inflammatory interleukin expression was correlated to properties of modified surfaces. A strong correlation was found in surface elasticity (Young's modulus) and peak-count roughness. The increase in vertically directed stiffness (Young's modulus) and an increase in roughness (by peak-count definition) induces a significant decrease in interleukin expression. Horizontally directed stiffness (shear modulus) and surface viscosity of plain modified surfaces show no correlation, however after protein adsorption form cell culture medium these parameters are changed and reveal a correlation to interleukin expression. A decrease in shear modulus or shear viscosity after protein adsorption decreases the interleukin expression. This important insight mediates that surface properties of plain materials are not set in stone and surface property changes by environment must be considered when studying the effect on biological cells.

Chapter 7 – Materials and Methods

This section details the materials and methods used for each measurement conducted in the thesis. The numbers in the headings correspond to the chapters where the measurement results are presented and discussed.

Surface modification with polyelectrolyte multilayers (PEM) – chapter 3

Polyelectrolyte multilayers (PEM) were constructed by alternating deposition of polyelectrolytes (PE) from watery solution on substrate surfaces. The polyelectrolytes poly(ethylene imine) (PEI, brenched, Mn 60 kDa by GPC, Mw 750 kDa by LS) and poly(styrene sulfonate (PSS, 70 kDa) and the electrolyte sodium chloride (NaCl >99 %) were purchased from Sigma Aldrich, Germany. Poly(allylamine hydrochloride) (PAH, 120-200 kDa) was purchased from Alfa Aeasar, Germany. Hyaluronic acid (HA, sodium hyaluronate, Mw 323 kDa) was purchased from Lifecore Biomedical, US. Chitosan (CHI, Chitosan 95/50, deacetylation degree > 92.6 %, 100-200 kDa) was purchased from Heppe Medical Chitsan, Germany. For deposition solutions PSS and PAH were dissolved at 2 g/L in water with sodium chloride concentrations of either 0 M (no NaCl), 0.5 M or 1 M (NaCl, Sigma Aldrich, Germany). The pH of deposition solutions was adjusted to 7.0. The polyelectrolytes HA and CHI were dissolved at 1 g/L in 5 mM sodium acetate trihydrate buffer (NaAc, Fluka Chemika-BioChemika, Germany) at pH of 5.5. After preparation the deposition solution were filtered to sterile conditions (Filtropur V25, Sarstedt, pore size = 0.45 µm). The subsequent coating procedure was performed in a laboratory workbench (class 1) to reduce the risk of contaminating the coatings before the cell experiments.

The PEM surface modifications were prepared on different substrates in regard to the characterization method and application. The substrates were cleaned extensively before the coating procedure by ultra-sonication in acetone and isopropanol. After nitrogen drying, the surface was activated by plasma cleaning for 5 min (Plasma Prep 2, GaLa Instrumente, Germany).

The PE were deposited on substrates with the Layer-by-Layer deposition technique [Decher *et al.* 1992] by either dipping the substrates in reservoirs filled with PE deposition solution or by adding and aspirating of PE deposition solution to substrates such as multiwell plates. All coatings were prepared using polyethyleneimine (PEI, 0.1 M in water at pH = 7.0) as adhesion promoting layer, which was followed by alternating deposition of negatively charged PEs (PSS, HA) and positively charged PEs (PAH, CHI). After each PE deposition step, the substrates were

rinsed three times for two minutes in either ultrapure water (resistivity = 18.2 MΩ·cm) for PSS/PAH or 5 mM NaAc buffer for HA/CHI.

The PEM coatings were prepared with positive termination (5 bilayers) or with negative termination (5.5 bilayers) governing the surface charge of the completed PEM surface. Following PEM coatings were prepared and used throughout the thesis:

PEM:	Composition	Termination (charge):	Solvent of deposition solution:
SP0	PEI/(PSS/PAH)5	PAH (+)	0 M (no NaCl)
SN0	PEI/(PSS/PAH)5/PSS	PSS (-)	0 M (no NaCl)
SP05	PEI/(PSS/PAH)5	PAH (+)	0.5 M NaCl
SN05	PEI/(PSS/PAH)5/PSS	PSS (-)	0.5 M NaCl
SP10	PEI/(PSS/PAH)5	PAH (+)	1.0 M NaCl
SN10	PEI/(PSS/PAH)5/PSS	PSS (-)	1.0 M NaCl
WP	PEI/(HA/CHI)5	CHI (+)	0.005 M NaAc
WN	PEI/(HA/CHI)5/HA	HA (-)	0.005 M NaAc

Contact angle of water measurements – chapters 3.2.1 and 3.3.1

The contact angle of water on PEM-coated Si-wafers and PEM-coated Au-Si-wafers was measured with contact angle measuring system OCA 15E (DataPhysics Instruments, Germany). Drop shapes analysis is based on the Young-Laplace fitting, using SCA 20 Software, DataPhysics. A minimum of four measurement at different points of the sample surface were tested. Each surface was measured in triplicate.

Zeta potential of PEM-modified surfaces – chapters 3.2.2 and 3.3.2

The zeta-potential was measured by Zetasizer Nano ZS (Malvern Instruments, Germany). The PEM coatings were prepared on non-sedimenting silica particles with radius of ~200 nm. Zeta-potential was measured in triplicate at each polyelectrolyte coating step. The tests were always performed in distilled water in equilibrium with the room atmosphere. This assures certain

conductivity of around 1 mS/cm of the suspensions of the PEM coated SiO_2 particles. All measurements were performed in triplicate.

AFM Characterization of surface roughness of PEM-modified surfaces – chapter 3.2.3

The contact-mode imaging was performed on a NanoWizard® I from JPK Instruments, Bruker, Germany in the department of nanobiotechnology at BOKU University of Natural Resources and Life Science, Vienna, Austria. The AFM probes used for contact mode were DNP-S10, non-conductive silicon nitride, tip: 600 nm, cantilever B with a base frequency of 23 kHz and a spring constant of 0.12 N/m from Bruker, Germany. The samples were PEM coated glass slides. The samples were immersed in liquid environment (0.1 M NaCl solution) during the measurements to measure topography in wet conditions. The topography of an area of 10 μm2 was measured on at least three points on three samples. The average roughness, peak-to-valley roughness and root mean squared roughness were calculated via the analytical software Data Processing, version 5.0.62 from JPK Instruments. The peak-count roughness was manually calculated from evaluation of two diagonal profile lines on 10 μm^2 on all topographic images.

AFM Characterization of mechanical stiffness (Young's modulus) of PEM-modified surfaces – chapter 3.2.4

The force spectroscopy was performed on a NanoWizard® I from JPK Instruments, Bruker, Germany in the department of nanobiotechnology at BOKU University of Natural Resources and Life Science, Vienna, Austria. The AFM probes used for force spectroscopy were DNP-S10, non-conductive silicon nitride, tip: 600 nm, cantilever B with a base frequency of 23 kHz and a spring constant of 0.12 N/m from Bruker, Germany. The PEM-coated glass slides were immersed in liquid environment (0.1 M NaCl solution) during the measurements. A UV-Cleaner (UV Ozone Cleaner – ProCleaner Plus, BioForce Nanosciences) was used to discharge the AFM probes before measurements. The thermal tune method by [Hutter & Bechhoefer 1993] was used to precisely determine the spring constant of the cantilevers. The tip-sample separation method was used to calculate the indentation of the sample [Saravia & Toca-Herrera, 2009]. By following physical description, it is possible to measure indentation of the sample when a cantilever with a defined spring constant is applied:

$$\delta = h - h_{contact} - \frac{F}{k}$$

, where δ is Indentation; h is displacement; $h_{contact}$ is displacement as the contact takes place; F is applied force; and k is cantilever spring constant. The force curves were measured by application of piezo extending speed of 0.5 µm/s and a setpoint of 3.0 nN.

The measured force curves were analyzed by a variation of the Hertz model for four-sided pyramidal indenters to calculate the Young's Modulus [Rico *et al.* 2005]:

Hertz equation:

$$F = \frac{E \cdot tan(\alpha) \cdot \delta^2}{(1 - \nu^2) \cdot \sqrt{2}}$$

which follows:

$$E = \left(\frac{F \cdot (1 - \nu^2) \cdot \sqrt{2}}{tan(\alpha)}\right) \cdot \delta^2 = constant \cdot \delta^2$$

where δ is measured indentation; F is applied force at 3 nN; ν is Poisson's ratio of 0.5; α is the front angle of the pyramidal tip is 15 ± 2.5°; and E is the Young's Modulus.

The measurements of force curves were performed on nine points per surface. Each sample was measured in triplicate.

<u>QCM-D Characterization of PEM build-up and protein adsorption on PEM-coated surfaces, measurement of adsorbed mass, shear modulus and shear viscosity – chapters 3.3.3, 3.3.4 and 4.2.2</u>

The measurements were performed online by performing a PEM film deposition or protein deposition on a running QCM-D measurement.

Gold-covered Quartz crystal microbalance sensor crystals (a = 1 cm^2, QSX 301 Gold) were purchased from QSense, Sweden and served as substrates for adsorption.

For characterization of the build-up process and protein adsorption the Quartz Crystal Microbalance with Dissipation monitoring (QCM-D) from QSense AB, Sweden was employed. Mass deposition on the sensor crystals decreases their oscillation frequency. The change in the oscillation frequency is converted to mass increase by applying the Sauerbrey equation. The change in the mass (Δm) can be calculated from measuring the oscillating frequency shift (Δf)

with the specific sensor material constant based on fundamental frequency, thickness and density of the quartz crystal (here 17.7 ng·cm^{-2}·Hz^{-1}) in relation to the overtone (n).

$$\Delta m = -C\,\frac{\Delta f}{n}$$

Several harmonic overtones of 5, 15, 25, 35, 45, 55 MHz were monitored. The presented data for Δf is always for the 5th overtone (basic frequency of 25 MHz), Sauerbrey mass calculations were also performed on the 5th overtone. All measurements were performed in watery environment at least in triplicate.

After the adsorption of proteins on top of PEM-films, the films were considered not strictly rigid and a different model was applied. The more complex modeling by Voigt model of the QCM-D data was used on the modelling software QTools (V. 3.1, Biolin Scientific AB, Sweden) to calculate mass of films after the deposition of protein and for calculation of the viscous and elastic properties. The model was used to simultaneously fit the third, fifth, seventh, ninth and eleventh overtones. The Voigt model regards the film-coated senor crystal setup as system with elastic shear moduli and viscosities, which are contributed by the bulk liquid, the film and the quartz crystal:

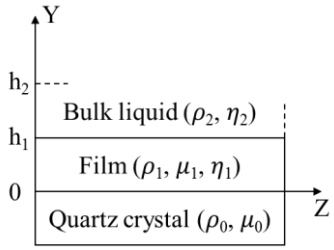

The dissipation (energy loss) and the frequency shift are used to model the elastic and viscous properties of the film by following equations:

$$\Delta f \approx -\frac{1}{2\pi\rho_0 h_0}\left\{\frac{\eta_2}{\delta_2} + h_1\rho_1\,\omega - 2h_1\left(\frac{\eta_2}{\delta_2}\right)^2 \frac{\eta_1\omega^2}{\mu_1^2 + \eta_1^2\omega^2}\right\}$$

$$\Delta D \approx \frac{1}{2\pi f\rho_0 h_0}\left\{\frac{\eta_2}{\delta_2} + 2h_1\left(\frac{\eta_2}{\delta_2}\right)^2 \frac{\mu_1\omega}{\mu_1^2 + \eta_1^2\omega^2}\right\}$$

There Δf and ΔD are frequency and dissipation changes; $\rho_{0,1,2}$ are densities of the quartz crystal (0), the film (1) and the bulk liquid (2); $\mu_{0,1}$ are elastic shear moduli of the quartz crystal (0) and the film (1); $\eta_{1,2}$ are viscosities of the film (1) and the bulk liquid (2).

For the modelling the densities of PEM-films and protein-films, as well as density and viscosity of water, were estimated. The density of PEM films was set to 1.1 $g \cdot cm^{-3}$ and the density of protein films was set to 1.2 $g \cdot cm^{-3}$ according to [Elzbieciak *et al.* 2009]. The density of bulk liquid (water) was set to 0.997 $g \cdot cm^{-3}$ and viscosity to 0.9544 $g \cdot m^{-1} \cdot s^{-1}$. All PEM films and PEM-protein films were measured and analyzed at least in triplicate.

Neutron reflectometry measurements of thickness and scattering length density of PEM films and of PEM films after BSA adsorption – chapters 3.3.5.1 and 4.3

PEM film samples were prepared on Si support blocks by dipping technique. For PEM-protein measurements, the completed PEM-coated Si blocks were immersed for 1 h in 1 mg/mL pure BSA solution in TRIS buffer (pH = 7.4). To ensure a high scattering contrast the completed PEMs were exposed to a D_2O environment, allowing all H_2O content to be replaced by D_2O driven by diffusion. All experiments were performed on D_2O soaked PEM films. The samples were studied against liquid D_2O directly after their preparation and without any intermediate drying. These experiments were performed using a solid/liquid experimental cell as described in [Delajon *et al.* 2005].

The reflectivity, R, which is the ratio between the intensity of the incoming to the reflected beam, was measured as a function of the momentum transfer, Q. The experiments were conducted with D_2O on the bottom of the experimental cell against a silicon block above it. In this setup, the lower medium has a higher scattering length density (SLD) than the upper one. Under these conditions, R = 1 for Q below a critical value Q_c. Above Q_c, R decays with Q, and the shape of the dependence is a function of the area-averaged scattering length density profile normal to the interface. A beam of rectangular cross section was set by a slit system on the sample side. At the neutron reflectometer AMOR at the Paul Scherrer Institute, Villigen, Switzerland, the experiments were performed in time-of-flight (ToF) mode at three angles of incidence (0.4°, 0.9°, and 1.5°), covering the entire necessary Q range. The background signal was directly subtracted from the specular signal to obtain the corrected intensity. The reflectivity data were footprint-corrected for the varying flux on the sample as θ increased.

A single neutron reflectometry (NR) experiment can provide information on the film thickness, d, the scattering length density profile, ρ(z), across the film, and the surface roughness, σ, between different layers. This technique determines the optical reflectivity of neutrons from planar surfaces using a calculation based on a recursion scheme for stratified media. The film is modeled as layers with specific thickness, scattering length density, and roughness, which serve as fitting parameters. The model reflectivity profile is calculated and compared to the measured data, and the fitting parameters are adjusted to achieve the best fit. For sufficiently large Q values, the layer thickness, d, can be estimated from the spacing, ΔQ, of the minima of two neighboring interference fringes using the relation $d \approx 2\pi/\Delta Q$ [Delajon et al. 2005].

The experimentally obtained reflectivity curves were analyzed by applying the standard fitting routine using the NCNR online reflectivity calculator, which was supplied by [Maranville 2017].

Cytotoxicity of PE and extracts of PEM from poly(styrene sulfonate)/poly(allylamine hydrochloride) (PSS/PAH) and hyaluronic acid/chitosan (HA/CHI) – chapter 3.3.6

The setup of experiments is based on suggestions from guidelines for biological evaluation of medical devises, ISO 10993-5 - Tests for in vitro cytotoxicity and ISO 10993-12 - Sample preparation and reference materials. The tested solutions were PE stock solutions and extracts from PEM coatings on stent substrates. The extraction was performed by incubation in DMEM cell culture medium with 10 % FCS under agitation for 24 h at 37 °C. The ratio of extraction medium volume to surface was conducted according to suggestions from ISO 10993-12:10.3.3. The extracts or PE stock solutions were diluted with DMEM medium and incubated for 24 h on confluent L929. Afterwards the cell viability was quantified by resazurin assay. Extracts of non-toxic polypropylene and toxic latex served as negative and positive controls. The absorption of the reaction product resorufin was spectroscopically measured at 570 nm wavelength. The growth inhibition ($G.I.in\ \%$) was calculated according to:

$$G.I.in\ \% = \frac{A_{570}(sample - blank) - A_{570}(negative\ control - blank)}{A_{570}(positive\ control - blank) - A_{570}(negative\ control - blank)} \cdot 100$$

where A_{570}-blank is the resazurin absorption in empty wells without cells; A_{570}-sample is the absorption from wells with cells after pretreatment for 24 h with PEM-extract dilutions; A_{570}-

negative-control is absorption from wells with cells after pretreatment with non-toxic polypropylene (0 % growth inhibition); and A_{570}-positive-control is the absorption from wells with cells after pretreatment with toxic latex (100 % growth inhibition).

Biological characterization of HUVECs adhesion and viability on PEMs from poly(styrene sulfonate)/poly(allylamine hydrochloride) (PSS/PAH) with variation of electrolyte concentration in the deposition solution – chapter 4.2.1

Cell adhesion, activity and proliferation were measured on PEM-modified poly(styrene) well plates and PEM-modified Au-coated Si-wafers (Silicon (Cz), orientation (100), type and doping agent: p-type and boric, spec. resistance 1 – 35 Ω·cm, polished) were purchased from CrysTec, Germany.

The number of adhered cells and were measured by optical microscopy. The activity was measured by metabolic assay via resazurin.

Pooled HUVEC Human Vein Endothelial Cells and optimized HUVEC cell culture medium with supplement mix were purchased from PromoCell, Germany. HUVECs up to the 10th passage were seeded (10,000 cell·cm^{-1}) and cultivated on PEM-coated non-tissue-culture-treated polystyrene (PS) microtiter plates (multiwell plate for suspension culture, poly(styrene), Greiner Bio-One, Germany). The untreated PS multiwell plates show very weak adhesion of HUVEC and served as control. Tissue-culture-treated (TCT) multiwell plates served as control for strong cell adhesion (Corning® Costar® cell culture plates from Sigma-Aldrich, Germany). After 24 h, 48 h or 72 h the cells were stained as following: cellular nucleolus was stained by Diamidine phenylindole dihydrochloride (DAPI, purchased from Sigma Aldrich, Germany) and actin filaments by fluorescent phalloidin conjugate (Life Technologies GmbH, Germany). The cells were fixed with 4 % (v/v) paraformaldehyde in PBS and stained by DAPI and phalloidin in PBS. Fluorescence images were taken on the Axiovert 200M from Zeiss, Germany.

The Resazurin Assay was performed on HUVECs cultivated on PEM-coated non-tissue-culture-treated polystyrene (PS) microtiter plates (multiwell plate for suspension culture, poly(styrene), Greiner Bio-One, Germany) and on PEM-coated Au-Si-Wafers. HUVECs were seeded on the substrates (10,000 cells·cm^{-2}) and incubated at 37 °C and 5 % CO_2. After 24 h, 48 h or 72 h the medium was exchanged by fresh medium containing 10 mg·L-1 resazurin sodium salt (Sigma Aldrich, Germany). Viable cells quantitatively reduce resazurin to resorufin by citrate cycle. The

concentrations of resazurin and resorufin in the supernatant were measured at 600 nm and 570 nm by multiplate reader PHERAstar (BMG LABTECH, Germany).

Measurement of activation and translocation of nuclear factor kappa B (NF-κB) – chapter 5.1

Pooled human umbilical vein endothelial cells (HUVEC) were purchased from PromoCell, Germany and cultivated according to PromoCells cultivation protocol in optimized endothelial cell growth medium with supplement mix. The cell growth medium contained fetal calf serum (FCS, 0.02 $mL \cdot mL^{-1}$), epidermal growth factor (0.1 $ng \cdot mL^{-1}$), heparin (90 $\mu g \cdot mL^{-1}$), hydrocortisone (1 $\mu g \cdot mL^{-1}$) and endothelial cell growth supplement from aqueous bovine hypothalamus extract (0.004 $mL \cdot mL^{-1}$). The HUVECs were seeded at numbers of 10,000 $cells \cdot cm^{-2}$ and incubated at 37 °C for 24 h on tissue-culture-treated well plates (TC-treated multiwell plates, tissue-culture treated poly(styrene), Corning Inc., US). The confluent cells were activated for 10 min by 40 $ng \cdot mL^{-1}$ TNFα in HUVEC medium and/or by addition of PEM-coated medical steel inlets. The cells were biologically activated by TNFα (Human TNF-alpha Protein in FN, Thermo Fisher) and by contact with the PEM-coated steel surfaces (Steel pins, A2-70, Würth, Germany). The following fixation and staining were carried out according to guidelines from Cell Signaling Technology, US. After activation, the cells were rinsed with PBS and fixed with 4 % (v/v) paraformaldehyde (PFA) in PBS for 20 min at room temperature. Unspecific binding sites were blocked with a blocking buffer of 5 % horse-serum (v/v) / 0.3 % Triton X-100 (v/v) in PBS for 1 h. The primary antibody (XP® NF-kappaB p65 (D14E12) XP® Rabbit mAb, Cell Signaling Technology, Inc., US) was diluted in 1 % horse-serum (v/v) / 0.3 % Triton X-100 (v/v) in BPS and applied for 2 h on the wells. The secondary fluorochrome-conjugated antibody (Goat anti-Rabbit IgG (H+L) Cross-Adsorbed Secondary Antibody, Alexa Fluor 546, Thermo Fisher Scientific, Germany) was applied for 2 h in the dark. DAPI (Sigma Aldrich) and fluorochrome-conjugated phalloidin (Phalloidin Oregon Green, Invitrogen) simultaneously applied for 3 h on the wells. The fluorescent imaging was performed on the Axiovert 200M microscope from Zeiss, Germany.

Measurement of pro-inflammatory interleukin mRNA expression of HUVEC in contact with PEM-modified surfaces – chapter 5.2

The expression of mRNA coding for pro-inflammatory interleukins IL-1ß, IL-6 and IL-8 by cells biologically activated by tumor necrosis factor alpha (TNF-α) and by physical contact with substrate surfaces was measured by real-time polymerase chain reaction (rt-PCR).

Pooled human umbilical vein endothelial cells (HUVEC; PromoCell, Germany) were seeded at cells·cm^{-2} in tissue-culture-treated 96-well plate (TC-treated multiwell plates, tissue-culture treated poly(styrene), Corning Inc., US) and cultivated in optimized endothelial cell growth medium with supplement mix (PromoCell, Germany) at 37 °C and 5 % CO_2. After 24 h, the cell growth medium was replaced. Half of the wells were filled with fresh cell growth medium, the other half with cell growth medium containing 40 ng·mL^{-1} TNF-α for biological activation. Immediately after changing the medium, PEM-coated and uncoated steel substrate inlets were put on top of the intact cell layer to introduce activation by cellular contact with surfaces. The flat pin heads, which are slightly smaller than the well bottom area, were directed towards the flat bottom of well to ensure high contact area between cells and inlet surface. The well plates were incubated for 4 h, in which the expression of mRNA took place.

The steel substrates and cell growth medium were removed, the cells were detached and the QIAshredder columns and RNeasy kit (from Qiagen, Germany) were applied according to manual to extract and isolate total mRNA. The application of the kit involved the separation of genomic DNA. Contents of three wells were pooled together to reach 0.1 µg total mRNA per sample. The Reverse Transcriptase Core kit from Eurogentec, Belgium was applied to translate mRNA in cDNA by reverse transcriptase (EuroScript, Moloney Murine leukemia virus rev. transcriptase, 50 U/µL) with the thermocycler Whatman from Biometra, Germany by a program of 10 min at 25 °C (primer binding), 30 min at 48 °C (reverse transcription) and 5 at 95 °C (inactivation of reverse transcriptase).

The sequence of primers for housekeeping gene and target interleukins was as followed:

Primer:	Primer Sequence (forward 5‘-3‘ & reverse 3‘-5‘):	Amplicon size (bp):
GAPDH	F: AGAAAAACCTGCCAAATATGATGAC	126
	R: TGGGTGTCGCTGTTGAAGTC	
IL-6	F: GGTACATCCTCGACGGCATCT	81
	R: GTGCCTCTTTGCTGCTTTCAC	
IL-8	F: TCTGTGTGAAGGTGCAGTTTTG	212
	R: CAACCCTCTGCACCCAGTTT	

A mastermix for each primer pair was prepared. The forward and reverse primer stocks were mixed with MESA GREEN qPCR MasterMix Plus for SYBR Assay I (Low ROX) from Eurogentec, Belgium. Molecular-biological clean water (VWR, Germany) was used for dilution steps. The mastermix was mixed with cDNA measured by the Fast Real-Time PCR System 7500 from Applied Biosystems, US. The main PCR program ran repeated cycles of 95 °C for 15 s, 60 °C for 20 s and 72 °C for 40 s to amplify cDNA. In the amplification plot the upper and lower limit of accurate measurements was identified and the middle value of colorimetric signal was used for evaluation of amplification cycles.

For evaluation by ΔΔCP method [Livak & Schmittgen 2001], the surface contact stimulation of cells with simultaneous biological TNF-α activation was defined as initiator. The PEM surface modifications were defined as treatment. The three groups of samples were measured. One control group was measured without initiator and without treatment. Two groups of cells were stimulated by the initiators, of which one was a measured in contact with uncoated surfaces (- treatment) and the other in contact with PEM-modified surfaces (+ treatment). The ratio of expression between the initiated groups with and without treatment is the relative expression ratio.

The relative expression ratio was calculated by ΔΔCT method as follows:

$$R = \frac{\left(E_{target\ gene}\right)^{\Delta CT_{target\ gene}(control-treatment)}}{\left(E_{reference\ gene}\right)^{\Delta CT_{reference\ gene}(control-treatment)}}$$

, where R is the relative expression ratio; $E_{target\ gene}$ is the relative expression of target molecules (IL-1ß, IL-6, IL-8); $E_{reference\ gene}$ is the relative expression of the house-keeping

gene (GAPDH); and CT values are the number of cycles of target molecules or housekeeping genes at the same colorimetric signal in PCR measurement data. As such, a relative expression ratio of 1 meant the PEM-modification had no effect on the expression. The relative expression ratio >1 meant the pro-inflammatory IL expression was increased by the treatment. The relative expression ratio <1 meant a decrease of interleukin expression by the treatment was measured. All sets of experiments were replicated at least six times (n = 6).

Measurement of pro-inflammatory interleukin expression of HUVEC in contact with PEM-modified surfaces – chapter 5.3

The expression of pro-inflammatory interleukins IL-1ß, IL-6 and IL-8 by cells biologically activated by tumor necrosis factor alpha (TNF-α) and by physical contact with substrate surfaces was measured by quantitative sandwich ELISA.

Pooled human umbilical vein endothelial cells (HUVEC; PromoCell, Germany) were seeded at 3000 cells·cm^{-2} in tissue-culture-treated 96-well plate (multiwell plate for suspension culture, poly(styrene), Greiner Bio-One, Germany) and cultivated in optimized endothelial cell growth medium with supplement mix (PromoCell, Germany) at 37 °C and 5 % CO_2. After 24 h, the cell growth medium was replaced. Half of the wells were filled with fresh cell growth medium, the other half with cell growth medium containing 40 ng·mL^{-1} TNF-α for biological activation. Immediately after change of medium, PEM-coated and uncoated steel substrate inlets were put on top of the intact cell layer to introduce activation by cellular contact with surfaces. The flat pin heads, which are slightly smaller than the well bottom area, were directed towards the flat bottom of well to ensure high contact area between cells and inlet surface. The well plates were incubated for 24 h, in which the expression of interleukin expression took place and was secreted by the cells into the medium.

The Quantikine ELISA Human IL-1ß, IL-6 and IL-8 Immunoassay kits were purchased from R&D Systems, US. The quantification of IL protein concentration in cell culture medium was performed according to manufacturer manuals. The sets of experiments were replicated six times for IL-1ß and IL-6, and 12 times for IL-8.

Literature

Allen *et al.* 2006	Allen LT, Tosetto M, Miller IS, O'Connor DP, Penney SC, Lynch I, *et al.* Surface-induced changes in protein adsorption and implications for cellular phenotypic responses to surface interaction. Biomaterials. 2006;27(16):3096–3108. doi:10.1016/j.biomaterials.2006.01.019.
Andrade & Hlady 1987	Andrade JD, Hlady V. Plasma protein adsorption: the big twelve. In: Blood in Contact with Artificial Surfaces. Ann NY Acad Sci. 1987;516(1):158-172. doi:10.1111/j.1749-6632.1987.tb33038.x.
Andreeva *et al.* 2016	Andreeva TD, Hartmann H, Taneva SG, Krastev R. Regulation of the growth, morphology, mechanical properties and biocompatibility of natural polysaccharide-based multilayers by Hofmeister anions. J Mater Chem B. 2016;4(44):7163-7174. doi:10.1039/C6TB01638C.
Bair *et al.* 1969	Bair RE, Dutton RC, Gott VL. Surface Chemistry of Biological System. In: Blank M, editor. On Surface Chemistry of Bio Systems. Proc Amer Chem Soc Symp. Plenum Press, N.Y.; 1969. p. 235.
Barbucci & Magnani 1994	Barbucci R, Magnani A. Surface Infrared Analysis of Standard Biomaterials. Biomaterials. 1994;15(12):955-960. doi:10.1016/0142-9612(94)90075-2.
Benbow *et al.* 2019	Benbow EJ, Smith AM, Jones RA, *et al.* Odd–even effect in polyelectrolyte multilayers: Influence on drying behavior. Macromolecules. 2019;52(4):1234-1242. doi:10.1021/acs.macromol.8b02234.
Bevilacqua *et al.* 1985	Bevilacqua MP, Pober JS, Wheeler ME, Cotran RS, Gimbrone MA Jr. Interleukin 1 acts on cultured human vascular endothelium to increase the adhesion of polymorphonuclear leukocytes, monocytes, and related leukocyte cell lines. J Clin Invest. 1985;76(5):2003-2011. doi:10.1172/JCI112200.
Billsten *et al.* 1995	Billsten M, Wahlgren M, Arnebrant T, McGuire J, Elwing H. Structural changes of T4 lysozyme upon adsorption to silica nanoparticles measured by circular dichroism. J Colloid Interface Sci. 1995;175(1):77-82. doi:10.1006/jcis.1995.1431.
Bjerrum *et al.* 1959	Bjerrum NJ. Obituary: Professor Niels J. Bjerrum. Trans Faraday Soc. 1959;55:X001. doi:10.1039/TF959550X001.
Büscher *et al.* 2002	Büscher K, Graf K, Laschewsky A, Ringsdorf H. Influence of polyelectrolyte deposition conditions on the structure of multilayers. Langmuir. 2002;18(9):3585-3591. doi:10.1021/la011657j.
Butt & Kappl 2018	Butt H-J, Kappl M. Surface and Interfacial Forces. 2nd ed. Weinheim: Wiley-VCH; 2018. doi:10.1002/9783527341658.
Cao *et al.* 2022	Cao G, Xuan X, Hu J, Zhang R, Jin H, Dong H. How vascular smooth muscle cell phenotype switching contributes to vascular disease. Cell Commun Signal. 2022;20:180. doi:10.1186/s12964-022-00993-2.
Carrière *et al.* 2004	Carrière D, Krastev R, Schönhoff M. Oscillations in solvent fraction of polyelectrolyte multilayers driven by the charge of the terminating layer. Langmuir. 2004;20(21):9533-9538. doi:10.1021/la049118m.
Chan & Schroder 2020	Chan AH, Schroder K. Inflammasome signaling and regulation of interleukin-1 family cytokines. J Exp Med. 2020;217(1):e20190314. doi:10.1084/jem.20190314.
Chattoraj & Mitra 1977	Chattoraj DK, Mitra SP. Adsorption of proteins at solid-liquid interfaces. Ind J Biochem Biophys. 1977;14:1-10.

Costa & Simon 2005	Costa MA, Simon DI. Molecular basis of restenosis and drug-eluting stents. Circulation. 2005;111(17):2257-2273. doi:10.1161/01.CIR.0000163587.36485.A7.
Cranford & Buehler 2012	Cranford SW, Buehler MJ. Materiomics: biological protein materials, from nano to macro. Prog Mater Sci. 2012;57(8):809-839. doi:10.1016/j.pmatsci.2012.03.001.
Curcio *et al.* 2011	Curcio A, Torella D, Indolfi C. Mechanisms of smooth muscle cell proliferation and endothelial regeneration after vascular injury and stenting. Circ J. 2011;75(6):1287–1296. doi:10.1253/circj.CJ-11-0366.
Debye & Hückel 1923	Debye P, Hückel E. Zur Theorie der Elektrolyte. I. Gefrierpunktserniedrigung und verwandte Erscheinungen. Phys Z. 1923;24:185–206. Translated by Braus MJ. 2019.
Decher & Schlenoff 2002	Decher G, Schlenoff JB, editors. Multilayer Thin Films. Weinheim: Wiley-VCH Verlag GmbH & Co. KGaA; 2002. ISBNs: 3-527-30440-1 (Hardback); 3-527-60057-4 (Electronic).
Decher 1997	Decher G. Fuzzy nanoassemblies: toward layered polymeric multicomposites. Science. 1997;277(5330):1232–1237. doi:10.1126/science.277.5330.1232.
Decher *et al.* 1992	Decher G, Hong JD, Schmitt J. Buildup of ultrathin multilayer films by self-assembly process. III. Consecutively alternating adsorption of anionic and cationic polyelectrolytes on charged surfaces. Thin Solid Films. 1992;210-211:831-835. doi:10.1016/0040-6090(92)90417-A.
Dee *et al.* 2002	Dee KC, Puleo DA, Bizios R. Protein-Surface Interactions. Wiley; 2002. ISBN: 978-0-471-25394-5.
Degasne *et al.* 1999	Degasne I, Baslé MF, Demais V, Hure G, Lesourd M, Grolleau B, Chappard D. Effects of roughness, fibronectin and vitronectin on attachment, spreading, and proliferation of human osteoblast-like cells (Saos-2) on titanium surfaces. Calcif Tissue Int. 1999;64(6):499-507. doi:10.1007/s002239900628.
Delajon *et al.* 2005	Delajon C, Gutberlet T, Steitz R, Möhwald H, Krastev R. Formation of Polyelectrolyte Multilayer Architectures with Embedded DMPC Studied in Situ by Neutron Reflectometry. Langmuir 2005, 21, 8509-8514. doi:10.1021/la050407n.
Delves & Roitt *et al.* 1998	Delves PJ, Roitt IM, editors. Encyclopedia of Immunology. 2nd ed. San Diego (CA): Academic Press; 1998.
Detzel *et al.* 2011	Detzel C, Hossfeld S, Schmitt-Sody M, *et al.* Linear and exponential growth regimes of polyelectrolyte multilayers: Mechanisms and applications. Langmuir. 2011;27(16):10016-10023. doi:10.1021/la2012345.
Dinarello 2005	Dinarello CA. Blocking IL-1 in systemic inflammation. J Exp Med. 2005;201(9):1355–1359. doi:10.1084/jem.20050640.
Dinarello *et al.* 2012	Dinarello CA, Simon A, van der Meer JW. Treating inflammation by blocking interleukin-1 in a broad spectrum of diseases. Nat Rev Drug Discov. 2012;11(8):633-652. doi:10.1038/nrd3800.
Dubas & Schlenoff 1999	Dubas ST, Schlenoff JB. Factors controlling the growth of polyelectrolyte multilayers. Macromolecules. 1999;32(24):8153-8160. doi:10.1021/ma990860+.
Dubas & Schlenoff 2001	Dubas ST, Schlenoff JB. Swelling and smoothing of polyelectrolyte multilayers by salt. Langmuir. 2001;17(25):7725-7727. doi:10.1021/la0112099.
Elbert *et al.* 1999	Elbert DL, Herbert CB, Hubbell JA. Thin polymer layers formed by polyelectrolyte multilayer techniques on biological surfaces. Langmuir. 1999;15(16):5355-5362. doi:10.1021/la990669a.

Elzbieciak *et al.* 2009	Elzbieciak M, Wysokinska E, Warszynski P. Influence of polyelectrolyte multilayer film structure on the adsorption of proteins. Colloids Surf B Biointerfaces. 2009;74(1):1-9. doi:10.1016/j.colsurfb.2009.06.001.
Fang & Szleifer 2001	Fang F, Szleifer I. Competitive adsorption of proteins. Biophys J. 2001;80(6):2568-2575. doi:10.1016/S0006-3495(01)76228-5.
Garcia & Boettiger 1999	Garcia AJ, Boettiger D. Integrin-fibronectin interactions at the cell-material interface: initial integrin binding and signaling. Biomaterials. 1999;20(23–24):2427–2433. doi:10.1016/S0142-9612(99)00183-3.
Geiger *et al.* 2009	Geiger B, Spatz JP, Bershadsky AD. Environmental sensing through focal adhesions. Nat Rev Mol Cell Biol. 2009;10(1):21-33. doi:10.1038/nrm2593.
Han *et al.* 2023	Han F, Shen Q, Zheng W, Zuo J, Zhu X, Li J, Peng C, Li B, Chen Y. The conformational changes of bovine serum albumin at the air/water interface: HDX-MS and interfacial rheology analysis. Foods. 2023;12(8):1601. doi:10.3390/foods12081601.
Hänni-Ciunel *et al.* 2007	Hänni-Ciunel K, Findenegg GH, von Klitzing R. Water contact angle on polyelectrolyte-coated surfaces: effects of film swelling and droplet evaporation. Soft Mater. 2007;5(2-3):61-73. doi:10.1080/15394450701554452.
Harada *et al.* 1994	Harada A, Mukaida N, Matsumoto T, Matsushima K. Inhibition of neutrophil-mediated acute inflammatory injury by an antibody against interleukin-8 (IL-8). Inflamm Res. 1994;43(12):551-556. doi:10.1007/BF01833493.
Hertz 1882	Hertz H. On the contact of elastic solids. J Reine Angew Math. 1882;92:156-171. doi:10.1515/crll.1882.92.156.
Horbett & Brash 1995	Horbett TA, Brash JL. In: Proteins at Interfaces II. Fundamentals and Applications. ACS Symp. Washington D.C.; 1995. doi:10.1021/bk-1995-0602.
Hu & Hassan 2019	Hu Z, Hassan MM. Effect of Poisson's ratio on material property characterization by nanoindentation with a cylindrical flat-tip indenter. J Mater Res. 2019;34(14):2482-2491. doi:10.1557/jmr.2019.160.
Hutter & Bechhoefer 1993	Hutter JL, Bechhoefer J. Calibration of atomic-force microscope tips. Rev Sci Instrum. 1993;64(7):1868-1873. doi:10.1063/1.1143970.
Huynh & Heo 2021	Huynh DTN, Heo KS. Role of mitochondrial dynamics and mitophagy of vascular smooth muscle cell proliferation and migration in progression of atherosclerosis. Arch Pharm Res. 2021;44(12):1051–1061. doi:10.1007/s12272-021-01360-4.
Indolfi *et al.* 2003	Indolfi C, Mongiardo A, Curcio A, Torella D. Molecular mechanisms of in-stent restenosis and approach to therapy with eluting stents. Trends Cardiovasc Med. 2003;13(4):142–148. doi:10.1016/S1050-1738(03)00061-2.
Inoue *et al.* 2003	Inoue T, Uchida T, Yaguchi I, Sakai Y, Takayanagi K, Morooka S. Stent-induced expression and activation of the leukocyte integrin Mac-1 is associated with neointimal thickening and restenosis. Circulation. 2003;107(14):1757-1763. doi:10.1161/01.CIR.0000060487.15126.56.
Inoue *et al.* 2008	Inoue T, Croce K, Morooka T, Sakuma M, Node K, Simon DI. Vascular inflammation and repair: implications for re-endothelialization, restenosis, and stent thrombosis. JACC Cardiovasc Interv. 2008;1(1):68-75. doi:10.1016/j.jcin.2007.10.009.
Istanbullu & Akdogan 2022	Istanbullu OB, Akdogan G. Influences of stent design on in-stent restenosis and major cardiac outcomes: a scoping review and meta-analysis. Cardiovasc Eng Technol. 2022;13(1):147–169. doi:10.1007/s13239-021-00569-0.

Istanbullu *et al.* 2021	Istanbullu E, Yildiz A, Koc M, *et al.* The impact of stent design on in-stent restenosis: a comparative study. J Cardiovasc Surg (Torino). 2021;62(3):345-352. doi:10.23736/S0021-9509.21.11634-5.
Jaminon *et al.* 2019	Jaminon A, Reesink K, Kroon A, Schurgers L. The role of vascular smooth muscle cells in arterial remodeling: focus on calcification-related processes. Int J Mol Sci. 2019;20(22):5694. doi:10.3390/ijms20225694.
Jandt & Cai 2007	Jandt KD, Cai K. Evolutions, revolutions and trends in biomaterials science – a perspective. Adv Eng Mater. 2007;9(12):1035-1041. doi:10.1002/adem.200700284.
Jorgenson *et al.* 1988	Jorgenson L, Richardson D, Neumann F. Mechanisms of in-stent restenosis. Circulation. 1988;78(6):1424-1432. doi:10.1161/01.CIR.78.6.1424.
Karimi *et al.* 2018	Karimi F, O'Connor AJ, Qiao GG, Heath DE. Integrin clustering matters: a review of biomaterials functionalized with multivalent integrin-binding ligands to improve cell adhesion, migration, differentiation, angiogenesis, and biomedical device integration. Adv Healthc Mater. 2018;7(12):e1701324. doi:10.1002/adhm.201701324.
Keselowsky *et al.* 2003	Keselowsky BG, Collard DM, Garcia AJ. Surface chemistry modulates fibronectin conformation and directs integrin binding and specificity to control cell adhesion. J Biomed Mater Res A. 2003;66(2):247–259. doi:10.1002/jbm.a.10537.
Keselowsky *et al.* 2004	Keselowsky BG, Collard DM, Garcia AJ. Surface chemistry modulates focal adhesion composition and signaling through changes in integrin binding. Biomaterials. 2004;25(28):5947–5954. doi:10.1016/j.biomaterials.2004.01.062.
Keselowsky *et al.* 2005	Keselowsky BG, Collard DM, Garcia AJ. Integrin binding specificity regulates biomaterial surface chemistry effects on cell differentiation. Proc Natl Acad Sci U S A. 2005;102(17):5953–5957. doi:10.1073/pnas.0407356102.
Kolasińka *et al.* 2005	Kolasińka M, Picart C, Mutterer J, *et al.* Exponential growth of polyelectrolyte multilayers: a scaling approach. Langmuir. 2005;21(18):8585-8590. doi:10.1021/la047451y.
Koźlik *et al.* 2023	Koźlik M, Harpula J, Chuchra PJ, Nowak M, Wojakowski W, Gąsior P. Drug-eluting stents: technical and clinical progress. Biomimetics. 2023;8(1):72. doi:10.3390/biomimetics8010072.
Kubiak *et al.* 2015	Kubiak K, Adamczyk Z, Wasilewska M. Mechanisms of fibrinogen adsorption at solid substrates. J Colloid Interface Sci. 2015;457:378-385. doi:10.1016/j.jcis.2015.07.009.
Kuramitsu *et al.* 2021	Kuramitsu S, Sonoda S, Ando K, Otake H, Natsuaki M, Anai R, Honda Y, Kadota K, Kobayashi Y, Kimura T. Drug-eluting stent thrombosis: current and future perspectives. Cardiovasc Interv Ther. 2021;36(2):158–168. doi:10.1007/s12928-021-00754-x.
Lan *et al.* 2005	Lan MA, Gersbach CA, Michael KE, Keselowsky BG, Garcia AJ. Myoblast proliferation and differentiation on fibronectin-coated self assembled monolayers presenting different surface chemistries. Biomaterials. 2005;26(22):4523–4531. doi:10.1016/j.biomaterials.2004.11.028.
Lawrence 2009	Lawrence T. The nuclear factor NF-κB pathway in inflammation. Cold Spring Harb Perspect Biol. 2009;1(6):a001651. doi:10.1101/cshperspect.a001651.
Lee *et al.* 1984	Lee CE, McCammon JE, Rossky PJ. The structure of liquid water at an extended hydrophobic surface. J Chem Phys. 1984;80(9):4448-4455. doi:10.1063/1.447226.

Lee *et al.* 2006	Lee MH, Ducheyne P, Lynch L, Boettiger D, Composto RJ. Effect of biomaterial surface properties on fibronectin-alpha5beta1 integrin interaction and cellular attachment. Biomaterials. 2006;27(9):1907-1916. doi:10.1016/j.biomaterials.2005.11.003.
Livak & Schmittgen 2001	Livak KJ, Schmittgen TD. Analysis of relative gene expression data using real-time quantitative PCR and the 2(-Delta Delta C(T)) Method. Methods. 2001;25(4):402-408. doi:10.1006/meth.2001.1262.
Lösche *et al.* 1998	Lösche M, Schmitt J, Decher G, Bouwman WG, Kjaer K. Detailed structure of molecularly thin polyelectrolyte multilayer films on solid substrates as revealed by neutron reflectometry. Macromolecules. 1998;31(25):8893-8906. doi:10.1021/ma980765t.
Majhy *et al.* 2021	Majhy B, Priyadarshini P, Sen AK. Effect of surface energy and roughness on cell adhesion and growth – facile surface modification for enhanced cell culture. RSC Adv. 2021;11(25):15467–15476. doi:10.1039/D1RA02402G.
Maleknia *et al.* 2020	Maleknia M, Ansari N, Haybar H, Maniati M, Saki N. Inflammatory growth factors and in-stent restenosis: effect of cytokines and growth factors. SN Compr Clin Med. 2020;2:397–407. doi:10.1007/s42399-020-00240-0.
Maranville 2017	Maranville BB. Interactive, web-based calculator of neutron and X-ray reflectivity. J Res Natl Inst Stan. 2017;122:34. doi:10.6028/jres.122.034.
Matsarskaia *et al.* 2020	Matsarskaia O, Selhuber-Unkel C, Erdmann T, López-García M, Kessler H, Schwarz US, Spatz JP. Cell adhesion strength is controlled by intermolecular spacing of adhesion receptors. Biophys J. 2020;98(4):543-551. doi:10.1016/j.bpj.2009.11.001.
McEver 2010	McEver RP. Selectins: initiators of leucocyte adhesion and signalling at the vascular wall. Cardiovasc Res. 2010;88(2):211-221. doi:10.1093/cvr/cvq230.
Mitra 2020	Mitra SP. Protein adsorption on biomaterial surfaces: subsequent conformational and biological consequences – a review. J Surf Sci Technol. 2020;36(1-2):7-38. doi:10.18311/jsst/2020/23282.
Mitra *et al.* 2006	Mitra AK, Agrawal DK. In stent restenosis: bane of the stent era. J Clin Pathol. 2006;59(3):232–239. doi:10.1136/jcp.2005.025742.
Nakashima *et al.* 1999	Nakashima Y, Sun DH, Trindade MC, Maloney WJ, Goodman SB, Schurman DJ, Smith RL. Signaling pathways for tumor necrosis factor-alpha and interleukin-6 expression in human macrophages exposed to titanium-alloy particulate debris. J Bone Joint Surg Am. 1999;81(5):603-615. doi:10.2106/00004623-199905000-00006.
Navarese *et al.* 2014	Navarese EP, Kowalewski M, Kandzari D, Lansky A, Górny B, Kołtowski L, Waksman R, Berti S, Musumeci G, Limbruno U, van der Schaaf RJ, Kelm M, Kubica J, Suryapranata H. First-generation versus second-generation drug-eluting stents in current clinical practice: updated evidence from a comprehensive meta-analysis of randomised clinical trials comprising 31,379 patients. Open Heart. 2014;1(1):e000064. doi:10.1136/openhrt-2014-000064.
Neumann *et al.* 1996	Neumann FJ, Kastrati A, Schömig A. Mechanisms of coronary in-stent restenosis. J Am Coll Cardiol. 1996;28(4):804-812. doi:10.1016/0735-1097(96)00219-1.
Newby & Zaltsman 1999	Newby AC, Zaltsman AB. Fibrous cap formation or destruction—the critical importance of vascular smooth muscle cell proliferation, migration and matrix formation. Cardiovasc Res. 1999;41(2):345–360. doi:10.1016/S0008-6363(98)00286-7.

O'Brien & Carroll 2009	O'Brien B, Carroll W. The evolution of cardiovascular stent materials and surfaces in response to clinical drivers: a review. Acta Biomater. 2009;5(4):945–958. doi:10.1016/j.actbio.2008.12.012.
Olarte-Plata *et al.* 2020	Olarte-Plata JD, Brekke-Svaland G, Bresme F. The influence of surface roughness on the adhesive interactions and phase behavior of suspensions of calcite nanoparticles. Nanoscale. 2020;12(20):11165–11173. doi:10.1039/D0NR00834F.
Pelham & Wang 1997	Pelham RJ Jr, Wang YL. Cell locomotion and focal adhesions are regulated by substrate flexibility. Proc Natl Acad Sci U S A. 1997;94(25):13661-13665. doi:10.1073/pnas.94.25.13661.
Petreaca & Martins-Green *et al.* 2007	Petreaca ML, Martins-Green M. Dynamics of Cell-ECM Interactions. In: Lanza R, Langer R, Vacanti J, editors. Principles of Tissue Engineering. 3rd ed. 2007. p. 123-145.
Pyrillou *et al.* 2020	Pyrillou K, Burzynski LC, Clarke MCH. Alternative pathways of IL-1 activation, and its role in health and disease. Front Immunol. 2020;11:613170. doi:10.3389/fimmu.2020.613170.
Renné *et al.* 2012	Renné T, Schmaier AH, Nickel KF, Blombäck M, Maas C. In vivo roles of factor XII. Blood. 2012;120(22):4296-4303. doi:10.1182/blood-2012-07-292094.
Richardson *et al.* 1990	Richardson PD, Davies MJ, Born GV. Influence of plaque configuration and stress distribution on fissuring of coronary atherosclerotic plaques. Lancet. 1990;336(8710):941-944. doi:10.1016/0140-6736(90)92213-3.
Richert *et al.* 2004/1	Richert L, Lavalle P, Payan E, Shu XZ, Prestwich GD, Stoltz JF, Schaaf P, Voegel JC, Picart C. Layer by layer buildup of polysaccharide films: physical chemistry and cellular adhesion aspects. Langmuir. 2004;20(2):448-458. doi:10.1021/la034118+.
Richert *et al.* 2004/2	Richert L, Engler AJ, Discher DE, Picart C. Elasticity of native and cross-linked polyelectrolyte multilayer films. Biomacromolecules. 2004;5(5):1908-1916. doi:10.1021/bm0496173.
Rico *et al.* 2005	Rico F, Roca-Cusachs P, Gavara N, Farré R, Rotger M, Navajas D. Probing mechanical properties of living cells by atomic force microscopy with blunted pyramidal cantilever tips. Phys Rev E. 2005;72(2):021914. doi:10.1103/PhysRevE.72.021914.
Ridley *et al.* 2003	Ridley AJ, Schwartz MA, Burridge K, Firtel RA, Ginsberg MH, Borisy G, Parsons JT, Horwitz AR. Cell migration: integrating signals from front to back. Science. 2003;302(5651):1704-1709. doi:10.1126/science.1092053.
Rudt 2016	Rudt A. Force Spectroscopy of Polyelectrolyte Multilayer Coatings for Stents. Master's degree thesis, Reutlingen University, 2016.
Rudt *et al.* 2021	Rudt A, Sun J, Qin M, Liu L, Syldatk C, Barbeck M, Xiong X, Krastev R. Controlled Adhesion of HUVEC on Polyelectrolyte Multilayers by Regulation of Coating Conditions. ACS Applied Bio Materials. 2021 4(2), 1441-1449. doi:10.1021/acsabm.0c01330
Rogers *et al.* 1998	Rogers C, Edelman ER, Simon DI. A mAb to the β2-integrin Mac-1 reduces neointimal thickening after angioplasty in rabbits. J Clin Invest. 1998;101(10):2510-2519. doi:10.1172/JCI7811.
Saravia & Toca-Herrera 2009	Saravia F, Toca-Herrera JL. Tip-sample separation method for calculating indentation in atomic force microscopy. Rev Sci Instrum. 2009;80(8):086101. doi:10.1063/1.3200955.
Schmidt *et al.* 2009	Schmidt DR, Waldeck H, Kao WJ. Biological Interactions on Materials Surfaces. 1st ed. Springer; 2009. doi:10.1007/978-0-387-98161-1.

Schmidt *et al.* 2009	Schmidt DR, Waldeck H, Kao WJ. Protein adsorption to biomaterials. In: Puleo DA, Bizios R, editors. Biological Interactions on Materials Surfaces. New York: Springer; 2009. p. 1-18. doi:10.1007/978-0-387-98161-1_1.
Schönhoff 2003	Schönhoff M. Self-assembled polyelectrolyte multilayers. Curr Opin Colloid Interface Sci. 2003;8(1):86-95. doi:10.1016/S1359-0294(03)00011-3.
Schönhoff 2003	Schönhoff M. Layered polyelectrolyte complexes: physics of formation and molecular properties. J Phys Condens Matter. 2003;15:R1781-R1808. doi:10.1088/0953-8984/15/49/R01.
Schönhoff 2003	Schönhoff M. Layered polyelectrolyte complexes: physics of formation and molecular properties. J Phys Condens Matter. 2003;15(49):R1781-R1808. doi:10.1088/0953-8984/15/49/R01.
Schönhoff *et al.* 2007	Schönhoff M, Ball V, Bausch AR, *et al.* Hydration and internal properties of polyelectrolyte multilayers. Colloids Surf A Physicochem Eng Asp. 2007;303(1-2):14-29. doi:10.1016/j.colsurfa.2007.02.054.
Schwarz & Schönhoff 2002	Schwarz B, Schönhoff M. Surface potential driven swelling of polyelectrolyte multilayers. Langmuir. 2002;18(8):2964-2966. doi:10.1021/la015636y.
Selhuber-Unkel *et al.* 2010	Selhuber-Unkel C, Erdmann T, López-García M, Kessler H, Schwarz US, Spatz JP. Cell adhesion strength is controlled by intermolecular spacing of adhesion receptors. Biophys J. 2010;98(4):543–551. doi:10.1016/j.bpj.2009.11.001.
Simon *et al.* 2000	Simon DI, Chen Z, Seifert P, Edelman ER, Ballantyne CM, Rogers C. Decreased neointimal formation in Mac-1–/– mice reveals a role for inflammation in vascular repair after angioplasty. J Clin Invest. 2000;105(3):293-300. doi:10.1172/JCI7811.
Singh *et al.* 2005	Singh M, Chand H, Gupta KC. The studies of density, apparent molar volume, and viscosity of bovine serum albumin, egg albumin, and lysozyme in aqueous and RbI, CsI, and DTAB aqueous solutions at 303.15 K. Chem Biodivers. 2005;2(6):809-824. doi:10.1002/cbdv.200590059.
Sun 2017	Sun SC. The non-canonical NF-κB pathway in immunity and inflammation. Nat Rev Immunol. 2017;17(9):545-558. doi:10.1038/nri.2017.52.
Sutterwala *et al.* 2014	Sutterwala FS, Haasken S, Cassel SL. Mechanism of NLRP3 inflammasome activation. Ann N Y Acad Sci. 2014;1319:82-95. doi:10.1111/nyas.12458.
Tak & Firestein 2001	Tak PP, Firestein GS. NF-κB: a key role in inflammatory diseases. J Clin Invest. 2001;107(1):7-11. doi:10.1172/JCI11830.
Turner *et al.* 2007	Turner NA, Mughal RS, Warburton P, O'Regan DJ, Ball SG, Porter KE. Mechanism of TNFα-induced IL-1α, IL-1β and IL-6 expression in human cardiac fibroblasts: effects of statins and thiazolidinediones. Cardiovasc Res. 2007;76(1):81–90. doi:10.1016/j.cardiores.2007.06.003.
Vaca *et al.* 2020	Vaca DJ, Thibau A, Schütz M, Kraiczy P, Happonen L, Malmström J, Kempf VAJ. Interaction with the host: the role of fibronectin and extracellular matrix proteins in the adhesion of Gram-negative bacteria. Med Microbiol Immunol. 2020;209(3):277-299. doi:10.1007/s00430-019-00644-3.
Vicente-Manzanares *et al.* 2009	Vicente-Manzanares M, Ma X, Adelstein RS, Horwitz AR. Non-muscle myosin II takes centre stage in cell adhesion and migration. Nat Rev Mol Cell Biol. 2009;10(11):778-790. doi:10.1038/nrm2786.
Vogl *et al.* 2021	Vogl LM, Schweizer P, Richter G, Spiecker E. Effect of size and shape on the elastic modulus of metal nanowires. MRS Adv. 2021;6(27):665-673. doi:10.1557/s43580-021-00103-3.

Vogler 1998	Vogler EA. Structure and reactivity of water at biomaterial surfaces. Adv Colloid Interface Sci. 1998;74:69-117. doi:10.1016/S0001-8686(97)00040-7.
Vogler 2012	Vogler EA. Protein adsorption in three dimensions. Biomaterials. 2012;33(5):1201-1237. doi:10.1016/j.biomaterials.2011.10.059.
Vrana *et al.* 2016	Vrana NE, editor. Cell and Material Interface: Advances in Tissue Engineering, Biosensor, Implant, and Imaging Technologies. Boca Raton: CRC Press; 2016. ISBNs: 978-1-138-02941-9 (Hardback); 978-1-315-21508-2 (eBook).
Vroman *et al.* 1980	Vroman L, Adams AL, Fischer GC, Munoz PC. Interaction of high molecular weight kininogen, factor XII, and fibrinogen in plasma at interfaces. Blood. 1980;55(1):156-159. doi:10.1182/blood.V55.1.156.
Warszynski & Kolasinska 2005	Warszynski P, Kolasinska M. The effect of support material and conditioning on wettability of PAH/PSS multilayer films. Bioelectrochemistry. 2005;66(1-2):65-70. doi:10.1016/j.bioelechem.2004.09.004.
Weisel & Litvinov 2017	Weisel JW, Litvinov RI. Fibrin Formation, Structure and Properties. In: Fibrous Proteins: Structures and Mechanisms. Subcellular Biochemistry. Vol 82. Springer; 2017. p. 405-456. doi:10.1007/978-3-319-49674-0_13.
Welt & Rogers 2002	Welt FG, Rogers C. Inflammation and restenosis in the stent era. Arterioscler Thromb Vasc Biol. 2002;22(11):1769-1776. doi:10.1161/01.ATV.0000037100.44766.5B.
William 2009	Williams DF. On the nature of biomaterials. Biomaterials. 2009;30(30):5879-5897. doi:10.1016/j.biomaterials.2009.07.027.
Wintermantel & Ha 2009	Wintermantel E, Ha SW, editors. Medizintechnik: Life Science Engineering. 5th ed. Berlin: Springer-Verlag; 2009. ISBNs: 978-3-540-93935-1 (Hardback); 978-3-540-93936-8 (eBook).
Zan *et al.* 2012	Zan X, Hoagland DA, Wang T, Su Z. Ion dispositions in polyelectrolyte multilayer films. Macromolecules. 2012;45(21):8805-8812. doi:10.1021/ma3014492.
Zaveri *et al.* 2014	Zaveri TD, Lewis JS, Dolgova NV, Clare-Salzler MJ, Keselowsky BG. Integrin-directed modulation of macrophage responses to biomaterials. Biomaterials. 2014;35(13):3504-3515. doi:10.1016/j.biomaterials.2014.01.038.

Acknowledgement (Danksagung)

Diese Dissertation entstand im Zuge von Forschungsprojekten, die durch das Land Baden-Württemberg, das Bundesministerium für Bildung und Forschung (BMBF) sowie das Zentrum für Angewandte Forschung an Fachhochschulen (ZAFH) finanziert wurden.

Zu diesen Projekten gehören:

MediFreiStent (Land BW): Medikamentenfreie, kontaktwirkende, immunosuppressive Beschichtungen für vaskulären Stents (Innovative Projekte BW, 2014.001-Krastev)

BioDegStent (BMBF): Beschichtung für kontrollierte Biodegradation vaskulärer Metallstents (FHprofUnt 2016, FKZ: 3FH155PX6).

PolyAntiBak (BMBF): Beschichtung zur Immobilisierung von Polymerkompartimenten auf Oberflächen (ProMatLeben - Polymere, FKZ: 13XP5073D)

InSeL (ZAFH): Innovative Schaumstrukturen für effizienten Leichtbau. Entwicklung neuartiger zellulärer Leichtbauwerkstoffe und Komposite auf Basis von offenporigen Metallschäumen sowie die Entwicklung eines Verfahrens zur Substitution des spezifischen Herstellungsprozesses. (Zentren für angewandte Forschung (ZAFH), FKZ: FEIH_ZAFH_798236)